GEOLOGICA CARPATHICA, OCTOBER 2020, 71, 5, 462–482 https://doi.org/10.31577/GeolCarp.71.5.6

Geochemistry and Sr–Nd–Pb isotope characteristics of Miocene basalt–trachyte rock association in transitional zone between the Outer Western Carpathians and Bohemian Massif

LUKÁŠ KRMÍČEK[1,2,✉], JAROMÍR ULRYCH[1], PETRA ŠIŠKOVÁ[3], SIMONA KRMÍČKOVÁ[1,3], PETR ŠPAČEK[4] and ŠÁRKA KŘÍŽOVÁ[1]

[1]Institute of Geology of the Czech Academy of Sciences, Rozvojová 269, 165 02 Praha 6, Czech Republic; ✉krmicek@gli.cas.cz
[2]Brno University of Technology, Faculty of Civil Engineering, Institute of Geotechnics, Veveří 95, 602 00 Brno, Czech Republic
[3]Department of Geological Sciences, Faculty of Science, Masaryk University, Kotlářská 2, 611 37 Brno, Czech Republic
[4]Institute of Physics of the Earth, Masaryk University, Tvrdého 12, 602 00 Brno, Czech Republic

(Manuscript received January 20, 2020; accepted in revised form June 12, 2020; Associate Editor: Igor Broska)

Abstract: Representative samples covering all petrographic types of the Miocene subvolcanic (dykes and sills) basalt–trachyte rock association from the Uherský Brod area (UB, Moravia) in the Czech Republic were studied. The UB area is associated with the Klippen Zone in the neighbourhood of the contact of the Carpathian–Pannonian Block with the Bohemian Massif. The petrographic and geochemical features of the subvolcanic rocks from the UB area only partly resemble those of the calc-alkaline rocks in a similar structural position in the coeval Pieniny area in Poland as well as of the transitional calc-alkaline rocks from the Central Slovakian volcanic field. The Miocene subvolcanic rocks were generated by melting of the variably metasomatised sub-lithospheric source and subsequent fractional crystallisation of the primary basaltic magma. The compositional characteristics of this rock series straddle the alkaline and subalkaline volcanic rock fields, while the rocks from the Pieniny area and from the Central Slovakian volcanic field are predominantly calc-alkaline andesites. The distribution of incompatible elements such as U, Th, REE, Nb, Ta, Sr, Ba as well as La_N/Yb_N ratios and Sr–Nd–Pb isotope composition of the rocks from the UB and Pieniny areas differ substantially, whereas the geochemical patterns of the UB rocks are slightly similar to those of the transitional rocks from the Central Slovakian volcanic field. The modest contents of incompatible trace elements in the andesitic rocks from the Pieniny area share several characteristics of the prevalent calc-alkaline andesitic rocks from the Carpathian–Pannonian region. Basaltic–trachytic series from the UB area are characterised by higher εNd (~2.5) and lower $^{87}Sr/^{86}Sr$ (~0.704) and $^{207}Pb/^{204}Pb$ (~15.65) initial values in comparison with the calc-alkaline rocks from the Carpathian–Pannonian region including the Pieniny area. Nevertheless, the basaltic–trachytic rocks from the UB, richer in some of the incompatible trace elements (e.g., U, Th, REE, Sr and Ba) partly resemble (including Sr–Nd–Pb isotopes) the Na-alkaline Miocene volcanic rock series of the NE shoulder of the Cheb–Domažlice Graben in the Bohemian Massif.

Keywords: Outer Western Carpathians, post-collisional high-K magmatism, mineralogy, geochemistry, Sr–Nd–Pb isotopes.

Introduction

Two main volcanic associations were formed in the Central European region in the Cenozoic (Lustrino & Wilson 2007 and references therein): (1) an orogenic [mostly calc-alkaline and (ultra)potassic] series and (2) an anorogenic (mostly sodic alkaline with minor tholeiitic) series. The mantle beneath Central Europe was affected both by Variscan subduction and by post-Variscan extension (e.g., Wilson & Downes 1991; Ulrych et al. 2006; Dostal et al. 2019; Krmíček et al. 2020).

A Miocene volcanic association is present in the Carpathian–Pannonian area close to the south-eastern margin of the Bohemian Massif. Here, basaltic to trachytic rocks with Middle Miocene cooling ages share several geochemical and mineralogical characteristics of the calc-alkaline Carpathian–Pannonian orogenic series (e.g., Harangi et al. 2007), as well as of Na-alkaline anorogenic volcanic suites of the Cheb–Domažlice Graben in the western Bohemian Massif (Ulrych et al. 2016). This magmatism is exposed in the vicinity of the Carpathian Klippen Belt near Uherský Brod (UB) in southern Moravia, Czech Republic, and extends to the Slovak Republic (Fig. 1). UB magmatic bodies are not deformed nor metamorphosed, testifying for their post-orogenic emplacement. The petrogenesis of these rocks has been the subject of debate for a long time (e.g., Nejbert et al. 2012; Hrouda et al. 2015 and references therein), partly because similar rock associations of Miocene age also occur near the Pieniny Klippen Belt in Poland (Nejbert et al. 2012).

A number of studies in the last two decades have presented the mineralogical, petrographic and geochemical data on subvolcanic rocks from the Moravian region in the Czech Republic (Fediuk & Gürtlerová 2006; Nejbert et al. 2012; Hrouda et al. 2015), and the Pieniny Mountains in Poland (Pin et al. 2004; Nejbert et al. 2012), the latter also including Sr–Nd–Pb data (Trua et al. 2006) and Sr–Nd–Hf data (Anczkiewicz & Anczkiewicz 2016). A Sr–Nd–Pb isotope survey for rocks from the UB region is still lacking, which does not permit a comparison of the parental melt sources of these

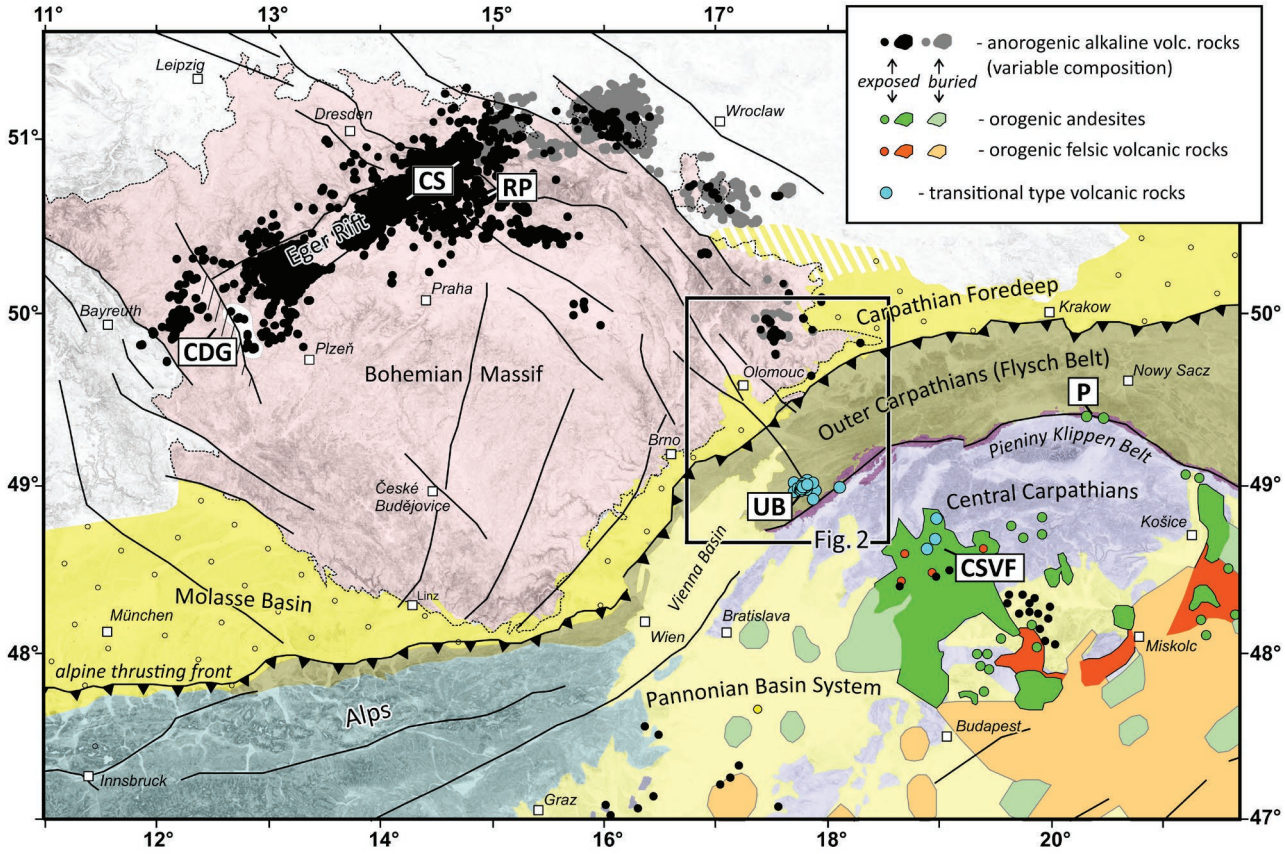

Fig. 1. Distribution and main typology of volcanics over the broader European plate–Western Carpathians–Alps junction region. Classification of volcanics into "orogenic" and "anorogenic" is *sensu* Lustrino & Wilson (2007). Occurrences of volcanic rocks are compiled from Harangi et al. (2007), Lexa et al. (2010), Ulrych et al. (2011) and Hrouda et al. (2015). Acronyms: CDG — Cheb–Domažlice Graben; CS — České Středohoří Volcanic Complex; CSVF — Central Slovakia Volcanic Field; P — Pieniny volcanics; RP — Ralská Pahorkatina Volcanic Complex; UB — Uherský Brod volcanics. The white marked area at the NE shoulder of CDG shows the location of samples used for reference further in this paper. Faults are very approximate. Rectangle shows the extent of the map in Fig. 2.

rocks with those of a similar age and composition from the Carpathian–Pannonian region and the Bohemian Massif. In this study we present a comparative petrological and geochemical investigation with the aim of discussing the sources of magma of this specific association, including Sr–Nd–Pb isotope data.

Geological setting and structural control of the magmatic rocks near Uherský Brod

The Carpathian Flysch Belt is particularly poor in subvolcanic rock occurrences (Pin et al. 2004; Pécskay et al. 2006; Nejbert et al. 2012; Hrouda et al. 2015). The most voluminous and differentiated subvolcanic rocks of Miocene age are exposed as more than 100 small bodies of ~10–1000 m size scattered over an area of ~120 km^2 in the clastic flysch-facies sediments, east and southeast of the town of Uherský Brod (Figs. 1, 2, 3). The rocks crop out as subvolcanic sills and dykes with basaltic, andesitic and trachytic composition (Hrouda et al. 2015). The published K–Ar ages are in the range of 15 to 13 Ma (Přichystal et al. 1998; Pécskay et al. 2002). These rocks are deformed only by small scale faults and are believed to be *in situ* intrusions postdating the large scale thrusting in the region (Přichystal et al. 1998; Krejčí & Poul 2010; Hrouda et al. 2015).

The UB subvolcanic rocks are located in the accretionary wedge of the Outer Western Carpathians, close to the Klippen Belt, a complex crustal structure marking the boundary with the Central Western Carpathians (Fig. 1). This boundary is generally assumed to coincide with the main suture between the two collided plates of the Alpine–Carpathian Orogen, i.e. the lower North European plate in the foreland *vs.* the upper Alcapa block in the hinterland (e.g., Nemcok et al. 1998; Froitzheim et al. 2008; Hrubcová & Środa 2015). The basement of the UB area is regarded as a part of the lower North European plate. In most tectonic models, it is suggested that the detachment of the steep subducted slab took place during the late collisional to early post-collisional phases (e.g., Nemcok et al. 1998; Konečný et al. 2002). The onset of the slab detachment can be dated since the youngest thrusting phase in the frontal part of accretionary wedge occurred in

the latest Early Miocene (~16–15 Ma). Therefore, at the time of emplacement of the subvolcanic rocks (~15–11 Ma), the lithosphere of the UB area might have been strongly influenced by the local effects of slab break-off (e.g., Nemcok et al. 1998) and by regional "back-arc" extension and related upwelling of asthenosphere commonly used to explain the origin of volcanic rocks in the inner parts of the Carpathian–Pannonian region (e.g., Konečný et al. 2002; Seghedi et al. 2004a). According to some models of lithospheric thickness (which, however, have limited resolution), the broader UB area is located close to the transitional zone between the normal lithosphere of the Bohemian Massif and the thinned lithosphere of the Pannonian domain (e.g., Praus et al. 1990; Majcin et al. 2015). Two models of magma generation have been proposed:

- The fault zones, especially where they intersect each other, may have acted as foci for asthenosphere diapirs, which impinged upon the mantle lithosphere of the European plate, promoting the partial melting of the lithosphere and leading to formation of primary magmas (Nejbert et al. 2012). Finger-like asthenosphere diapirs offer heat flux additional to that of asthenosphere updoming in response to the delamination of the subducting European plate (Trua et al. 2006).
- The primary magmas were generated within the lithosphere by decompression melting associated with pull-apart extension at transcurrent fault zones (Nejbert et al. 2012). Magma genesis associated with the decompression melting was focused entirely within hydrated and/or metasomatised mantle lithosphere (Seghedi & Downes 2011).

The upward migration of magma through the lithosphere, on the other hand, may have been controlled largely by pre-existing structures in the basement of the Carpathian accretionary wedge. A major fault structure on a NW–SE trend – the Haná Fault Zone (HFZ) – continues towards the UB area from the eastern Bohemian Massif (Fig. 2). There, the HFZ is well defined, correlating with a distinct negative Bouguer gravity anomaly and hosting a system of sedimentary grabens with late Miocene, Pliocene and Pleistocene fills (e.g., Špaček et al. 2015 and references therein). Some faults of the HFZ show evidence of significant oblique normal slip as young as the latest Pleistocene (Špaček et al. 2017). HFZ makes part of a broader zone with multiple expressions of regionally anomalous Cenozoic activity (Nysa–Morava Zone; e.g., Špaček et al. 2015) where small-volume basaltic volcanic eruptions occurred repeatedly in the Oligocene to Early Miocene and Pliocene to Early Pleistocene periods (e.g., Ulrych et al. 2013).

At present, an increased CO_2 flux and high-rate micro-seismicity are observed over the whole zone, including the direct neighbourhood of the UB area. An isolated patch of carbonated water springs surrounds the UB area and the seismically active domain extends to the basement of the Outer Western Carpathians just NW of the UB area. The continuation of the HFZ farther to the NE is also marked by a conspicuous interruption of the negative gravity anomaly of Outer Western Carpathians (Fig. 2) and by mapped faults of NW–SE to

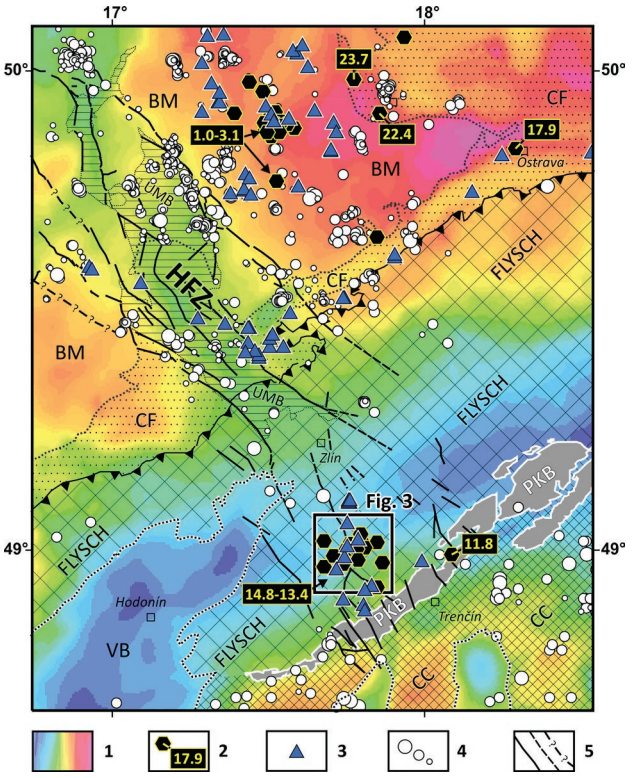

Fig. 2. Major structural, volcanic and tectonic features of the broader UB area. 1 — Bouguer anomaly map modified from Lenhardt et al. (2007), range: −60 to 5 mgal; 2 — Cenozoic volcanic rocks and their K–Ar ages in Ma taken from Pécskay et al. (2002) and Ulrych et al. (2013); 3 — Springs of carbonated mineral water modified from Špaček et al. (2015), some extinct springs included; 4 — Epicentres of natural earthquakes (M<0|M=0–1.5|M>1.5) compiled from IPE-MONET catalogue (Sýkorová et al. 2018) and catalogue of Slovak Academy of Sciences; 5 — Faults of the Haná Fault Zone (verified|indicated| assumed) compiled or interpreted from various sources, including geological maps of Czech and Slovak Geological Surveys (geometry is schematic). Acronyms: BM — Bohemian Massif; CF — Carpathian Foredeep; CC — Central Carpathians; FLYSCH — Flysch Belt, Outer Carpathians; HFZ — Haná Fault Zone; PKB — Pieniny Klippen Belt; UMB — Upper Morava Basin; VB — Vienna Basin.

NNW–SSE strike (e.g., the Nezdenice Fault; Krejčí & Poul 2010; Hrouda et al. 2015). Subvolcanic rocks at a similar position in the Pieniny Mountains in Poland (~13.3–10.8 Ma; Birkenmajer & Pécskay 2000) concentrate around the intersection of the NW–SE-striking Rieka and Dunajec faults and the Pieniny Klippen Belt.

Sampling and analytical methods

The distribution of the UB subvolcanic rocks and the localities sampled are presented in Fig. 3. The localities together with their geographic coordinates and brief geological and petrographic characteristics are listed in Table 1 and Fig. 4.

Representative rock samples (~3 to 5 kg each) from the UB area were crushed in a jaw crusher with tungsten carbide

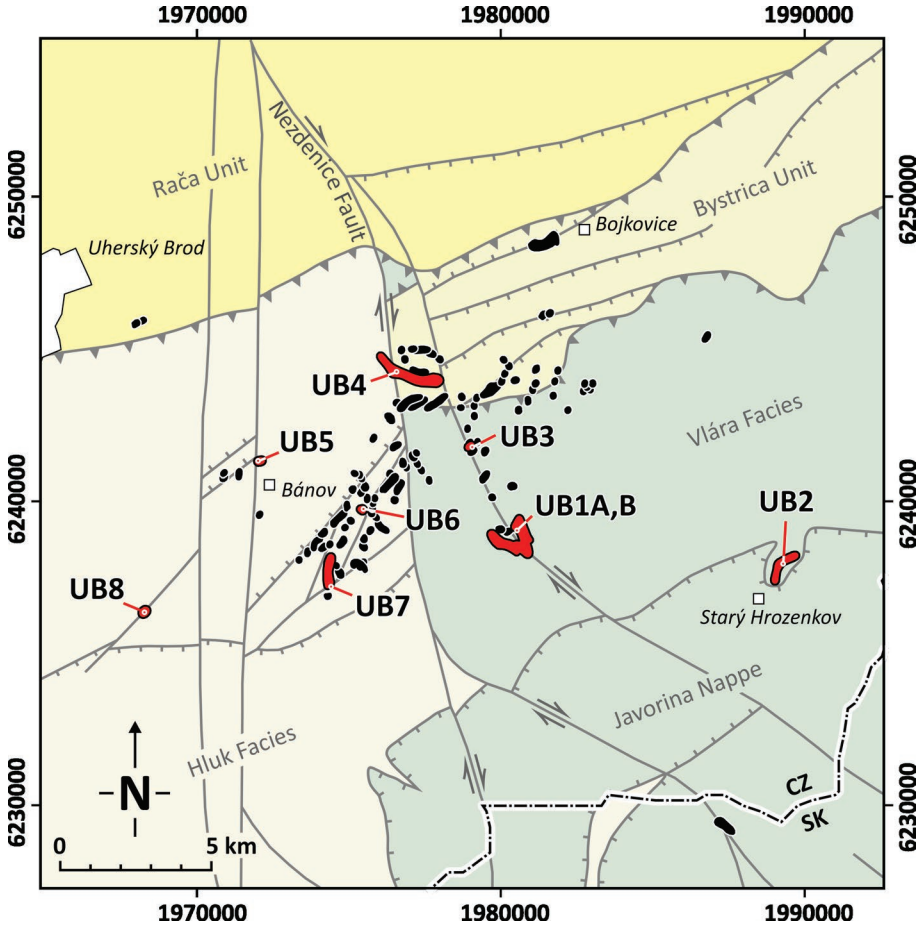

Fig. 3. Uherský Brod volcanic area – situation and sampling. Volcanic bodies are shown as black spots. Sampled occurrences are highlighted in red colour. Map adopted from Hrouda et al. (2015) and modified. The distribution of volcanic bodies is based largely on maps of Krejčí (1990) and Krejčí & Poul (2010).

plates. These samples were selected to cover all petrographic types of the studied subvolcanic rocks. Aliquots of crushed fragments were ground to a fine powder in an agate swing mill. Whole-rock major element and trace element analyses were performed at the Bureau Veritas Analytical Laboratories Ltd. (Vancouver, Canada) using inductively coupled plasma atomic emission spectrometry (ICP-AES; major oxides, Ba, Ni, Cu, Pb, Zn) and inductively coupled plasma mass spectrometry (ICP-MS; Co, Cs, Hf, Nb, Rb, Sr, Ta, Th, U, V, Zr, Y and REE). Loss on ignition (LOI) was determined by mass difference after ignition at 1000 °C. Detection limits for major oxides and trace elements ranged between 0.002–0.04 wt. % and 0.02–1 ppm, respectively. For further analytical details, see www.acmelab.com.

The major element mineral compositions (amphibole, clinopyroxene, mica, feldspars) were determined using a CAMECA SX 100 electron microprobe operated in wavelength-dispersive mode. Measurements were performed using a 15 keV acceleration voltage, 10 nA beam current and 2 m m beam diameter. Both natural and synthetic minerals were used as reference standards. The concentrations of the following elements were measured (standard, spectrometer crystals and detection limit for analysed elements are given in parentheses): Si (diopside, LTAP, 222 ppm), Ti (rutile, LPET, 357 ppm), Al (jadeite, LTAP, 272 ppm), Cr (Mn–Cr spinel, LIF, 910 ppm), Fe (haematite, LIF, 1047 ppm), Mn (rhodonite, LIF, 965 ppm), Ni (Ni_2Si, LTAP, 1404 ppm), Mg (periclase, LTAP, 422 ppm), Ca (diopside, LPET, 341 ppm), Na (jadeite, LTAP, 262 ppm), K (leucite, LPET, 300 ppm), F (fluorite, PC0, 1575 ppm), Cl (tugtupite, LPET, 320 ppm), Rb (RbCl, LTAP, 217 ppm) and Ba (baryte, LPET, 503 ppm). Counting times on peaks were 10 s for Mg, Al, K, Ca, Cl, Ti; 20 s for Na, Si, Rb, Ba, Ni and Mn; and 30 s for Cr, Ca and Al. The X-phi correction procedure (Merlet 1992) was used for spectra processing. Mineral compositions and formulas are listed and discussed in atoms per formula unit (*apfu*). The coefficient X_{Mg} is defined as X_{Mg}=Mg/(Mg+Fe). Abbreviations of mineral names are used according to Whitney & Evans (2010).

The Sr–Nd–Pb isotope analyses were carried out at the Institute of Geology of the Czech Academy of Sciences (GLI CAS) following the chemical protocol outlined in detail in Pin et al. (2014). Approximately 0.15 g of the sample was weighed in pre-cleaned Savillex beakers and decomposed using 4 ml of concentrated HF (23M) and 2 ml of 7M HNO_3 for 72 hours on

Table 1: Geological and petrographic characteristics of the basaltic–trachytic volcanic rocks from the Uherský Brod area.

Sample No.	Location	Longitude N	Latitude E	Geological characteristics	Rock type	Petrographic characteristics
UB1A	Bučník near Komňa (active quarry)	48°58.745'	17°47.457'	Sill, (laccolith?)	Trachydacite light	Holocrystalline, porphyritic, glomerophyric Phenocrysts: pl>>cpx, amp, bt, opq Microphenocrysts: pl>>cpx, opq, ap Groundmass: trachytic, pl>>, Kfs, opq
UB1B	Bučník near Komňa (active quarry)	48°58.745'	17°47.457'	Sill, (laccolith?) enclave	Basaltic trachyandesite greish-black	Holocrystalline, porphyritic Phenocrysts: pl>cpx, amp, ol?, opq Microphenocrysts: pl>>cpx, opq, ap Groundmass: microlithic, pl>cpx, opq
UB2	Starý Hrozenkov (abandoned quarry)	48° 58.360'	17° 52.171'	Sill	(Olivine) basalt	Holocrystalline, porphyritic, glomerophyric Phenocrysts: pl>>cpx, amp, ol, opq Microphenocrysts: pl>>cpx, opq, ap Groundmass: trachytic, pl>>cpx, opq
UB3	Modrá voda near Komňa (abandoned quarry)	48°59.709'	17°46.692'	Sill	Trachybasalt	Holocrystalline, porphyritic, glomerophyric Phenocrysts: pl>>cpx, amp, phl, opq Microphenocrysts: pl>>cpx, opq, ap Groundmass: trachytic, pl>>cpx, opq
UB4	U Kyselky near Nezdenice (abandoned quarry)	49°00.581'	17°45.321'	Sill, dyke	Trachyandesite light	Holocrystalline, porphyritic, glomerophyric Phenocrysts: pl>>cpx, amp, bt, opq Microphenocrysts: pl>>cpx, opq, ap Groundmass: trachytic, pl>>Kfs?, opq
UB5	Hrádek near Bánov (abandoned quarry)	48° 59.547'	17° 42.866'	Feeding channel with volcanic breccia – angular clast	Trachyandesite partly altered	Holocrystalline, porphyritic, glomerophyric Phenocrysts: pl>>amp, cpx, bt, opq Microphenocrysts: pl>>cpx, opq, ap Groundmass: trachytic, pl>>Kfs?, opq
UB6	Skalky near Bystřice pod Lopeníkem (abandoned quarry)	48°58.989'	17°44.740'	Sill	Trachybasalt fine-grained	Holocrystalline, porphyritic, glomerophyric Phenocrysts: pl>>cpx, amp, opq Microphenocrysts: pl>>cpx, opq, ap Groundmass: trachytic, pl>>cpx, opq
UB7	Bouda near Ordějov (abandoned quarry)	48°58.086'	17°44.168'	Sill	Basaltic andesite	Holocrystalline, porphyritic, glomerophyric Phenocrysts: pl>>cpx, amp, opq Microphenocrysts: pl>>cpx, opq, ap Groundmass: trachytic, pl>>cpx, opq
UB8	Na Hrádku near Suchá Loz (abandoned quarry)	48°57.800'	17°40.849'	Sill	Altered vesicular (olivine) basalt	Holocrystalline, porphyritic, glomerophyric Phenocrysts: pl>>cpx, amp, ol, opq Microphenocrysts: pl>>cpx, opq, ap Groundmass: trachytic, pl>>cpx, opq

Apatite and Ti-magnetite are common minerals of matrix of all presented rocks.

a hot plate at 140 °C. After that, the solution was dried at 120 °C and re-dissolved several times in 2 ml of 14M HNO_3 and 2 ml of 10M HCl until a clear solution was obtained. Thereafter, the solution was evaporated, and the residue was re-dissolved in 2 ml of 1M HNO_3. Before Sr–Nd–Pb separation, 100–200 mg of ascorbic acid (depending on Fe^{3+} content) was added in order to reduce the Fe^{3+} amount, and the resulting solution was placed in an ultrasonic bath for 10 minutes to ensure complete dissolution of ascorbic acid. Strontium–Pb and REE fractions were extracted from the matrix by ion-exchange chromatography using the column setup described in detail in Pin et al. (2014). For Sr–Pb isolation, a Sr resin (TrisKem) was used, while a combination of TRU and LN resins (TrisKem) was used for REE isolation and Nd extraction from bulk REE, respectively. The strontium fraction was collected by 0.05M HNO_3, the Pb fraction by 6M HCl and Nd by 0.25M HCl. The Sr and Nd solutions were dried and re-dissolved for isotope analyses in 1 µl of 1M HNO_3 and 6M HCl, respectively. In the case of Pb, ~50 µl of H_3PO_4 was added to the Pb cut, followed by a slow evaporation to about half of the solution. Finally, ~50 µl of H_2O_2 was added, the solution was evaporated, and the residue was re-dissolved for the isotope analyses in 1 µl of the emitter, consisting of silica gel and diluted phosphoric acid. The isotope analyses of Sr–Nd–Pb were performed on a Thermo Triton thermal ionisation mass spectrometer (TIMS) housed at the GLI CAS. Strontium was loaded on the degassed W filaments in the presence of a Ta activator and analysed in a static mode using a single configuration and a $^{88}Sr/^{86}Sr$ ratio of 8.3752 was applied for the mass fractionation correction. Neodymium was loaded onto degassed Re filaments and analysed in a static mode using a double configuration and a $^{146}Nd/^{144}Nd$ ratio of 0.7219 for the mass fractionation correction. The external reproducibility of Sr and Nd analyses was monitored by the long-term reproducibility of the NIST SRM 987 yielding $^{87}Sr/^{86}Sr$ of 0.710247 ±0.000013 (2σ, n=34) and JNdi-1 with $^{143}Nd/^{144}Nd$ value of 0.512100±0.000008 (2σ, n=24). Lead was loaded onto degassed Re filaments and analysed in static mode using a single filament configuration. The instrumental mass bias was corrected using the long-term replicate analyses of a NIST SRM 981 Pb standard. An average mass fractionation factor of 0.136 ‰ per mass unit relative to the reference values (Todt

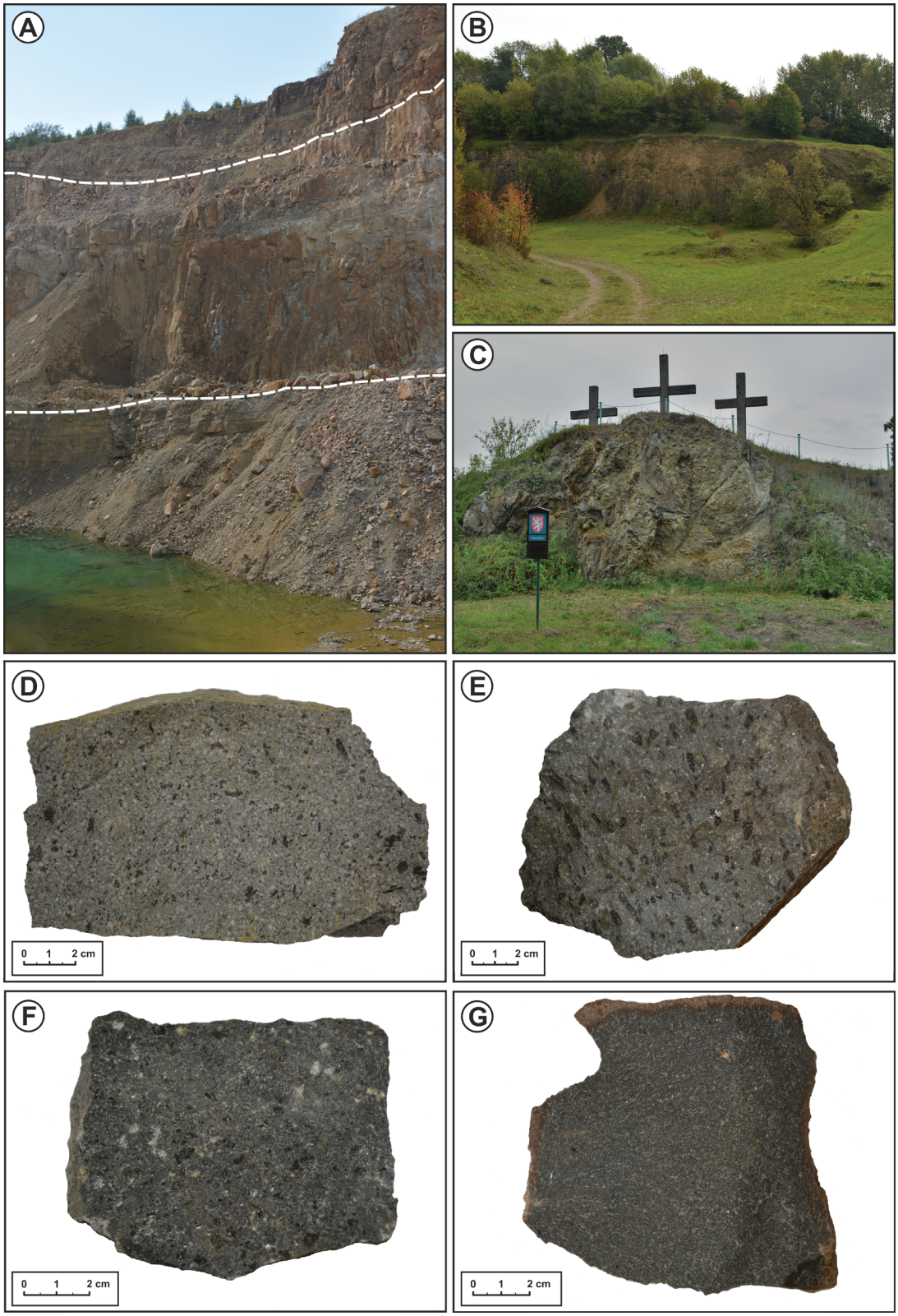

Fig. 4. General view of representative localities and rock samples of basaltic, andesitic and trachytic volcanic rocks from the Uherský Brod area. **A** — Bučník near Komňa, active quarry. An about 8 m thick basaltic trachyandesite sill with traces of columnar jointing in contact with metamorphosed sediments of the Magura Group of Nappes; **B** — Starý Hrozenkov, abandoned quarry with uncovered sill of olivine basalt; **C** — Hrádek near Bánov, abandoned quarry with uncovered feeding channel with volcanic breccia of trachyandesite composition; **D** — Microporphyritic light trachydacite (sample UB1A, Bučník near Komňa); **E** — Porphyritic basaltic trachyandesite from dark enclave (sample UB1B, Bučník near Komňa); **F** — Porphyritic olivine basalt (sample UB2, Skalka near Starý Hrozenkov); **G** — Fine-grained trachybasalt (sample UB6; Skalky near Bystřice pod Lopeníkem).

et al. 1996) was applied to all Pb isotope ratios. The external reproducibility (2SD) of $^{206}Pb/^{204}Pb$ was approximately 0.007, $^{207}Pb/^{204}$ approximately 0.008 and of $^{208}Pb/^{204}Pb$ approximately 0.030, as determined from the long-term reproducibility of the NIST SRM 981 with a determined value of 16.934±0.002 for $^{206}Pb/^{204}Pb$, 15.491±0.002 for $^{207}Pb/^{204}Pb$ and 36.703± 0.006 $^{208}Pb/^{204}Pb$ (errors as 2SE, n=32). The accuracy of the whole analytical protocol was monitored through the analyses of a BCR-2 (USGS) reference material (see table with isotope results) with values in excellent agreement with those previously published (Jochum & Nohl 2008).

Results

Petrography and mineral chemistry

The main petrographic features of the basaltic–andesitic–trachytic rocks and their phenocryst assemblages are presented in Table 1. Representative compositions of mafic minerals are listed in Table 2, while the complete dataset of mineral analyses is provided in Supplement A.

The rocks are porphyritic with a fine-grained trachytic groundmass (pl>>Na-Kfs±cpx, bt, opq). The common phenocryst assemblage is partly different in basaltic rocks (pl>>cpx>amp>ol, opq) from those in trachybasaltic to trachydacitic rocks (pl>>cpx>amp, bt) and trachyandesitic rocks (pl>>amp>cpx, bt) (see Table 1). This assemblage is very similar to that found in andesitic rocks of the Pieniny Mountains, Poland (Trua et al. 2006; Nejbert et al. 2012). Olivine is present only in a completely altered form in basaltic rocks from Starý Hrozenkov and Suchá Loz, whereas scarce dark mica is present in the samples from Bučník near Komňa. The trachytic groundmass is strictly leucocratic, dominated by feldspars (plagioclase and rarer Na–K feldspar), Fe–Ti oxides and rare chevkinite-group minerals and zirconolite (Macdonald et al. 2018). An altered volcanic breccia with altered clasts occurs in a feeding channel of Hrádek near Bánov.

Olivine

Olivine is the primary mineral forming almost subhedral phenocrysts in the sample from Starý Hrozenkov and Suchá Loz. It is completely transformed in a fine aggregate of calcite and serpentine (Fig. 5A).

Clinopyroxene

Subhedral to euhedral clinopyroxene represents the most abundant mafic phenocrysts (Fig. 5B, Starý Hrozenkov) and rare grains in the groundmass. Short columnar clinopyroxene commonly displays both sector and oscillatory zoning in trachybasalt (Fig. 5C, Modrá voda near Komňa) and basalt (Fig. 5B and Table 2, Starý Hrozenkov). Cores of the phenocrysts are rich in Mg, while the rims are rich in Fe (Supplement A). Prismatic sectors of the sector-zoned clinopyroxenes are enriched in elements such as Ti and Al, as well as Fe and Na, relative to the pyramidal sector which concentrates Mg and Si during partial equilibration with the melt. The relative diffusion rates of cations in the melt and the growth rates of crystal faces play a dominant role in the formation of the sector zoning and the oscillations in clinopyroxenes (e.g., Downes 1974). The clinopyroxene is predominantly diopside with a substantial compositional variation (X_{Mg}=0.6–0.9; Ca=0.86–0.95 *apfu*; Fig. 6A, Table 2 and Supplement A). Inclusions are represented by Fe-Ti oxides and apatite. Partial chloritisation of marginal parts of clinopyroxene grains is common.

Amphibole

Subhedral, usually zoned columns of brown and dark green amphibole (Fig. 5D,E) show a broad range of compositions from pargasite to magnesio-hastingsite (X_{Mg}=0.6–0.8; Si=5.69–6.43 *apfu*; Ca=1.73–1.99 *apfu*; Ti=0.24–0.45 *apfu*; Fig. 6B, Table 2 and Supplement A). The chemical compositions of amphibole resemble those of typical Ti-poor members of the magnesio-hastingsite–pargasite–kaersutite series (Ulrych et al. 2018). Resorbed edges of elongated and oval-shaped cross sections are characteristic (Fig. 5B, Starý Hrozenkov). Carbonatisation and opacite rims of amphibole are common (Fig. 5F, Hrádek near Bánov and Fig. 5E, Bučník near Komňa).

Feldspars

Subhedral plagioclase laths represent the most abundant phenocrysts, often forming cross twins to isometric glomerophyres (Fig. 5G, Bučník near Komňa and Fig. 5H, Hrádek near Bánov). The plagioclase compositions (Fig. 6C, Table 2 and Supplement A) range from andesine to anorthite ($An_{33–92}$). The zonality of plagioclase phenocrysts is highlighted by varying degrees of hydrothermal alteration, sericitisation and carbonatisation of individual zones. The transitions of basicity between the individual zones are quite sharp. The strongest alterations are characteristic of the most basic central parts of phenocrysts. The alteration of thin columnar to acicular plagioclase of the groundmass is not significant. Rare partially resorbed plagioclase cores show signs of sieve textures (Fig. 5H, Hrádek near Bánov). This texture is usually interpreted as a result of magma mixing (Streck 2008) but it may also occur by rapid decompression in a feeding channel of Hrádek near Bánov, where heat loss is minor relative to the ascent rate (Nelson & Montana 1992). Rarer Na–K feldspars ($Ab_{46–67}$, $Or_{16–52}$) are, together with plagioclase, confined to the groundmass.

Biotite

Rare subhedral (micro)phenocryst flakes of dark mica occur in some light varieties of trachyandesite and trachydacite (Bučník near Komňa). The compositions of mica correspond to biotite (X_{Mg}=0.5–0.6; Si=2.70–2.75 *apfu*; Table 2 and Supplement A).

Table 2: Representative compositions of dark mica, amphibole and clinopyroxene.

Mineral	**Dark mica**		**Amphibole**					**Clinopyroxene**				
Sample	**UB1A**	**UB1A**	**UB1A**	**UB1A**	**UB1A**	**UB2**	**UB2**	**UB2**	**UB2**	**UB2**	**UB2**	**UB2**
Petrographic type	**TD**	**TD**	**TD**	**TD**	**TD**	**BA**	**BA**	**BA-PY**	**BA**	**BA-PR**	**BA-PY**	**BA**
SiO_2	36.3	36.0	43.2	41.9	42.8	40.6	40.4	54.2	50.1	48.2	53.2	49.9
TiO_2	4.29	4.30	2.65	3.15	2.87	2.96	2.92	0.17	0.93	1.67	0.34	0.98
Al_2O_3	14.7	14.4	10.7	13.0	11.1	14.0	14.5	1.48	5.09	5.32	2.31	5.66
Cr_2O_3	<BDL	<BDL	<BDL	<BDL	<BDL	0.05	<BDL	0.62	0.19	<BDL	0.50	0.28
FeO	19.2	18.5	13.9	10.9	13.6	11.6	9.50	2.64	5.39	8.97	3.54	5.36
BaO	1.00	0.99	<BDL	0.16	0.12	0.11	0.11	<BDL	<BDL	<BDL	<BDL	<BDL
MnO	0.27	0.24	0.27	0.12	0.32	0.12	0.12	0.11	0.11	0.21	0.08	0.09
MgO	12.2	12.5	12.9	14.2	13.0	12.8	14.6	17.7	14.5	12.7	16.7	14.1
CaO	<BDL	<BDL	11.1	11.9	11.5	12.3	12.3	23.7	23.6	23.0	23.9	23.7
Na_2O	0.57	0.51	2.20	2.44	2.40	2.27	2.28	0.19	0.22	0.35	0.20	0.24
K_2O	8.63	8.66	0.88	0.93	0.90	1.28	1.29	<BDL	<BDL	<BDL	<BDL	<BDL
H_2O	3.69	3.66	1.97	2.00	1.97	1.98	2.01					
F	0.54	0.54	0.21	0.25	0.25	0.20	0.22					
Cl	0.13	0.12	0.10	0.04	0.07	0.02	<BDL					
O = −F	−0.23	−0.23	−0.09	−0.11	−0.10	−0.09	−0.09					
O = −Cl	−0.03	−0.03	−0.02	−0.01	−0.02	−0.01	0.00					
Total	101.2	100.2	100.3	101.0	101.0	100.4	100.3	100.8	100.1	100.4	101.0	100.3
Empirical formula (*apfu*)												
Si	2.74	2.74	6.32	6.06	6.25	5.98	5.87	1.96	1.85	1.81	1.93	1.84
Al^{IV}	1.26	1.26	1.68	1.94	1.75	2.02	2.13	0.04	0.15	0.19	0.07	0.16
ΣT*	4.00	4.00	8.00	8.00	8.00	8.00	8.00	2.00	2.00	2.00	2.00	2.00
Ti	0.24	0.25	0.29	0.34	0.32	0.33	0.32	0.00	0.03	0.05	0.01	0.03
Al	1.30	1.29	1.85	2.21	1.91	2.44	2.48	0.06	0.22	0.24	0.10	0.25
Al^{VI}	0.04	0.02	0.16	0.26	0.15	0.42	0.35	0.02	0.07	0.04	0.03	0.08
Cr	0.00	0.00	0.00	0.00	0.00	0.01	0.00	0.02	0.01	0.00	0.01	0.01
Fe^{tot}	1.21	1.18	1.70	1.32	1.66	1.43	1.15	0.08	0.17	0.28	0.11	0.17
Fe^{3+}	–	–	0.55	0.33	0.42	0.04	0.37	0.02	0.06	0.12	0.04	0.05
Mg	1.37	1.41	2.81	3.06	2.83	2.81	3.16	0.95	0.80	0.71	0.90	0.78
Ca	0.00	0.00	1.73	1.85	1.80	1.95	1.91	0.91	0.93	0.93	0.93	0.94
Mn	0.02	0.02	0.03	0.01	0.04	0.01	0.01	0.00	0.00	0.01	0.00	0.00
Fe^{2+}	–	–	1.15	1.00	1.24	1.39	0.79	0.06	0.11	0.17	0.07	0.12
Ba	0.03	0.03	0.00	0.01	0.01	0.01	0.01	0.00	0.00	0.00	0.00	0.00
Na	0.08	0.08	0.62	0.68	0.68	0.65	0.64	0.01	0.02	0.03	0.01	0.02
K	0.83	0.84	0.16	0.17	0.17	0.24	0.24					
OH	1.86	1.86	1.88	1.88	1.87	1.90	1.90					
F	0.13	0.13	0.10	0.11	0.11	0.10	0.10					
Cl	0.02	0.02	0.02	0.01	0.02	0.01	0.00					
O	11.0	11.0	22.7	22.8	22.7	23.0	22.8	6.00	6.00	6.00	6.00	6.00
Mg/(Mg+Fe)	0.53	0.55	0.71	0.75	0.69	0.67	0.80	0.94	0.88	0.81	0.93	0.87
Species	B	B	M	M	M	P	M	D	D	D	D	D

Empirical formula of dark mica is calculated on the basis of O=11.
Empirical formula of amphibole is calculated on the basis of T+C=13.
Empirical formula of clinopyroxene is calculated on the basis of O=6.
Petrographic type: TD — trachydacite; BA — basalt; PR — prismatic sector; PY — pyramidal sector
Species: B — biotite; M — magnesiohastingsite; P — pargasite; D — diopside
BDL: below detection limit
apfu: atoms per formula unit

Fe–Ti oxides

Subhedral isometric grains and their clusters and rare microphenocrysts of Ti-magnetite occur in various quantities in all samples. Microphenocrysts are present in trachybasalt from Modrá voda near Komňa. Fine grains of magnetite and ilmenite are present in the groundmass of the dark-coloured trachyandesite samples (Hrádek near Bánov).

Major, minor and trace elements

The Miocene UB subvolcanic rocks share similar geochemical patterns, transitional between the composition of the Miocene sodic alkaline volcanic rocks from the Bohemian Massif (NE shoulder of the Cheb–Domažlice Graben; Cajz et al. 2009; Ulrych et al. 2010, 2016) and the Miocene calc-alkaline volcanic rocks from the Carpathian–Pannonian area (e.g.,

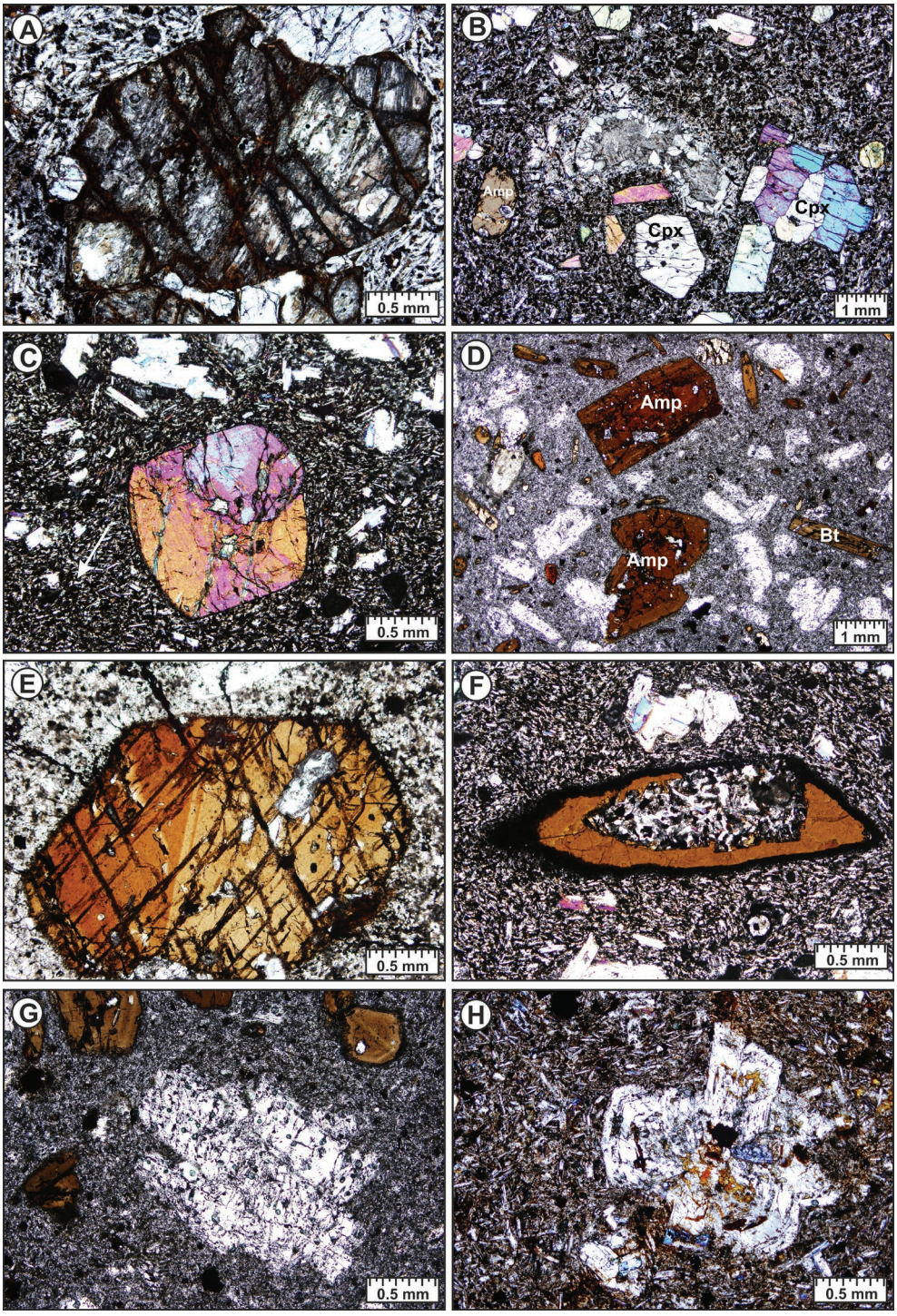

Fig. 5. Principal petrographic features of the Miocene volcanic rocks from the Uherský Brod area (XPL=crossed polarised light, PPL=plain polarised light). **A** — Completely carbonatised and serpentinised subhedral phenocryst of olivine in fine-grained groundmass (UB8; PPL); **B** — Numerous euhedral phenocrysts of clinopyroxene (Cpx), rare subhedral-oval phenocrysts of amphibole (Amp) and an amygdule filled with carbonates and zeolites in central part of the photomicrograph surrounded by a fine-grained groundmass with a trachytic texture (UB2; XPL); **C** — Clinopyroxene phenocryst displaying hour-glass sector zoning and microphenocrysts of plagioclases (light) and clinopyroxenes (dark) in fine-grained trachytic groundmass (UB3; XPL); **D** — Phenocrysts of amphibole (Amp) and biotite (Bt) in a fine-grained groundmass with trachytic texture (UB1A; PPL); **E** — Partly altered phenocrysts of amphibole twin with a thin opacite rim formed mostly by magnetite. Apatite inclusions are predominantly concentrated in amphibole (UB1B; PPL); **F** — Elongated, partly resorbed amphibole phenocryst with thick opacite rim. The fine-grained feldspar groundmass penetrates into the central part of the altered amphibole (UB3; XPL); **G** — Altered cross-twin phenocrysts of plagioclase along with amphibole phenocrysts concentrated in the upper-left part of the photomicrograph (UB1A; PPL); **H** — Glomerophyric aggregate of altered plagioclase phenocrysts with sieve textures in the central part of phenocrysts sitting in a trachytic groundmass (UB5; XPL).

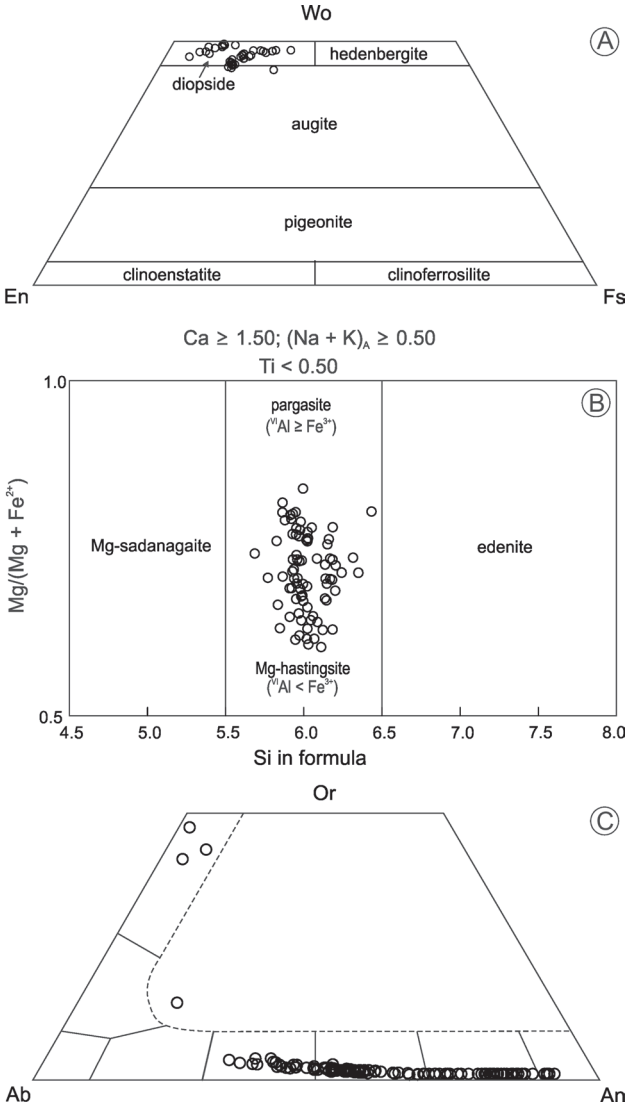

Fig. 6. Mineral compositions of rocks from the Uherský Brod area. **A** — Clinopyroxenes in the classification diagram of Morimoto et al. (1988); **B** — Amphiboles in the classification diagram of Leake et al. (1997); **C** — Ternary classification plot showing the composition of feldspars.

Harangi & Lenkey 2007; Harangi et al. 2007), including those from the Pieniny Mts. in Poland (Pin et al. 2004; Trua et al. 2006; Nejbert et al. 2012). However, several calc-alkaline volcanic rocks from the Central Slovakian volcanic field, classified as transitional between K-alkaline (orogenic) to Na-alkaline (anorogenic) volcanic rocks by higher Nb and Nb/Y values (Harangi et al. 2007; Seghedi & Downes 2011; Seghedi et al. 2013), are partly geochemically similar to the UB basaltic–trachytic series (Figs. 7, 8, 9, 10).

The UB rocks have SiO_2 content ranging from 45 to 62 wt. % (Table 3). For classification of the rocks we used the most common TAS classification despite the high LOI (2–8 wt. %) contents. In the TAS (Na_2O+K_2O *vs.* SiO_2) classification diagram, the rocks display a substantial variation from basic (basalt, trachybasalt, basaltic andesite and basaltic trachyandesite) to trachytic (trachyandesite and trachydacite) composition (Fig. 7). Members of these series straddle the line dividing alkaline and subalkaline volcanic rocks. In the K_2O *vs.* SiO_2 diagram applicable to the subdivision of subalkaline volcanic rocks, they plot close to the boundary between the high-K calc-alkaline series and the shoshonite series. Regardless the degree of possible alteration, the rocks follow the same high-K differentiation trend (Fig. 8).

Overall, rocks of the basaltic–trachytic series from the UB area show coherent trends of some oxides/elements (Al_2O_3, CaO, Ni, La, Ce), partly coherent (Sr, Zr, TiO_2) in binary variation diagrams, using mg# [molar $100\times MgO/(MgO+FeO_{total})$] as a differentiation index (Fig. 9). The rocks have positive correlations of CaO and Ni, and negative correlation of Al_2O_3, Sr, Zr and LREE with decreasing mg#. These trends reflect different fractionating mineral assemblages.

The primitive mantle-normalised incompatible element patterns (Fig. 10A) show similar trends with distinct relative enrichment of Th, U, La, Sr, and Nd and depletion in Rb, Nb, Ta, Pb, P, Zr and Ti negative anomalies. Moreover, the samples from the Bučník laccolith partly differ in the higher content of Pb (~63 ppm), probably associated with a post-magmatic fluid-induced enrichment (hydrothermal alteration) reflected in the occurrence of Fe–Cu–Pb–Hg mineralisation at the Bučník locality (Fojt & Přichystal 1979; Fig. 10A). In comparison with the UB samples, the rocks from the Pieniny Mts. show lower Nb, Ta, U, Th and REE and rather overlap with the Miocene calc-alkaline volcanic rocks from the Carpathian–Pannonian area (Fig. 10A).

The basaltic to trachytic rocks from the UB area show overlapping chondrite-normalised REE patterns (Fig. 10B) with a substantial LREE/HREE enrichment (La_N/Yb_N=12–33), coupled with a lack of a significant Eu-anomaly (Eu/Eu*= 0.9–1.0).

Sr–Nd–Pb isotope compositions

The initial Sr–Nd isotope ratios are given in Table 4 and plotted in Fig. 11. The suite has a relatively restricted range of initial $^{87}Sr/^{86}Sr$ ratios (0.7038–0.7048) and positive εNd values (from +1.8 to +3.3). The Sr–Nd isotope compositions define a two-component mixing line (Fig. 11). From a regional point of view, the initial Sr–Nd isotope signatures of basaltic–trachytic series from the UB area differ significantly from those of Miocene andesitic rocks from the Pieniny, which have more radiogenic $^{87}Sr/^{86}Sr_{(i)}$ (0.7053–0.7070) and notably variable negative $\varepsilon Nd_{(i)}$ between −4.7 and −10.1 (Pin et al. 2004; Trua et al. 2006). On the other hand, isotope compositions of the rocks from the UB area partly overlap those from the Miocene off-rift volcanic rock series of the NE shoulder of the Cheb–Domažlice Graben in western Bohemia (Ulrych et al. 2016; Fig. 11).

Lead isotope data are given in Table 4, and initial Pb isotope ratios are plotted as $^{206}Pb/^{204}Pb$ *vs.* $^{207}Pb/^{204}Pb$ and $^{206}Pb/^{204}Pb$ *vs.* $^{208}Pb/^{204}Pb$ in Fig. 12. The rocks show a relatively limited

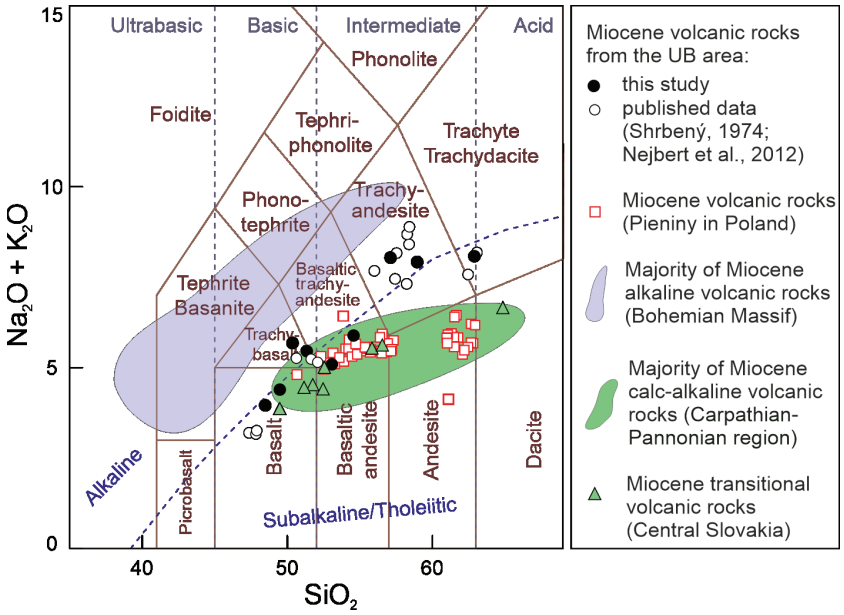

Fig. 7. The total alkali *vs.* silica (TAS) diagram (Le Maitre 2002) showing the composition of Miocene volcanics from Uherský Brod. Published data for Pieniny taken from Pin et al. (2004), Trua et al. (2006) and Nejbert et al. (2012), and for Central Slovakian volcanic field from Harangi et al. (2007). Fields for the majority of Miocene calc-alkaline volcanic rocks from the Carpathian–Pannonian area (Harangi & Lenkey 2007) and Miocene alkaline volcanic rocks from the Bohemian Massif (Cajz et al. 2009; Ulrych et al. 2010, 2016) are plotted for comparison.

overlapping variation in the initial $^{206}Pb/^{204}Pb$ (19.1–19.4), $^{207}Pb/^{204}Pb$ (15.6–15.7) and $^{208}Pb/^{204}Pb$ (39.0–39.2) ratios. The rocks plot along an inferred two-component mixing trend that crosses the Northern Hemisphere Reference Line (NHRL) of Hart (1984) in the $^{206}Pb/^{204}Pb$ *vs.* $^{208}Pb/^{204}Pb$ diagram (Fig. 12B). Initial Pb isotope signatures of the basaltic–trachytic series from the UB area partly deviate towards upper crustal $^{207}Pb/^{204}Pb$ values from Variscan inherited orogenic Pb growth component sampled by various volcanic rocks from the České Středohoří and Ralská Pahorkatina volcanic complexes in the Bohemian Massif (Fig. 12A). Additionally, the initial Pb isotope compositions are closely comparable to the Pb isotope compositions of the Miocene off-rift volcanic rocks from the NE shoulder of the Cheb–Domažlice Graben in western Bohemia (Ulrych et al. 2016; Fig. 12A).

P–T conditions of amphibole crystallisation

Amphibole is one of the most useful minerals for the estimation of the P–T conditions under which magma crystallised (Mutch et al. 2016). Several thermobarometers based on the composition of amphibole have been proposed for different igneous systems. Regarding the compositional characteristic of the host rocks and the high content of Ca and Mg in the amphibole, the thermometer of Ridolfi & Renzulli (2012) was selected as the most suitable. On the other hand, the barometer proposed by the same authors may be too sensitive to subtle compositional variations in amphibole and may generate a large uncertainty in the pressure estimates. Consequentially, we preferred to use the empirical barometer of Pál-Molnár et al. (2015) based on the Al_2O_3 contents in amphibole, which is calibrated using data for experimental amphiboles.

Temperature and pressure ranges calculated for the UB amphiboles are 910–990 °C ±24 °C and 0.4–1.2 GPa (i.e., ~15–45 km; Fig. 13). Calculated P–T conditions are compatible with experimental data on the stability of amphiboles of the magnesio-hastingsite–pargasite–kaersutite series supposedly derived from the upper mantle (Green et al. 2010; Pilet et al. 2010 and references therein) and fall into the stability field of amphibole in mafic lavas (Green et al. 2010). Generally, analyses of outer rims and/or BSE-light [i.e., with relatively lower $Mg/(Mg+Fe^{2+})$ ~0.6] zones in amphibole with reverse zoning displayed a parallel trend with the major P–T range yielding lower pressures (the lowest values are ~0.3 GPa) at the same temperature (Fig. 13), suggesting their late appearance.

Crystallisation temperatures of the amphibole are lower than the temperature estimates (at comparable pressures) for amphibole of the magnesio-hastingsite–pargasite–kaersutite series from the volcnic rocks from the Bohemian Massif (Ulrych et al. 2018), which crystallised from a Ti-enriched Na-alkaline system under rift conditions with elevated heat flow due to uplifted asthenospheric mantle.

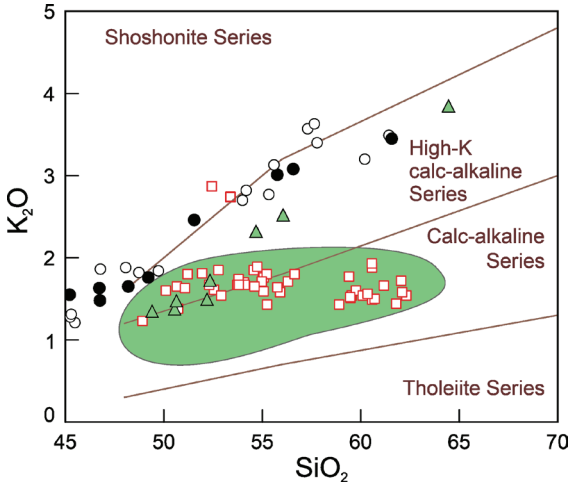

Fig. 8. The SiO_2 *vs.* K_2O plot (Pecerillo & Taylor 1976) showing the composition of Miocene volcanic rocks from the Uherský Brod area. Analyses were not recalculated on a volatile-free basis before plotting. Symbols are corresponding to the legend in Fig. 7.

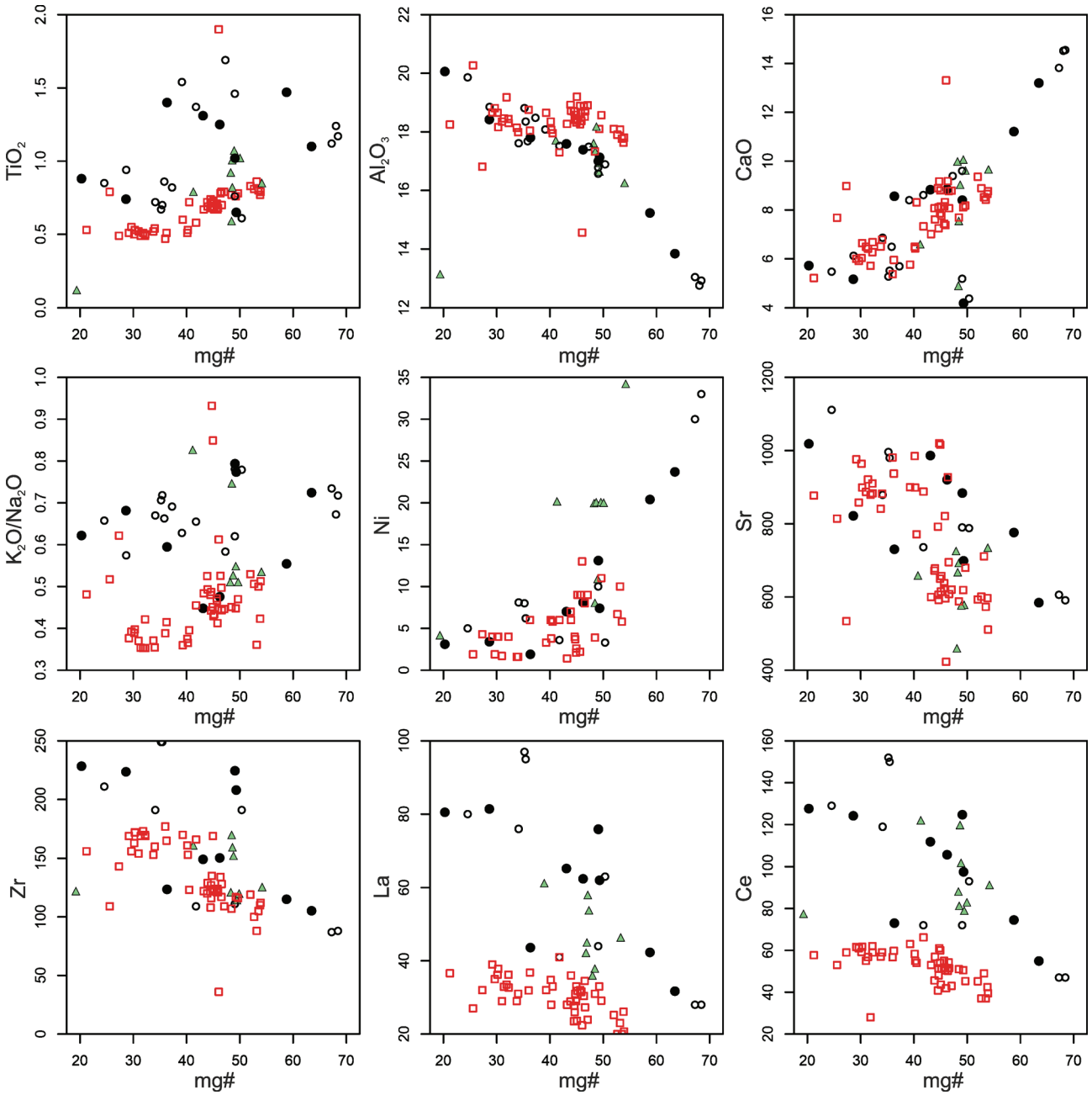

Fig. 9. Selected major and trace element contents *vs.* mg# of Miocene igneous rocks from the Uherský Brod area (black circles: new analyses; white circles: Shrbený 1974; Nejbert et al. 2012). Published data for Pieniny (red squares: Pin et al. 2004; Trua et al. 2006; Nejbert et al. 2012) and for the Central Slovakian volcanic field (green triangles: Harangi et al. 2007) are plotted for comparison.

Discussion

Nature of magma source

Majority of Miocene andesites from the Intra-Carpathian part of the Carpathian–Pannonian region are relatively poor in K_2O and total alkali contents (Lexa & Konečný 1998; Seghedi et al. 2004a,b, 2005; Harangi & Lenkey 2007; Harangi et al. 2007; Lustrino & Wilson 2007; Harangi 2009) and plot exclusively in the calc-alkaline field in TAS and K_2O *vs.* SiO_2 diagrams (Figs. 7, 8; Table 5). A post-collisional change in the geochemical character of calc-alkaline rocks from the Carpathian–Pannonian region from more K-enriched ones derived from a metasomatically enriched lithospheric source to Na-alkaline ones generated from a depleted asthenospheric mantle source was presented, e.g., by Mason et al. (1996); Seghedi et al. (2004a,b); Harangi & Lenkey (2007) and Harangi et al. (2007). Seghedi & Downes (2011) and Seghedi et al. (2013) classified such calc-alkaline rocks as transitional, characterised by higher Nb contents (>35 ppm)

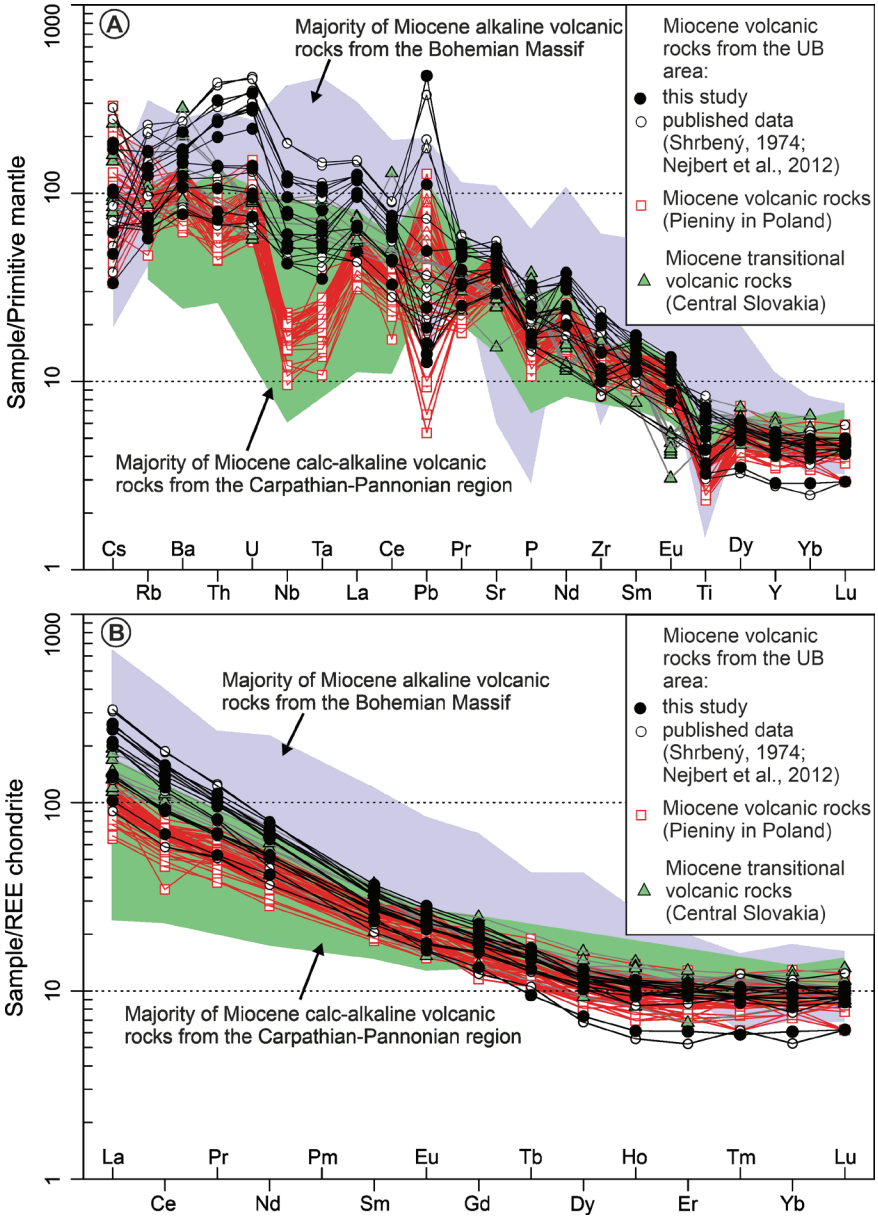

Fig. 10. A — Primitive mantle-normalised (McDonough & Sun 1995) multielemental patterns of Miocene volcanic rocks from Uherský Brod; **B** — Chondrite-normalised (Boynton 1984) REE content for the same rocks. Published data for Pieniny taken from Pin et al. (2004), Trua et al. (2006) and Nejbert et al. (2012), and for Central Slovakian volcanic field from Harangi et al. (2007). Fields for the majority of Miocene calc-alkaline volcanic rocks from the Carpathian–Pannonian area (Harangi & Lenkey 2007) and Miocene alkaline volcanic rocks from the Bohemian Massif (Cajz et al. 2009; Ulrych et al. 2010, 2016) are plotted for comparison.

and Nb/Y ratios (>1). Seghedi (2004a,b) emphasised that the typical calc-alkaline magmas of the Carpathian–Pannonian region were formed by decompression melting of a heterogeneous crust and mantle lithosphere, while those of the UB and Pieniny Mts. type resulted from fluid-dominated melting of the mantle lithosphere in the same region.

Major and trace element compositions of the basaltic–trachytic series from the UB area suggest a thermal initiation in the asthenospheric mantle, causing the partial melting of metasomatised lithospheric mantle rich in alkalis and some incompatible elements, such as Sr, Ba, REE, Th and U. In such a model, the melted material is usually considered to be represented by mantle peridotite with significant proportions of amphibole-bearing clinopyroxenite veins (e.g., Bailey 1982; Powell et al. 2004; Harangi et al. 2015) and the compositions of the resulted magma reflect such a heterogeneous metasomatised lithospheric source and variable degrees of melting (e.g., Haase & Renno 2008; Dostal et al. 2017). The large major and trace element variations in the UB suite (Fig. 7) and the covariations between mg# and major/trace elements (Fig. 9) indicate that the parental basaltic melt underwent fractional crystallisation during ascent. The decrease in CaO, MgO, Ni and increase in SiO_2, Na_2O and K_2O can be attributed to olivine, clinopyroxene, feldspar, amphibole, biotite and Ti-magnetite fractionation. Olivine is, however, present only as carbonatised pseudomorphs. Nevertheless, the most primitive samples of (olivine) basalts having 7.3 wt.% MgO, 281 ppm Cr and 24 ppm Ni, are rather far from values typical of primitive mantle melts. Moreover, elevated contents of TiO_2, K_2O/Na_2O, U, Th, REE, Nb, Ta, Sr, Ba of the UB rocks in comparison with samples with the same mg# from the Pieniny Mountains point probably to significant differences in source composition, melting grade and/or degree of melt fractionation (Fig. 9).

Miocene subvolcanic rocks from the Pieniny area exhibit a coupled, negative Nb–Ta anomaly (Fig. 10A). Lustrino & Wilson (2007) argued that a negative Nb-Ta anomaly can indicate either shallow-level crustal contamination, the introduction of subducted sediment into the mantle source of the magma or fluid-induced enrichment of the elements adjacent to Nb–Ta in the trace element pattern. Arndt and Christensen (1992) interpreted this negative anomaly in basaltic lavas as a consequence of Nb–Ta fractionation during passage of the deep asthenospheric magma through metasomatised peridotite in the lithospheric mantle. Transitional calc-alkaline rocks from the Central Slovakian volcanic field lack this Nb–Ta negative anomaly and their

Table 3: Chemical analyses of the basaltic–trachytic volcanic rocks from the Uherský Brod area.

Locality	UB1A Bučník, Komňa	UB1B Bučník enclave	UB2 Skalka, Starý Hrozenkov	UB3A Modrá voda, Komňa	UB4A U Kyselky, Nezdenice	UB5 Hrádek, Bánov	UB6A Skalky, Bystřice p. L.	UB7 Bouda, Ordějov	UB8 Suchá Loz
Rock type	light TD	dark BTA	ol. BA	TB	light TA	TA clast	fine-gr. TB	BAA	ol. BA
SiO_2 (wt. %)	61.6	51.5	45.2	48.2	56.6	55.8	46.7	49.2	46.8
TiO_2	0.65	1.02	1.10	1.25	0.74	0.88	1.31	1.40	1.47
Al_2O_3	17.1	17.0	13.8	17.4	18.4	20.1	17.6	17.8	15.2
Fe_2O_3	3.99	6.78	8.36	8.55	5.83	6.00	8.87	8.09	8.74
MnO	0.14	0.19	0.16	0.15	0.14	0.07	0.16	0.15	0.17
MgO	1.96	3.30	7.33	3.71	1.18	0.77	3.39	2.33	6.29
CaO	4.19	8.40	13.2	8.85	5.16	5.72	8.83	8.56	11.2
Na_2O	4.46	3.10	2.14	3.47	4.52	4.84	3.64	2.96	2.67
K_2O	3.45	2.46	1.55	1.65	3.08	3.01	1.63	1.76	1.48
P_2O_5	0.36	0.67	0.37	0.65	0.33	0.52	0.64	0.47	0.47
LOI	1.80	5.10	6.30	5.80	3.60	2.00	6.80	7.00	5.10
Total	99.7	99.6	99.6	99.7	99.6	99.6	99.6	99.7	99.6
Ni (ppm)	7.4	13.1	23.7	8.1	3.4	3.1	7.0	1.9	20.4
Cr	<BDL	27.4	281	20.5	20.5	<BDL	13.7	<BDL	164
Co	8.2	19.7	28.7	21.5	10.2	11.9	23.0	16.8	31.3
Sc	8	16	39	15	9	6	16	16	32
Rb	99.2	74.6	44.7	38.7	99.5	82.3	43.1	43.9	34.5
Sr	699	884	585	920	822	1019	986	730	776
Y	12.4	23.2	17.4	21.2	18.4	19.9	21.7	20.3	22.1
Zr	208	225	105	150	224	228	149	124	115
Nb	39.9	62.8	33.4	50.4	80.7	75.4	52.5	27.9	35.6
Cs	1.3	3.8	2.1	2.1	3.6	1.0	3.9	2.2	0.7
Ba	1105	1038	707	816	1395	1128	956	709	511
La	62.0	75.9	31.7	62.4	81.4	80.5	65.2	43.6	42.3
Ce	97.5	124.7	54.9	105.7	124.2	127.6	111.9	73.0	74.5
Pr	9.96	13.60	6.42	11.64	12.26	12.88	12.21	8.28	8.40
Nd	30.9	47.0	24.8	41.0	38.5	43.2	42.5	30.5	31.3
Sm	4.75	7.16	4.57	6.39	5.52	6.22	6.78	5.32	5.62
Eu	1.21	2.08	1.32	1.89	1.60	1.79	2.00	1.56	1.69
Gd	3.45	5.88	4.17	5.45	4.55	4.99	5.70	4.72	5.13
Tb	0.45	0.80	0.62	0.76	0.62	0.72	0.80	0.69	0.76
Dy	2.36	4.20	3.40	3.86	3.28	3.75	4.18	3.76	3.86
Ho	0.44	0.80	0.70	0.80	0.67	0.76	0.82	0.77	0.78
Er	1.28	2.24	1.96	2.32	2.11	2.08	2.30	2.19	2.18
Tm	0.19	0.33	0.28	0.33	0.31	0.33	0.34	0.30	0.30
Yb	1.27	2.19	1.74	2.03	2.17	2.19	2.17	2.03	1.93
Lu	0.20	0.34	0.28	0.32	0.34	0.34	0.33	0.31	0.29
Hf	5.0	4.7	2.7	3.4	4.7	4.6	3.3	3.1	2.8
Ta	2.0	3.0	1.9	2.3	3.8	4.0	2.5	1.3	2.3
Th	19.4	15.9	6.4	11.0	24.9	19.1	11.2	8.5	5.8
U	5.5	4.4	1.5	2.7	6.8	5.7	2.8	2.0	1.9
V	88	166	235	201	124	131	211	220	274
Cu	12.6	51.7	52.0	31.9	26.5	8.9	26.5	5.0	48.5
Pb	63.1	16.7	2.1	2.4	2.9	7.4	1.9	3.7	1.9
Zn	95	66	48	66	75	76	72	64	58
#mg	49	49	63	46	29	20	43	36	59
ΣREE	216	287	137	245	278	287	257	177	179
La_N/Yb_N	32.9	23.4	12.3	20.7	25.3	24.8	20.3	14.5	14.8
Eu/Eu*	0.91	0.98	0.92	0.98	0.98	0.98	0.98	0.95	0.96

#mg=[molar 100×MgO/(MgO+FeO total)]
TD — trachydacite; BTA — basaltic trachyandesite; BA — basalt; TB — trachybasalt; TA — trachyandesite; BAA — basaltic andesite
BDL: below detection limit

Table 4: Whole-rock Sr, Nd, and Pb isotope data for the basaltic–trachytic volcanic rocks of the Uherský Brod area.

Sample	Rock type	Locality	Age (Ma)	$^{87}Sr/^{86}Sr_{(m)}$	$^{87}Sr/^{86}Sr_{(i)}$	$^{143}Nd/^{144}Nd_{(m)}$	$^{143}Nd/^{144}Nd_{(i)}$	$\varepsilon Nd_{(i)}$	$^{206}Pb/^{204}Pb_{(m)}$	$^{207}Pb/^{204}Pb_{(m)}$	$^{208}Pb/^{204}Pb_{(m)}$	$^{206}Pb/^{204}Pb_{(i)}$	$^{207}Pb/^{204}Pb_{(i)}$	$^{208}Pb/^{204}Pb_{(i)}$
UB1A	light TD	Bučník, Komňa	14	0.704448±6	0.70437	0.512753±6	0.51274	2.6	19.146	15.650	39.047	19.13	15.65	39.03
UB1B	dark BTA, enclave	Bučník, Komňa – enclave	14	0.704823±4	0.70477	0.512711±11	0.51270	1.8	19.129	15.649	39.043	19.09	15.65	39.00
UB2	ol. BA	Skalka, Starý Hrozenkov	14	0.704552±4	0.70451	0.512744±4	0.51273	2.4	19.277	15.676	39.169	19.18	15.67	39.03
UB3	TB	Modrá voda, Komňa	14	0.704140±5	0.70412	0.512777±5	0.51277	3.0	19.384	15.653	39.236	19.22	15.65	39.02
UB4	light TA	U Kyselky, Nezdenice	14	0.703976±4	0.70391	0.512788±7	0.51278	3.3	19.401	15.654	39.155	19.08	15.63	38.85
UB5	TA angular clast	Hrádek, Bánov – clast	14	0.703799±5	0.70375	0.512773±5	0.51276	3.0	19.411	15.646	39.245	19.29	15.65	39.03
UB6	fine-gr. TB	Skalky, Bystřice p. L.	14	0.704000±5	0.70397	0.512777±6	0.51277	3.0	19.376	15.650	39.192	19.17	15.64	38.92
UB7	BAA	Bouda, Ordějov	14	0.704668±4	0.70463	0.512724±7	0.51271	2.0	19.100	15.641	38.993	19.02	15.64	38.89
BCR-2	Basalt, Columbia River, USGS Reference material			0.705008±5		0.512625±18			18.748	15.614	38.697			
BCR-2	Basalt, Columbia River, USGS Reference material			0.705008±5		0.512622±6			18.748	15.615	38.696			

$^{87}Sr/^{86}Sr$ and $^{143}Nd/^{144}Nd$ were normalised to $^{86}Sr/^{88}Sr$=0.1194 and $^{146}Nd/^{144}Nd$=0.7219, respectively. Analytical uncertainties are given at 2σm level. $^{87}Sr/^{86}Sr_{(i)}$ and $\varepsilon Nd_{(i)}$ were calculated for 14 Ma using $\lambda^{87}Rb$=1.42E−11 y^{-1} and $\lambda^{147}Sm$= 6.54E−12 y^{-1}, $(^{147}Sm/^{144}Nd)^0_{CHUR}$=0.1960, and $(^{143}Nd/^{144}Nd)^0_{CHUR}$=0.512630 (Bouvier et al. 2008), respectively, and the concentration data are given in Table 2.

Lead isotope data were recalculated for 14 Ma using the constants recommended by IUGS ($\lambda^{232}Th$=4.9475E−11 y^{-1}, $\lambda^{235}U$=9.8485E−10 y^{-1}, $\lambda^{238}U$=1.55125E−10 y^{-1}), and the concentration data listed in Table 2.

Rock type: TD = trachydacite; BTA = basaltic trachyandesite; BA = basalt; TB = trachybasalt; TA = trachyandesite; BAA = basaltic andesite

primitive mantle-normalised geochemical patterns mostly overlap with the UB subvolcanic rocks, except for the pronounced Eu negative anomaly (Fig. 10A).

The REE enrichment of the UB rocks is a characteristic feature of Miocene Na-alkaline rocks from the Bohemian Massif compared to that of prevalent calc-alkaline rocks from the Carpathian–Pannonian area (Fig. 10B). However, the REE patterns correspond to those of the transitional calc-alkaline rocks from the Central Slovakian volcanic field (Figs. 9, 10B).

The geochemical signatures, including the isotope data of the basaltic–trachytic series from the UB area, show that the magma was mainly derived from a metasomatised lithospheric source largely enriched in large-ion lithophile elements (LILE) such Cs, Rb or Ba. The contents of these characteristic elements, such as Ba (511–1395 ppm) and Sr (585–1019 ppm), are substantially higher than those of average continental crust (~260 ppm Ba, ~350 ppm Sr; Rudnick & Gao 2003) and should be interpreted in the context of the metasomatically transformed lithospheric sources. This is attested by the observed variations in Sr–Nd isotopes which define a two-component mixing line (Fig. 12). This is indicative of the presence of a metasomatised lithospheric mantle source with variable changing contributions from the (amphibole-bearing) metasome and ambient mantle (Supplement B). Such a metasomatised mantle type shows affinity towards the Enriched Mantle 2 (EM2)-type and points to a different mode of

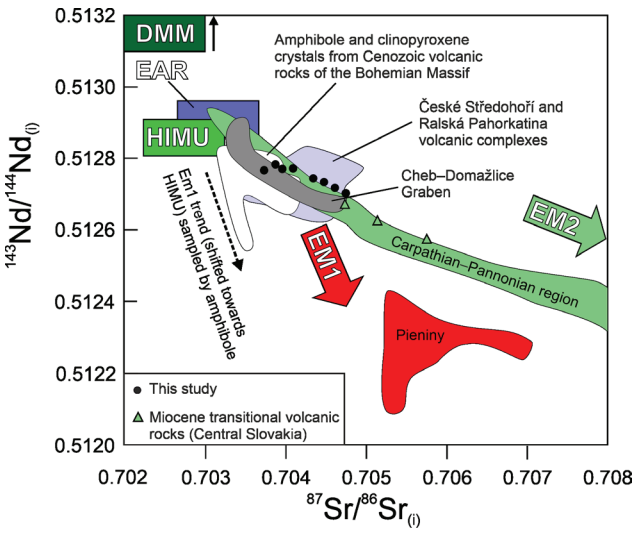

Fig. 11. Initial $^{143}Nd/^{144}Nd$ *vs.* $^{87}Sr/^{86}Sr$ isotope ratios for rocks from the Uherský Brod area in comparison with Sr–Nd isotope composition of Cenozoic volcanic rocks (and their amphibole and clinopyroxene) of the Bohemian Massif (Lustrino & Wilson 2007; Haase & Renno 2008; Ulrych et al. 2008, 2013, 2016, 2017, 2018; Dostal et al. 2017) and from the Carpathian–Pannonian region (Harangi & Lenkey 2007) including the Central Slovakian volcanic field (Harangi et al. 2007) and the Pieniny area (Pin et al. 2004; Trua et al. 2006). BSE=Bulk Silicate Earth; CHUR=Chondritic Uniform Reservoir; DMM=Depleted MORB Mantle; EAR=European Asthenospheric Reservoir; HIMU=high μ ($^{238}U/^{204}Pb$); EM1=Enriched Mantle 1; EM2=Enriched Mantle 2 (Ulrych et al. 2018 and references therein).

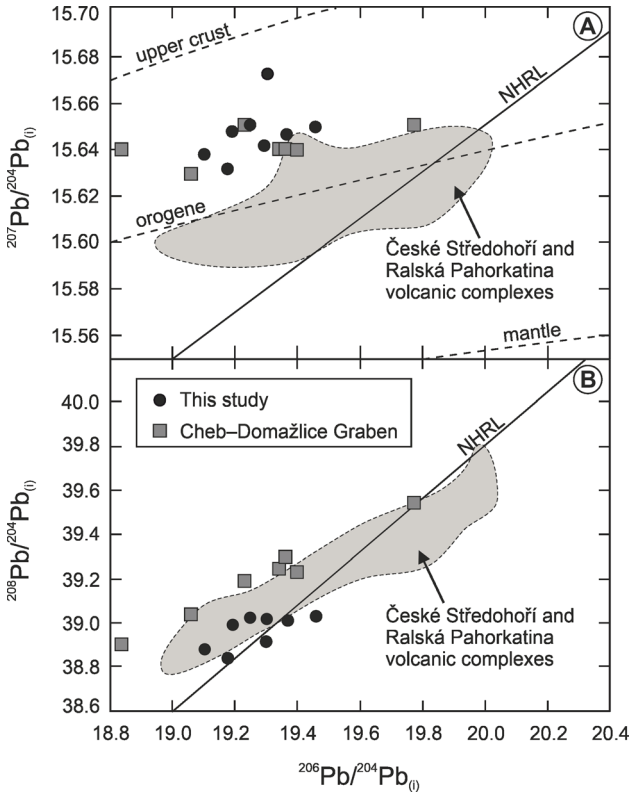

Fig. 12. Initial $^{207}Pb/^{204}Pb$ *vs.* $^{206}Pb/^{204}Pb$ (**A**) and $^{208}Pb/^{204}Pb$ *vs.* $^{206}Pb/^{204}Pb$ (**B**) isotope ratios for rocks of the Uherský Brod area. The rocks plot along two-component mixing trend which crosses the Northern Hemisphere Reference Line (NHRL) of Hart (1984) in the $^{208}Pb/^{204}Pb$ *vs.* $^{206}Pb/^{204}Pb$ diagram. Upper crust, orogenic and mantle growth curves are taken from Zartman & Doe (1981). The values for volcanic rocks of the same age from the Cheb–Domažlice Graben (Ulrych et al. 2016) and for the various volcanic rock in the České Středohoří and Ralská Pahorkatina volcanic complexes in the Bohemian Massif (Krmíčková et al. 2020*)* are plotted for comparison.

metasomatism compared to the subvolcanic rocks from the Pieniny area (Fig. 11). Moreover, the positive values of εNd in all studied rock types and the presence of numerous mafic trachyandesite enclaves with large amphibole phenocrysts (sample UB1B) found in the felsic trachydacite (sample UB1A) from the Bučník laccolith probably reflect magma differentiation within the same magmatic cycle rather than contamination by surrounding crustal material.

The first combined Sr–Nd–Pb isotope study of the UB basaltic–trachytic series has shown that the rocks partly differ from the prevalent isotope signature of Miocene calc-alkaline andesitic rocks from the Carpathian–Pannonian region (e.g., Seghedi et al. 2007) but significantly differ from those of the Pieniny Mountains in Poland having very high $^{207}Pb/^{204}Pb$ ratios and less radiogenic $^{206}Pb/^{204}Pb$ ratios (Fig. 14; Trua et al. 2006). However, the UB samples show a modest similarity to several more primitive calc-alkaline samples from the Central Slovakian volcanic field and from the Pieniny Mts. having lower $^{87}Sr/^{86}Sr$ (~0.705) isotope ratios (Fig. 11; Pin et al. 2004; Trua et al. 2006; Harangi et al. 2007). Despite the certain Sr isotope similarity to the Pieniny area, their Nd isotope composition is diametrically opposed, which is best demonstrated by εNd values yielding +1.8 to +3.3 for UB samples *vs.* −10.1 to −5.4 for Pieniny samples (cf. Pin et al. 2004; Trua et al. 2006), indicating lower Sm/Nd ratios in the source region of the UB subvolcanic rocks. Generally, an important isotope feature of the UB samples is the lack of an isotope component characterised by very high $^{87}Sr/^{86}Sr$ (~0.709) ratios (Fig. 11; Table 5) and $^{207}Pb/^{204}Pb$ (~15.7) values (Fig. 14; Table 5). This component is recognisable in the majority of the mantle-derived rocks in the Carpathian–Pannonian region and reflects the presence of lithospheric mantle metasomatised during the Alpine Orogeny and mixed with melts from the lower crust in the case of andesitic rocks as a consequence of magma stagnation below a thick continental lithosphere (cf. Krmíčková et al. 2020).

On the other hand, Miocene UB subvolcanic rocks isotopically overlap with the Miocene Na-alkaline volcanic rocks

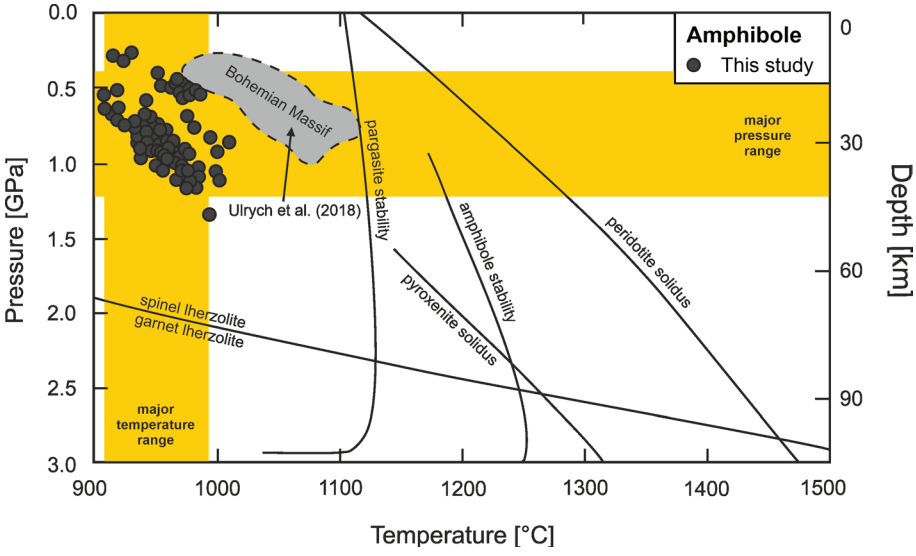

Fig. 13. Pressures and temperatures of amphibole formation of the Miocene volcanic rocks from the Uherský Brod area were calculated using the equations of Pál-Molnár et al. (2015) and Ridolfi & Renzulli (2012), respectively. The orange fields indicate the major temperature and pressure range of the samples. For comparison, P–T estimates of Ulrych et al. (2018) for amphibole are also shown. For peridotite/pyroxenite solidus, spinel/garnet lherzolite and pargasite/amphibole stability fields see Ulrych et al. (2018) and references therein.

from the Carpathian–Pannonian region as well as with the Na-alkaline volcanic rocks from the NE shoulder of the Cheb–Domažlice Graben in the Bohemian Massif, having low $^{87}Sr/^{86}Sr$ ratios, positive εNd values (Fig. 11) and lower $^{207}Pb/^{204}Pb$ ratios at slightly higher $^{206}Pb/^{204}Pb$ ratios (Fig. 14) compared to the majority of calc-alkaline rocks from the Carpathian–Pannonian region. Specific isotope signature of the volcanic rocks from the Cheb–Domažlice Graben is connected to their off-rift position (in relation to ENE–WSW trending Ohře/Eger Rift) and the rocks partly deviate towards elevated $^{207}Pb/^{204}Pb$ values from a Variscan inherited orogenic Pb growth component sampled by various post-collisional mantle-derived melts (e.g., Abdelfadil et al. 2013; Krmíček et al. 2014, 2016; Krmíčková et al. 2020; Fig. 14).

Regional position of the subvolcanic rocks of the Uherský Brod area

The magmatic activity was located in a singular structural setting near the Klippen Belt Zone where the UB and the Pieniny Mts. areas are close to the contact of the Carpathian–Pannonian block with the Bohemian Massif. We agree with Jurewicz & Nejbert (2005) and Nejbert et al. (2012) who considered the generally NW–SE trending structures to act as zones of lithospheric weakness that possibly controlled the emplacement of magmas in the UB and Pieniny areas (cf. Krejčí 1990; Krejčí & Poul 2010; Ulrych et al. 2011; Špaček et al. 2015 for UB case).

Local extension or transtension at the HFZ (Figs. 2, 3) in late-to post-collisional phases may have been promoted by asymmetric loading due to lithospheric bending of the lower (North European) plate and the hypothetical slab break-off. Both the bending and the break-off of the lithosphere could be expected to have migrated eastward along the Carpathian arc around the time of UB magmatism (Middle Miocene), consistent with the eastward advance of the collision zone observed at general scale of the Alpine–Carpathian orogenic system (e.g., Nemcok et al. 1998).

As described by this study and Pécskay et al. (2006), the (sub)volcanic rocks of the Klippen Belt have similar age and chemical compositions to the Na-alkaline volcanic rocks of both the Carpathian–Pannonian region (Harangi 2009; Seghedi & Downes 2011 and Harangi et al. 2015) and the NE shoulder of the Cheb–Domažlice Graben (Ulrych et al. 2016; cf. Fig. 1 and Table 5).

The latter developed during the late-rift episode of the Bohemian Massif – the major Late Miocene rejuvenation of the main Early Eocene to early Mid Miocene magmatic activity (Ulrych et al. 2011). Minor occurrences of Late Miocene volcanics are also found in the České Středohoří Mountains (Cajz et al. 2009)

Table 5: Comparison of geological, petrographical and geochemical characteristics of predominantly Miocene volcanic rocks from the Carpathian–Pannonian region and the Bohemian Massif.

	Carpathian-Pannonian Region					**Bohemian Massif**	
	Outer Western Carpathians		**Inner Carpathians**			**Cheb-Domažlice Graben**	**České Středohoří Mts.**
	Uherský Brod	**Pieniny**	**Calc-alkaline rocks**	**High-K-rich rocks**	**Alkaline rocks**	**Alkaline and calc-alk. rocks**	**Alkaline rocks**
	New data	Pin et al. (2004) Trua et al. (2006)	Embey-Isztin et al. (1993a,b), Harangi & Lenkey (2007), Harangi et al. (2007)			Ulrych et al. (2016)	Cajz et al. (2009)
Age in Ma	14.8–13.4	13.3–10.9	14.0–7.4	15.0–0.06	11.7–0.2	15.5–6.6	13.4–9.6
Geological body	Dykes, sills, laccolith	Dykes, sills	Volcanoes, complexes, effusive/pyroclastic cones	Volcanoes, flows	Volcanoes, maars, scoria–cones, tuff–rings	Volcanoes, flows	Volcanoes, flows
Rock association	Basaltic–trachytic	Andesitic	Basaltic–andesitic	K–andesitic–trachytic	Nephelinitic–basaltic	Basaltic–rhyolitic	Basaltic
Geochemical characteristics							
mg#	63–20	54–21	65–43	67–50	69–52	70–7	71–63
ΣNa_2O+K_2O (wt. %)	3.7–7.9	2.9–6.4	4.1–5.0	7.2–9.5	4.9–9.6	4.1–12.4	3.3–5.7
ΣREE (ppm)	137–287	95–171	42–213	112–402	111–473	158–462	205–872
La_N/Yb_N	12.3–32.9	6.5–14.7	2.2–13.5	8.2–73.6	9.5–30.2	19.9–37.2	19.5–27.8
Eu/Eu	0.91–0.98	0.90–1.20	0.88–0.99	1.01–1.18	1.04	0.88–1.01	0.86–1.06
Nb (ppm)	28–63	4.3–15	4.0–61	12–57	41–147	87–135	73–100
Ta (ppm)	1.3–4.0	0.31–1.45				5.2–9.1	4.4–6.2
Isotope composition							
$^{87}Sr/^{86}Sr_{(i)}$	0.70375–0.70477	0.70529–0.70696	0.70475–0.70734	0.70438–0.70943	0.70322–0.70443	0.70332–0.70471	0.70347–0.70361
$^{143}Nd/^{144}Nd_{(i)}$	0.51270–0.51277	0.51211–0.51238	0.51221–0.51268	0.51228–0.51290	0.51255–0.51278	0.51268–0.51283	0.51279–0.51284
$^{206}Pb/^{204}Pb_{(i)}$	19.02–19.29	18.62–18.82	18.75–18.94	18.78	18.62–19.71	18.84–19.78	
$^{207}Pb/^{204}Pb_{(i)}$	15.63–15.67	15.66–15.75	15.66–15.75	15.68	15.61–15.67	15.56–15.64	
$^{208}Pb/^{204}Pb_{(i)}$	38.99–39.25	38.75–39.88	38.90–39.73	38.89–38.92	38.45–39.46	38.91–39.55	

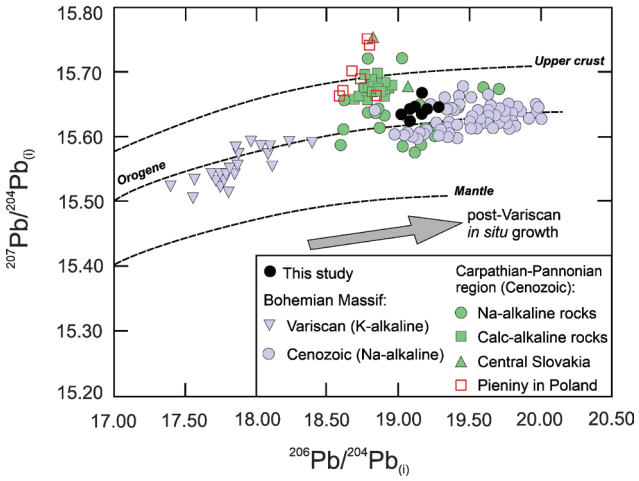

Fig. 14. Initial Pb isotope composition of Variscan and Cenozoic mantle-derived rocks from Eastern Central Europe including the samples from this study and the samples from the Bohemian Massif (Blusztajn & Hart 1989; Haase & Renno 2008; Abdelfadil et al. 2013; Krmíček et al. 2016; Ulrych et al. 2016; Krmíčková et al. 2020), and the Carpathian–Pannonian region (Embey-Isztin et al. 1993a,b; Dobosi et al. 1995; Trua et al. 2006; Harangi & Lenkey 2007; Harangi et al. 2007). The shift from less radiogenic Pb isotope compositions in Variscan rocks to more radiogenic Pb isotope compositions in Cenozoic mantle-derived rocks is shown schematically by an arrow. Upper crust, orogenic and mantle growth curves are taken from Zartman and Doe (1981).

and the Krušné Hory/Erzgebirge Mountains (Ulrych et al. 2010). This renewed anorogenic Late Miocene volcanic activity took place in a compressional tectonic regime and it is likely associated with asthenospheric upwelling controlled by tectonic processes in the Alpine-Carpathian orogenic system. The similarities in both geochemical characteristics and age between the subvolcanic rocks of the UB and the western Bohemian Massif suggest that their magmas may both have been generated by the same heat pulse from the complexly metasomatised mantle lithosphere underlying the Central European Volcanic Province (Ulrych et al. 2011; Dostal et al. 2017; Krmíčková et al. 2020).

Conclusions

The Uherský Brod (UB) Miocene subvolcanic area is associated with local fault reactivation near the Klippen Zone and the NW–SE striking faults associated with the Haná Fault Zone. The compositions of the UB rocks in TAS diagram straddle the line dividing alkaline and subalkaline fields of volcanic rocks, whereas the transitional volcanic rocks from the Central Slovakian volcanic field and andesites from the coeval Pieniny area, located in a similar structural position in Poland, are unambiguously subalkaline. The distribution of incompatible elements, such as U, Th, REE, Nb, Ta, as well as La_N/Yb_N ratios, is different in the UB and Pieniny areas, but similar to the transitional calc-alkaline rocks from the Central Slovakian volcanic field. The moderate contents of these trace elements in andesitic rocks from Pieniny are mostly similar to the prevalent calc-alkaline series of the Carpathian–Pannonian block. The UB rocks are enriched in these elements and partly resemble the Na-alkaline Miocene volcanic rock series of the NE shoulder of the Cheb–Domažlice Graben in western Bohemia in the Bohemian Massif.

The Sr–Nd–Pb isotope signatures of the UB basaltic–trachytic series mirror the isotope variations in their source rocks, represented by metasomatised lithosphere with amphibole-bearing clinopyroxenite veins (e.g., Bailey 1982; Powell et al. 2004; Harangi et al. 2015). The UB rocks lack an isotope component characterised by high $^{207}Pb/^{204}Pb$ (~15.7) values typical of the majority of the calc-alkaline mantle-derived rocks in the Carpathian–Pannonian region including those from the Pieniny area in Poland. Their Sr isotope signature also does not reach such high values up to 0.709 as most of the Carpathian–Pannonian calc-alkaline rocks. Although the $^{87}Sr/^{86}Sr$ ratios of the UB samples fluctuating around 0.704 partly resemble those of the Pieniny area, their Nd isotope composition completely differs. The isotope signature of the UB subvolcanic rocks is more similar to the Na-alkaline off-rift volcanic rocks from the Cheb–Domažlice Graben as well as to several more primitive (transitional) calc-alkaline and Na-alkaline rocks from the Carpathian–Pannonian region.

The UB basaltic–trachytic series was generated by melting of the variably metasomatised sub-lithospheric source and subsequent fractional crystallisation of the primary basaltic magma. Partial melting of the metasomatised lithospheric mantle may have been initiated by interaction with ascending sub-lithospheric melts. Such melts would exploit zones of weakness created by the juxtaposition of rocks of different competence, as is seen in the Klippen Zone. Crustal faulting would have the potential to create localised low pressure towards which rising melts would be drawn (*sensu* Bailey, 1977). Model P–T estimates of amphibole crystallisation in the parental rocks (~910–990 °C at ~0.4–1.2 GPa) correspond to ~15–45 km, suggesting a greater depth of the magma generation and subsequent progressive crystallisation of amphibole during the magma ascent.

Acknowledgements: This research was financially supported by the institutional project RVO 67985831 of the Institute of Geology of the Czech Academy of Sciences, as well as by the EXPRO 2019 project of the Czech Science Foundation [19-29124X]. Contributions of P. Špaček were supported by project CzechGeo/EPOS-Sci (CZ.02.1.01/0.0/0.0/16_013/0001800), funded from the OP RDE ERDF. We thank Jiří Adamovič (Prague) for careful reading of an early version of the manuscript and Ray Macdonald (Lancaster) and Felicity E. Lloyd (Bristol) for brilliant final assessment. The authors thank Lukáš Ackerman, Eva Vosáhlová and Jan Rejšek for their kind help with Sr–Nd–Pb separation and TIMS measurement. The authors greatly appreciate Jaroslav Dostal, Ioan Seghedi and Ján Spišiak for their very constructive and helpful comments and suggestions.

References

Abdelfadil K.M., Romer R.L., Seifert T. & Lobst R. 2013: Calc-alkaline lamprophyres from Lusatia (Germany) – Evidence for a repeatedly enriched mantle source. *Chemical Geology* 353, 230–245. https://doi.org/10.1016/j.chemgeo.2012.10.023

Anczkiewicz A.A. & Anczkiewicz K. 2016: U–Pb zircon geochronology and anomalous Sr–Nd–Hf isotope systematics of late orogenic andesites: Pieniny Klippen Belt, Western Carpathians, South Poland. *Chemical Geology* 427, 1–16. https://doi.org/10.1016/j.chemgeo.2016.02.004

Arndt N.T. & Christensen U. 1992: The role of lithospheric mantle in continental flood volcanism: thermal and geochemical constraints. *Journal of Geophysical Research: Solid Earth* 97, 10967–10981. https://doi.org/10.1029/92JB00564

Bailey D.K. 1977: Lithosphere control of continental rift magmatism. *Journal of the Geological Society* 133, 103–106. https://doi.org/10.1144/gsjgs.133.1.0103

Bailey D.K. 1982: Mantle metasomatism – continuing chemical change within the Earth. *Nature* 296, 525–530. https://doi.org/10.1038/296525a0

Birkenmajer K. & Pécskay Z. 2000: K–Ar dating of the Miocene andesite intrusions, Pieniny Mts, West Carpathians, Poland: a supplement. *Studia Geologica Polonica* 117, 7–25.

Blusztajn J. & Hart S.R. 1989: Sr, Nd and Pb isotopic character of Tertiary basalts from southwest Poland. *Geochimica Cosmochimica Acta* 53, 2689–2696. https://doi.org/10.1016/0016-7037(89)90140-3

Bouvier A., Vervoort J.D. & Patchett P.J. 2008: The Lu–Hf and Sm–Nd isotopic composition of CHUR: constraints from unequilibrated chondrites and implications for the bulk composition of terrestrial planets. *Earth and Planetary Science Letters* 273, 48–57. https://doi.org/10.1016/j.epsl.2008.06.010

Boynton W.V. 1984: Cosmochemistry of the rare earth elements: meteorite studies. In: Henderson P. (Ed.): Rare Earth Element Geochemistry. *Elsevier*, Amsterdam, 63–114. https://doi.org/10.1016/B978-0-444-42148-7.50008-3

Cajz V., Rapprich V., Erban V. Pécskay, Z. & Radoň M. 2009: Late Miocene volcanic activity in the České středohoří Mountains (Ohře/Eger Graben, northern Bohemia). *Geologica Carpathica* 60, 519–533. https://doi.org/10.2478/v10096-009-0038-8

Dobosi G., Fodor R.V. & Goldberg S.A. 1995: Late-Cenozoic alkali basalt magmatism in Northern Hungary and Slovakia: Petrology, source compositions and relationship to tectonics. *Acta Vulcanologica* 7, 199–207.

Dostal J., Murphy J.B. & Shellnutt J.G. 2019: Secular isotopic variation in lithospheric mantle through the Variscan orogen: Neoproterozoic to Cenozoic magmatism in continental Europe. *Geology* 47, 637–640. https://doi.org/10.1130/G46067.1

Dostal J., Shellnutt J.G. & Ulrych J. 2017: Petrogenesis of the Cenozoic alkaline volcanic rock series of the České Středohoří Complex (Bohemian Massif), Czech Republic: A case for two lineages. *American Journal of Science* 317, 677–706. https://doi.org/10.2475/06.2017.02

Downes M.J. 1974: Sector and oscillatory zoning in calcic augites from M. Etna, Sicily. *Contributions to Mineralogy and Petrology* 47, 187–196. https://doi.org/10.1007/BF00371538

Embey-Isztin A., Dobosi G., James D., Downes H., Poultidis C. & Scharbert H.G. 1993a: A compilation of new major, trace element and isotope geochemical analyses of the young alkali basalts from the Pannonian Basin. *Fragmenta Geologica et Petrographica* 16, 5–26.

Embey-Isztin A., Downes H., James D.E., Upton B.G.J., Dobosi G., Ingram G.A., Harmon R.S. & Scharbert H.G. 1993b: The petrogenesis of Pliocene alkaline volcanic rocks from the Pannonian Basin, Eastern Central Europe. *Journal of Petrology* 34, 317–343. https://doi.org/10.1093/petrology/34.2.317

Fediuk F. & Gürtlerová P. 2006: Adakitic trends in andesitic volcanics of SE-Moravia. *Bulletin mineralogicko-petrologického oddělení Národního muzea v Praze* 13, 121–124 (in Czech).

Fojt B. & Přichystal A. 1979: Sphalerite and carbonate from ore veins in propylitised andesite from Komňa (Southeast Moravia). *Scripta facultatis scientiarum naturalium Universitatis Purkynianae Brunensis: Geologia* 1, 17–28 (in Czech).

Froitzheim N., Plašienka D. & Schuster R. 2008: Alpine tectonics of the Alps and Western Carpathians. In: McCann T. (Ed.): The Geology of Central Europe. Vol. 2: Mesozoic and Cenozoic. *Geological Society Publishing House*, London, 1141–1232. https://doi.org/10.1144/CEV2P.6

Green D.H., Hibberson W.O., Kovacs I. & Rosenthal A. 2010: Water and its influence on the lithosphere–asthenosphere boundary. *Nature* 467, 448–451. https://doi.org/10.1038/nature09369

Haase K.M. & Renno A.D. 2008: Variation of magma generation and mantle sources during continental rifting observed in Cenozoic lavas from the Eger Rift, Central Europe. *Chemical Geology* 257, 195–205. https://doi.org/10.1016/j.chemgeo.2008.09.003

Harangi S. 2009: Volcanism of the Carpathian–Pannonian region, Europe: The role of subduction, extension and mantle plumes. http://www.mantleplumes.org/CarpathianPannonian.html

Harangi S. & Lenkey L. 2007: Genesis of the Neogene to Quaternary volcanism in the Carpathian–Pannonian region: Role of subduction, extension, and mantle plume. *Geological Society of America Special Papers* 418, 67–92. https://doi.org/10.1130/2007.2418(04)

Harangi S., Downes H, Thirlwall M. & Gmeling, K. 2007: Geochemistry, petrogenesis and geodynamic relationships of Miocene calc-alkaline volcanic rocks in the Western Carpathian Arc, Eastern Central Europe. *Journal of Petrology* 48, 2261–2287. https://doi.org/10.1093/petrology/egm059

Harangi S., Jankovics M.É., Sági T., Kiss B., Lukács R. & Soós I. 2015: Origin and geodynamic relationships of the Late Miocene to Quaternary alkaline basalt volcanism in the Pannonian basin, eastern–central Europe. *International Journal of Earth Sciences* 104, 2007–2032. https://doi.org/10.1007/s00531-014-1105-7

Hart S.R. 1984: A large-scale isotope anomaly in the Southern Hemisphere mantle. *Nature* 309, 753–757. https://doi.org/10.1038/309753a0

Hrouda F., Buriánek D., Krejčí O. & Chadima M. 2015: Magnetic fabric and petrology of Miocene sub-volcanic sills and dykes emplaced into the SW Flysh Belt of the Western Carpathians (S Moravia, Czech Republic) and their volcanological and tectonic implications. *Journal of Volcanology and Geothermal Research* 290, 23–38. https://doi.org/10.1016/j.jvolgeores.2014.12.001

Hrubcová P. & Środa P. 2015: Complex local Moho topography in the Western Carpathians: Indication of the ALCAPA and the European Plate contact. *Tectonophysics* 638, 63–81. https://doi.org/10.1016/j.tecto.2014.10.013

Jochum K.P. & Nohl U. 2008: Reference materials in geochemistry and environmental research and the GeoReM database. *Chemical Geology* 253, 50–53. https://doi.org/10.1016/j.chemgeo.2008.04.002

Jurewicz E. & Nejbert K. 2005: Geotectonic position of the so-called "Pieniny Mts. andesites". *Mineralogical Society of Poland – Special Papers* 25, 179–183.

Konečný V., Kováč M., Lexa J. & Šefara J. 2002: Neogene evolution of the Carpatho-Pannonian region: an interplay of subduction and back-arc diapiric uprise in the mantle. *EGU Stephan Mueller Special Publication Series* 1, 165–194.

Krejčí O. 1990: Basic geological map 1:25 000 sheet 35–112 Bánov, Explanatory text to the map. *Czech Geological Survey*, Prague (in Czech).

Krejčí O. & Poul I. 2010: Evidence of Middle Miocene thrust tectonics in the Bílé Karpaty Unit (Carpathian Flysh Belt). *Geological Research in Moravia and Silesia* 17, 58–63 (in Czech).

Krmíček L., Halavínová M., Romer R.L., Vašinová Galiová M. & Vaculovič T. 2014: Phlogopite/matrix, clinopyroxene/matrix and clinopyroxene/phlogopite trace-element partitioning in a calc-alkaline lamprophyre: new constrains from the Křižanovice minette dyke (Bohemian Massif). *Journal of Geosciences* 59, 87–96. https://doi.org/10.3190/jgeosci.160

Krmíček L., Romer R.L., Ulrych J., Glodny J. & Prelević D. 2016: Petrogenesis of orogenic lamproites of the Bohemian Massif: Sr–Nd–Pb–Li isotope constraints for Variscan enrichment of ultra-depleted mantle domains. *Gondwana Research* 35, 198–216. https://doi.org/10.1016/j.gr.2015.04.012

Krmíček L., Ackerman L., Hrubý J. & Kynický J. 2020: The highly siderophile elements and Re–Os isotope geochemistry of Variscan lamproites from the Bohemian Massif: implications for regionally dependent metasomatism of orogenic mantle. *Chemical Geology* 532, 119290. https://doi.org/10.1016/j.chemgeo.2019.119290

Krmíčková S., Krmíček L., Romer R.L. & Ulrych J. 2020: Lead isotope evolution of the Central European upper mantle: constraints from the Bohemian Massif. *Geoscience Frontiers* 11, 925–942. https://doi.org/10.1016/j.gsf.2019.09.009

Le Maitre R.W. 2002: Igneous Rocks. A Classification and Glossary of Terms. *Cambridge University Press*, Cambridge, 1–236. https://doi.org/10.1017/CBO9780511535581

Leake B.E. et al. 1997: Nomenclature of amphiboles: Report of the subcommittee on amphiboles of the international association, commission on new minerals and mineral names. *American Mineralogist* 82, 1019–1037.

Lenhardt W., Švancara J., Melichar P., Pazdírková J., Havíř J. & Sýkorová Z. 2007: Seismic activity of the Alpine–Carpathian–Bohemian Massif region with regard to geological and potential field data. *Geologica Carpathica* 58, 397–412.

Lexa J. & Konečný V. 1998: Geodynamic aspects of the Neogene to Quaternary volcanism. In: Rakús M. (Ed.): Geodynamic development of the Western Carpathians. *Geological Survey of Slovak Republic*, Bratislava, 219–240.

Lexa J., Seghedi I., Németh K., Szakács A., Konečný V., Pécskay Z., Fülöp A. & Kovacs M. 2010: Neogene–Quaternary Volcanic forms in the Carpathian–Pannonian Region: a review. *Central European Journal of Geosciences* 2, 207–270. https://doi.org/10.2478/v10085-010-0024-5

Lustrino M. & Wilson M. 2007: The circum-Mediterranean anorogenic Cenozoic igneous province. *Earth-Science Reviews* 81, 1–65. https://doi.org/10.1016/j.earscirev.2006.09.002

Macdonald R., Nejbert K., Baginski B. & Jurewicz E. 2018: Ti–Zr–Nb-bearing accessory minerals in high-K trachyandesitic rocks from the Western Outer Carpathians, Moravia, Czech Republic. *European Journal of Mineralogy* 30, 138–147. https://doi.org/10.1127/ejm/2017/0029-2693

Majcin D., Bilčík D. & Klučiar T. 2015: Thermal state of the lithosphere in the Danube Basin and its relation to tectonics. *Contributions to Geophysics and Geodesy* 45, 193–218. https://doi.org/10.1515/congeo-2015-0020

McDonough W.F. & Sun S. 1995: The composition of the Earth. *Chemical Geology* 120, 223–253. https://doi.org/10.1016/0009-2541(94)00140-4

Merlet C. 1992: Quantitative electron probe microanalysis: new accurate Φ (ρz) description. *Microchimica Acta* 12, 107–115. https://doi.org/10.1007/978-3-7091-6679-6_8

Morimoto N., Fabries J., Ferguson A.K., Ginzburg I.V., Ross M., Seifert F.A., Zussman L., Aoki K. & Gottardi G. 1988: Nomenclature of pyroxenes. *Mineralogy and Petrology* 39, 201–211. https://doi.org/10.1007/BF01226262

Mason P.R.D., Downes H., Thirlwall M.F., Seghedi I., Szakács A., Lowry D., Mattey D. 1996: Crustal assimilation as a major petrogenetic process in east Carpathian Neogene to Quaternary continental margin arc magmas. *Journal of Petrology* 37, 927–959. https://doi.org/10.1093/petrology/37.4.927

Mutch E.J.F., Blundy J.D., Tattich B.C., Cooper F.J. & Brooker R.A. 2016: An experimental study of amphibole stability in low-pressure granitic magmas and a revised Al-in-hornblende geobarometer. *Contributions to Mineralogy and Petrology* 171, 85. https://doi.org/10.1007/s00410-016-1298-9

Nejbert K., Jurewicz E. & Macdonald R. 2012: Potassium-rich magmatism in the Western Outer Carpathians: Magmagenesis in the transitional zone between the European Plate and Carpathian–Pannonian region. *Lithos* 146–147, 34–42. https://doi.org/10.1016/j.lithos.2012.04.026

Nelson S.T. & Montana A. 1992: Sieve-textured plagioclase in volcanic rocks produced by rapid decompression. *American Mineralogist* 77, 1242–1249.

Nemcok M., Pospisil L., Lexa J. & Donelick R.A. 1998: Tertiary subduction and slab break-off model of the Carpathian–Pannonian. *Tectonophysics* 295, 307–340. https://doi.org/10.1016/S0040-1951(98)00092-4

Pál-Molnár E., Batki A., Almasi E., Kiss B., Upton B.G.J., Markl G., Odling N. & Harangi S. 2015: Origin of mafic and ultramafic cumulates from the Ditrău Massif, Romania. *Lithos* 239, 1–18. https://doi.org/10.1016/j.lithos.2015.09.022

Peccerillo A. & Taylor S.R. 1976: Geochemistry of Eocene calc-alkaline volcanic rocks from the Kastamonu area, northern Turkey. *Contributions to Mineralogy and Petrology* 58, 63–81. https://doi.org/10.1007/BF00384745

Pécskay Z., Konečný V., Lexa J., Přichystal A. 2002: K/Ar dating of Neogene volcanic rocks in surrounding of Uherský Brod, Moravia. In: Ulrych J., Cajz V., Adamovič J. & Bosák P. (Eds.): Hibsch 2002 Symposium. Excursion Guide and Abstracts. *Czech Geological Survey*, Prague, 100.

Pécskay Z., Lexa J., Szakács A., Seghedi I., Balogh K., Konečný V., Márton E., Kovacs M., Poka T., Fülöp A. & Márton E. 2006: Geochronology of Neogene magmatism in the Carpathian arc and intra-Carpathian area. *Geologica Carpathica* 57, 511–530.

Pilet S., Ulmer P. & Villiger S. 2010: Liquid line of descent of a basanitic liquid at 1.5 GPa: constraints on the formation of metasomatic veins. *Contributions to Mineralogy and Petrology* 159, 621–643. https://doi.org/10.1007/s00410-009-0445-y

Pin C., Bouvier A. & Aleksandrowski P. 2004: Major trace element and Sr–Nd isotope data on Neogene andesitic rocks from the Pieniny Klippen Belt (southern Poland) and geodynamic inferences. *Mineralogical Society of Poland – Special Papers* 24, 323–328.

Pin C., Gannoun A. & Dupont A. 2014: Rapid, simultaneous separation of Sr, Pb, and Nd by extraction chromatography prior to isotope ratios determination by TIMS and MC-ICP-MS. *Journal of Analytical Atomic Spectrometry* 29, 1858–1870. https://doi.org/10.1039/C4JA00169A

Powell W., Zhang M., O'Reilly S. & Tiepolo M. 2004: Mantle amphibole trace-element and isotopic signatures trace multiple metasomatic episodes in lithospheric mantle, western Victoria, Australia. *Lithos* 75, 141–171. https://doi.org/10.1016/j.lithos.2003.12.017

Praus O., Pěčová J., Petr V., Babuška V. & Plomerová J. 1990: Magnetotelluric and seismological determination of lithosphere-asthenosphere transition in central Europe, *Physics of the Earth and Planetary Interiors* 60, 212–228. https://doi.org/10.1016/0031-9201(90)90262-V

Přichystal A., Repčok I. & Krejčí O. 1998: Radiometric dating of trachyandesites from Uherský Brod (Magurian section of the flysch zone). *Geological Research in Moravia and Silesia* 4, 33–34 (in Czech).

Ridolfi F. & Renzulli A. 2012: Calcic amphiboles in calc-alkaline and alkaline magmas: thermobarometric and chemometric empirical equations valid up to 1,130 °C and 2.2 GPa. *Contributions to Mineralogy and Petrology* 163, 877–895. https://doi.org/10.1007/s00410-011-0704-6

Rudnick R.L. & Gao S. 2003: Composition of the continental crust. In: Rudnick R.L. (Ed.): Treatise on Geochemisty, Vol. 3, The Crust. *Elsevier*, Oxford, 1–64. https://doi.org/10.1016/B0-08-043751-6/03016-4

Seghedi I. & Downes H. 2011: Geochemistry and tectonic development of Cenozoic magmatism in the Carpathian–Pannonian region. *Gondwana Research* 20, 655–672. https://doi.org/10.1016/j.gr.2011.06.009

Seghedi I., Downes H., Szakacs A., Mason P.R.D., Thirlwall M.F., Rosu E., Pécskay Z., Marton E. & Panaiotu C. 2004a: Neogene–Quaternary magmatism and geodynamics in the Carpathian–Pannonian region: a synthesis. *Lithos* 72, 117–146. https://doi.org/10.1016/j.lithos.2003.08.006

Seghedi I., Downes H., Vaselli O., Szakacs A., Balogh K. & Pécskay Z. 2004b: Post-collisional Tertiary-Quaternary mafic alkalic magmatism in the Carpathian–Pannonian region: a review. *Tectonophysics* 393, 43–62. https://doi.org/10.1016/j.tecto.2004.07.051

Seghedi I., Downes H., Harangi S., Mason P.R.D., Pécskay Z. 2005: Geochemical response of magmas to Neogene–Quaternary continental collision in the Carpathian–Pannonian region: A review. *Tectonophysics* 410, 485–499. https://doi.org/10.1016/j.tecto.2004.09.015

Seghedi I., Ersoy Y.E. & Helvacı C. 2013: Miocene–Quaternary volcanism and geodynamic evolution in the Pannonian Basin and the Menderes Massif: A comparative study. *Lithos* 180, 25–42. https://doi.org/10.1016/j.lithos.2013.08.017

Shrbený O. 1974: The petrochemical relations of the south-Moravian neovolcanic rocks to the neighbouring volcanic area. *Bulletin of the Czech Geological Survey* 49, 275–279.

Špaček P., Bábek O., Štěpančíková P., Švancara J., Pazdírková J. & Sedláček J. 2015: The Nysa-Morava Zone: an active tectonic domain with Late Cenozoic sedimentary grabens in the Western Carpathians' foreland (NE Bohemian Massif). *International Journal of Earth Sciences* 104, 963–990. https://doi.org/10.1007/s00531-014-1121-7

Špaček P., Valenta J., Tábořík P., Ambrož V., Urban M. & Štěpančíková P. 2017: Fault slip versus slope deformations: Experience from paleoseismic trenches in the region with low slip-rate faults and strong Pleistocene periglacial mass wasting (Bohemian Massif). *Quaternary International* 451, 56–73. https://doi.org/10.1016/j.quaint.2017.05.006

Streck M.J. 2008: Mineral textures and zoning as evidence for open system processes. *Reviews in Mineralogy and Geochemistry* 69, 595–622.

Sýkorová Z., Pazdírková J., Zacherle P., Vlach R. & Špaček P. 2018: Catalog of natural earthquakes in the NE Czech Republic IPE-MONET, release 2018. https://www.researchgate.net/publication/323906777_IPE-MONET_EARTHQUAKE_CATALOG. Accessed 1.3.2019

Todt W., Cliff R.A., Hanser A. & Hofmann A.W. 1996: Evaluation of a ^{202}Pb – ^{205}Pb double spike for high-precision lead isotope analysis. *Earth Processes: Reading the Isotopic Code* 95, 429–437. https://doi.org/10.1029/GM095p0429

Trua T., Serri G., Birkenmajer K. & Pécskay Z. 2006: Geochemical and Sr–Nd–Pb isotopic compositions of Mts Pieniny dykes and sills (West Carpathians): Evidence for melting in the lithospheric mantle. *Lithos* 90, 57–76. https://doi.org/10.1016/j.lithos.2006.01.001

Ulrych J., Pešek J., Štěpánková-Svobodová J., Bosák P., Lloyd F.E., von Seckendorff V., Lang M. & Novák J.K. 2006: Permo–Carboniferous volcanism in late Variscan continental basins of the Bohemian Massif (Czech Republic): geochemical characteristic. *Chemie der Erde – Geochemistry* 66, 37–56. https://doi.org/10.1016/j.chemer.2004.02.001

Ulrych J., Dostal J., Hegner E., Balogh K. & Ackerman L. 2008: Late Cretaceous to Paleocene melilitic rocks of the Ohře/Eger Rift in northern Bohemia, Czech Republic: insights into the initial stages of continental rifting. *Lithos* 101, 141–161. https://doi.org/10.1016/j.lithos.2007.07.012

Ulrych J., Jelínek E., Řanda Z., Lloyd F.E., Balogh K., Hegner E. & Novák J.K. 2010: Geochemical characteristics of the high- and low-Ti basaltic rocks from the uplifted shoulder of the Ohře (Eger) Rift, Western Bohemia. *Chemie der Erde – Geochemistry* 70, 319–333. https://doi.org/10.1016/j.chemer.2010.05.001

Ulrych J., Dostal J., Adamovič J., Jelínek E., Špaček P., Hegner E. & Balogh K. 2011: Recurrent Cenozoic volcanic activity in the Bohemian Massif (Czech Republic). *Lithos* 123, 133–144. https://doi.org/10.1016/j.lithos.2010.12.008

Ulrych J., Ackerman L., Balogh K., Hegner E., Jelínek E., Pécskay Z., Přichystal A., Upton B.G.J., Zimák J. & Foltýnová R. 2013: Plio-Pleistocene basanitic and melilititic series of the Bohemian Massif: K–Ar ages, major/trace element and Sr–Nd isotopic data. *Chemie der Erde – Geochemistry* 73, 429–450. https://doi.org/10.1016/j.chemer.2013.02.001

Ulrych J., Krmíček L., Tomek Č., Lloyd F.E., Ladenberger A., Ackerman L. & Balogh K. 2016: Petrogenesis of Miocene alkaline volcanic suites from western Bohemia: whole rock geochemistry and Sr–Nd–Pb isotopic signatures. *Chemie der Erde – Geochemistry* 76, 77–93. https://doi.org/10.1016/j.chemer.2015.11.003

Ulrych J., Krmíček L., Teschner C., Řanda Z., Skála R., Jonášová Š., Fediuk F., Adamovič J. & Pokorný R. 2017: Tachylyte in Cenozoic basaltic lavas from the Czech Republic and Iceland: contrasting compositional trends. *Mineralogy and Petrology* 111, 761–775. https://doi.org/10.1007/s00710-016-0483-x

Ulrych J., Krmíček L., Teschner C., Skála R., Adamovič J., Ďurišová J., Křížová Š., Kubošková S. & Radoň M. 2018: Chemistry and Sr–Nd isotope signature of amphiboles of the magnesio-hastingsite–pargasite–kaersutite series in Cenozoic volcanic rocks: Insight into lithospheric mantle beneath the Bohemian Massif. *Lithos* 312–113, 308–321. https://doi.org/10.1016/j.lithos.2018.05.017

Whitney D.L. & Evans B.W. 2010: Abbreviations for names of rock-forming minerals. *American Mineralogist* 95, 185–187. https://doi.org/10.2138/am.2010.3371

Wilson M. & Downes H. 1991: Tertiary–Quaternary extension-related alkaline magmatism in western and central Europe. *Journal of Petrology* 32, 811–849. https://doi.org/10.1093/petrology/32.4.811

Zartman R.E. & Doe B.R. 1981: Plumbotectonics – the model. *Tectonophysics* 75, 135–162. https://doi.org/10.1016/0040-1951(81)90213-4

Supplement A

Table S1: Representative compositions of amphibole.

Sample	**UB1A**	**UB1A**	**UB1A**	**UB1A**	**UB1A**	**UB1A**	**UB1A**	**UB1A**	**UB1A**	**UB1A**	**UB1A**	**UB1A**	**UB1A**
Petrographic type	**TD**	**TD**	**TD**	**TD**	**TD**	**TD**	**TD**	**TD**	**TD**	**TD**	**TD**	**TD**	**TD**
SiO_2	41.8	42.1	41.5	42.4	42.0	42.7	41.6	41.3	41.9	41.5	42.2	42.3	44.3
TiO_2	2.69	3.20	3.15	2.60	3.79	2.99	2.95	3.71	2.73	3.15	2.89	2.96	2.20
Al_2O_3	11.8	11.3	11.7	11.8	11.8	10.4	12.6	11.7	11.8	11.5	12.0	11.5	10.5
MgO	14.0	12.6	12.4	14.2	12.5	13.2	12.9	12.1	12.8	12.2	13.3	12.3	15.1
CaO	11.6	11.1	11.0	11.6	11.4	11.2	11.2	11.1	11.4	11.1	11.6	11.1	11.5
MnO	0.19	0.16	0.21	0.20	0.15	0.17	0.13	0.17	0.22	0.26	0.21	0.26	0.12
FeO	11.2	14.1	13.7	11.4	13.5	12.4	12.2	13.6	13.2	14.4	12.2	14.4	10.2
BaO	<BDL	<BDL	0.05	<BDL	<BDL	<BDL	0.04	0.04	<BDL	0.09	0.05	<BDL	0.04
Na_2O	2.63	2.71	2.73	2.52	2.82	2.50	2.66	2.62	2.81	2.51	2.62	2.64	2.43
K_2O	0.93	0.87	0.78	0.88	0.85	0.80	0.77	0.87	0.90	0.81	0.73	0.91	0.79
H_2O	2.03	2.04	2.02	2.06	2.05	2.02	2.03	2.02	2.03	2.03	2.05	2.04	2.07
Total	99.0	100.3	99.5	99.7	100.9	98.5	99.2	99.4	99.9	99.5	100.0	100.4	99.4
Empirical formula (*apfu*)													
Si	6.16	6.18	6.14	6.18	6.15	6.35	6.14	6.14	6.17	6.15	6.19	6.20	6.43
Al^{IV}	1.84	1.82	1.86	1.82	1.85	1.65	1.86	1.86	1.83	1.85	1.81	1.80	1.57
ΣT	8.00	8.00	8.00	8.00	8.00	8.00	8.00	8.00	8.00	8.00	8.00	8.00	8.00
Ti	0.30	0.35	0.35	0.29	0.42	0.33	0.33	0.41	0.30	0.35	0.32	0.33	0.24
Al	2.05	1.96	2.04	2.03	2.03	1.83	2.18	2.05	2.05	2.00	2.06	1.99	1.80
Al^{VI}	0.21	0.14	0.18	0.22	0.18	0.18	0.32	0.19	0.22	0.15	0.25	0.19	0.23
Fe^{tot}	1.39	1.73	1.70	1.39	1.65	1.54	1.50	1.69	1.63	1.78	1.49	1.77	1.24
Fe^{3+}	0.43	0.56	0.54	0.53	0.32	0.36	0.15	0.09	0.45	0.60	0.42	0.55	0.44
Mg	3.09	2.76	2.74	3.08	2.73	2.93	2.83	2.68	2.82	2.68	2.91	2.68	3.27
Ca	1.84	1.74	1.75	1.81	1.78	1.79	1.78	1.76	1.80	1.76	1.81	1.75	1.79
Mn	0.02	0.02	0.03	0.02	0.02	0.02	0.02	0.02	0.03	0.03	0.03	0.03	0.01
Fe^{2+}	0.96	1.17	1.16	0.86	1.33	1.18	1.36	1.61	1.18	1.18	1.08	1.23	0.80
Ba	0.00	0.00	0.00	0.00	0.00	0.00	0.00	0.00	0.00	0.01	0.00	0.00	0.00
Na	0.75	0.77	0.78	0.71	0.80	0.72	0.76	0.76	0.80	0.72	0.74	0.75	0.68
K	0.18	0.16	0.15	0.16	0.16	0.15	0.14	0.16	0.17	0.15	0.14	0.17	0.15
OH	2.00	2.00	2.00	2.00	2.00	2.00	2.00	2.00	2.00	2.00	2.00	2.00	2.00
O	22.8	22.7	22.7	22.7	22.8	22.8	22.8	22.8	22.8	22.7	22.8	22.7	22.8
$Mg/(Mg+Fe^{2+})$	0.76	0.70	0.70	0.78	0.67	0.71	0.68	0.63	0.70	0.69	0.73	0.69	0.80
Species	M	M	M	M	M	M	P	P	M	M	M	M	M

Empirical formula is calculated on the basis of T+C=13.

Petrographic type: TD — trachydacite; BTA — basaltic trachyandesite; BA — basalt; TB — trachybasalt; TA — trachyandesite; BAA — basaltic andesite

Species: M - magnesiohastingsite; P - pargasite

BDL: below detection limit

apfu: atoms per formula unit

Table S1 (continued): Representative compositions of amphibole.

Sample	**UB1A**	**UB1A**	**UB1A**	**UB1B**	**UB1B**	**UB1B**	**UB1B**	**UB1B**	**UB1B**	**UB1B**	**UB1B**	**UB1B**	**UB1B**
Petrographic type	**TD**	**TD**	**TD**	**BTA**	**BTA**	**BTA**	**BTA**	**BTA**	**BTA**	**BTA**	**BTA**	**BTA**	**BTA**
SiO_2	41.8	39.9	41.1	39.9	40.0	40.6	40.1	39.8	40.0	40.5	39.8	40.3	40.2
TiO_2	2.82	3.14	2.90	2.98	3.16	3.19	2.39	2.78	2.84	2.92	2.80	2.97	2.95
Al_2O_3	11.5	13.5	13.8	13.9	13.7	13.0	13.2	12.9	13.5	13.6	14.2	12.9	13.8
MgO	12.9	14.0	15.7	12.9	12.0	12.1	11.9	11.0	11.4	11.8	12.9	11.8	12.8
CaO	11.1	11.8	12.2	12.1	11.8	11.8	11.8	11.8	11.6	11.9	12.3	11.8	12.1
MnO	0.28	0.13	<BDL	0.13	0.17	0.13	0.22	0.27	0.24	0.19	0.15	0.18	0.13
FeO	13.5	10.1	7.39	11.3	12.8	12.8	13.3	14.6	14.1	13.6	10.7	13.4	11.1
BaO	<BDL	<BDL	<BDL	<BDL	0.06	<BDL	<BDL	<BDL	<BDL	<BDL	<BDL	<BDL	<BDL
Na_2O	2.29	2.47	2.55	2.57	2.38	2.65	2.60	2.58	2.50	2.82	2.36	2.50	2.44
K_2O	0.88	1.05	1.24	1.10	1.18	1.12	1.12	1.12	1.10	1.09	1.22	1.08	1.08
H_2O	2.04	2.02	2.05	2.01	2.01	2.00	1.99	1.98	2.00	2.02	2.00	1.99	2.01
Total	99.4	98.4	99.1	98.9	99.4	99.3	98.7	98.9	99.5	100.6	98.7	98.9	98.8
Empirical formula (*apfu*)													
Si	6.15	5.92	6.00	5.95	5.96	6.07	6.04	6.05	5.98	6.00	5.96	6.06	6.00
Al^{IV}	1.85	2.08	2.00	2.05	2.04	1.93	1.96	1.95	2.02	2.00	2.04	1.94	2.00
ΣT	8.00	8.00	8.00	8.00	8.00	8.00	8.00	8.00	8.00	8.00	8.00	8.00	8.00
Ti	0.31	0.35	0.32	0.33	0.35	0.36	0.27	0.32	0.32	0.32	0.31	0.34	0.33
Al	2.00	2.36	2.37	2.44	2.41	2.28	2.34	2.30	2.38	2.38	2.51	2.29	2.42
Al^{VI}	0.15	0.28	0.37	0.39	0.37	0.35	0.37	0.34	0.36	0.38	0.47	0.34	0.42
Fe^{tot}	1.66	1.26	0.90	1.41	1.59	1.60	1.68	1.85	1.76	1.68	1.34	1.68	1.39
Fe^{3+}	0.74	0.45	0.23	0.18	0.25	0.11	0.04	0.00	0.35	0.00	0.00	0.18	0.12
Mg	2.84	3.10	3.41	2.87	2.68	2.69	2.68	2.49	2.55	2.62	2.87	2.64	2.86
Ca	1.76	1.87	1.91	1.93	1.89	1.89	1.90	1.91	1.86	1.89	1.98	1.91	1.94
Mn	0.03	0.02	0.00	0.00	0.00	0.00	0.00	0.00	0.00	0.00	0.00	0.00	0.00
Fe^{2+}	0.92	0.81	0.68	1.23	1.34	1.48	1.64	1.85	1.41	1.68	1.34	1.50	1.27
Ba	0.00	0.00	0.00	0.00	0.00	0.00	0.00	0.00	0.00	0.00	0.00	0.00	0.00
Na	0.65	0.71	0.72	0.74	0.69	0.77	0.76	0.76	0.73	0.81	0.69	0.73	0.71
K	0.17	0.20	0.23	0.21	0.22	0.21	0.22	0.22	0.21	0.21	0.23	0.21	0.20
OH	2.00	2.00	2.00	2.00	2.00	2.00	2.00	2.00	2.00	2.00	2.00	2.00	2.00
O	22.6	22.8	22.9	22.9	22.9	22.9	22.9	22.9	22.8	22.9	23.0	22.9	22.9
$Mg/(Mg+Fe^{2+})$	0.75	0.79	0.83	0.70	0.67	0.64	0.62	0.57	0.64	0.61	0.68	0.64	0.69
Species	M	M	P	P	P	P	P	P	P	P	P	P	P

Empirical formula is calculated on the basis of T+C=13.

Petrographic type: TD — trachydacite; BTA — basaltic trachyandesite; BA — basalt; TB — trachybasalt; TA — trachyandesite; BAA — basaltic andesite

Species: M - magnesiohastingsite; P - pargasite

BDL: below detection limit

apfu: atoms per formula unit

Table S1 (continued): Representative compositions of amphibole.

Sample	**UB1B**	**UB1B**	**UB1B**	**UB1B**	**UB1B**	**UB1B**	**UB1B**	**UB1B**	**UB1B**	**UB1B**	**UB2**	**UB2**	**UB2**
Petrographic type	**BTA**	**BTA**	**BTA**	**BTA**	**BTA**	**BTA**	**BTA**	**BTA**	**BTA**	**BTA**	**BA**	**BA**	**BA**
SiO_2	40.8	40.3	40.2	41.3	40.1	40.4	40.3	39.2	39.1	40.2	39.5	39.4	40.5
TiO_2	2.98	3.62	2.96	2.99	2.77	2.54	2.56	3.15	3.09	3.00	2.90	2.49	3.00
Al_2O_3	12.0	13.4	13.6	11.7	12.6	14.7	14.9	13.8	14.4	13.7	14.2	14.3	14.3
MgO	11.8	12.8	12.1	11.3	10.9	14.6	14.6	12.3	11.0	12.7	12.6	11.8	13.9
CaO	11.6	11.9	11.8	11.1	11.5	12.4	12.4	11.9	11.8	12.0	12.2	12.1	12.7
MnO	0.32	<BDL	0.11	0.38	0.23	<BDL	0.10	0.15	0.21	0.15	0.11	0.14	<BDL
FeO	13.9	10.9	12.6	14.8	14.7	8.37	8.18	11.9	14.3	11.5	11.3	13.0	9.75
BaO	<BDL	<BDL	<BDL	<BDL	<BDL	<BDL	<BDL	<BDL	<BDL	0.06	<BDL	<BDL	<BDL
Na_2O	2.88	2.40	2.45	2.62	2.47	2.41	2.38	2.33	2.53	2.75	2.31	2.58	2.72
K_2O	1.10	0.99	1.11	1.04	1.14	1.20	1.31	1.10	1.10	1.20	1.35	1.35	1.28
H_2O	1.99	2.01	2.01	2.00	1.98	2.04	2.04	1.99	2.00	2.01	2.00	2.00	2.04
Total	99.5	98.4	98.9	99.3	98.6	98.9	99.0	98.0	99.6	99.3	98.6	99.3	100.3
Empirical formula (*apfu*)													
Si	6.14	6.02	6.00	6.21	6.08	5.94	5.92	5.92	5.86	5.99	5.92	5.91	5.94
Al^{IV}	1.86	1.98	2.00	1.79	1.92	2.06	2.08	2.08	2.14	2.01	2.08	2.09	2.06
ΣT	8.00	8.00	8.00	8.00	8.00	8.00	8.00	8.00	8.00	8.00	8.00	8.00	8.00
Ti	0.34	0.41	0.33	0.34	0.32	0.28	0.28	0.36	0.35	0.34	0.33	0.28	0.33
Al	2.13	2.35	2.40	2.07	2.26	2.55	2.59	2.46	2.54	2.41	2.51	2.52	2.48
Al^{VI}	0.27	0.38	0.40	0.28	0.34	0.49	0.51	0.38	0.40	0.40	0.43	0.43	0.42
Fe^{tot}	1.75	1.37	1.57	1.86	1.87	1.03	1.01	1.50	1.79	1.44	1.41	1.63	1.20
Fe^{3+}	0.00	0.09	0.23	0.30	0.27	0.21	0.00	0.23	0.31	0.06	0.16	0.17	0.00
Mg	2.64	2.85	2.69	2.52	2.47	3.20	3.20	2.76	2.46	2.82	2.81	2.64	3.05
Ca	1.87	1.90	1.89	1.79	1.86	1.95	1.95	1.93	1.90	1.92	1.95	1.95	1.99
Mn	0.00	0.00	0.00	0.00	0.00	0.00	0.00	0.00	0.00	0.00	0.01	0.02	0.00
Fe^{2+}	1.75	1.27	1.34	1.56	1.59	0.82	1.01	1.28	1.48	1.38	1.26	1.46	1.20
Ba	0.00	0.00	0.00	0.00	0.00	0.00	0.00	0.00	0.00	0.00	0.00	0.00	0.00
Na	0.84	0.70	0.71	0.76	0.73	0.69	0.68	0.68	0.73	0.79	0.67	0.75	0.77
K	0.21	0.19	0.21	0.20	0.22	0.22	0.25	0.21	0.21	0.23	0.26	0.26	0.24
OH	2.00	2.00	2.00	2.00	2.00	2.00	2.00	2.00	2.00	2.00	2.00	2.00	2.00
O	23.0	23.0	22.9	22.9	22.9	22.9	22.9	22.9	22.8	23.0	22.9	22.9	23.0
$Mg/(Mg+Fe^{2+})$	0.60	0.69	0.67	0.62	0.61	0.80	0.76	0.68	0.62	0.67	0.69	0.64	0.72
Species	P	P	P	M	P	P	P	P	P	P	P	P	P

Empirical formula is calculated on the basis of T+C=13.

Petrographic type: TD — trachydacite; BTA — basaltic trachyandesite; BA — basalt; TB — trachybasalt; TA — trachyandesite; BAA — basaltic andesite

Species: M - magnesiohastingsite; P - pargasite

BDL: below detection limit

apfu: atoms per formula unit

Table S1 (continued): Representative compositions of amphibole.

Sample	**UB2**	**UB2**	**UB2**	**UB3**	**UB4**	**UB4**	**UB4**	**UB4**	**UB4**	**UB4**	**UB4**	**UB4**	**UB4**
Petrographic type	**BA**	**BA**	**BA**	**TB**	**TA**	**TA**	**TA**	**TA**	**TA**	**TA**	**TA**	**TA**	**TA**
SiO_2	39.8	39.9	38.4	40.0	40.1	41.0	40.7	39.4	40.1	38.6	40.4	40.0	40.6
TiO_2	2.54	2.51	2.55	4.00	2.82	2.51	2.60	2.66	2.67	2.70	2.50	2.58	2.55
Al_2O_3	14.7	14.6	15.9	13.3	12.4	13.3	13.8	13.4	11.9	14.4	13.8	12.3	12.3
MgO	14.5	14.6	13.0	13.1	11.0	13.8	13.2	11.1	10.9	11.6	14.3	11.2	11.7
CaO	12.4	12.3	12.6	11.9	11.6	12.0	12.1	11.8	11.4	11.7	12.1	11.7	11.7
MnO	0.14	<BDL	0.10	0.15	0.36	0.14	<BDL	0.21	0.42	0.22	0.14	0.37	0.31
FeO	8.82	9.04	11.1	11.2	15.7	10.9	11.8	14.2	15.0	13.1	9.4	15.2	14.2
BaO	<BDL	0.04	<BDL	<BDL	<BDL	<BDL	0.06	<BDL	<BDL	<BDL	<BDL	0.08	<BDL
Na_2O	2.38	2.42	2.35	2.63	2.46	2.55	2.54	2.63	2.53	2.78	2.54	2.39	2.55
K_2O	1.41	1.50	1.34	0.81	1.28	0.93	0.98	1.08	1.42	0.98	1.05	1.35	1.28
H_2O	2.03	2.04	2.03	2.02	1.99	2.04	2.04	1.98	1.96	1.98	2.02	1.98	1.99
Total	98.8	99.1	99.6	99.4	99.8	99.2	99.9	98.6	98.5	98.2	98.2	99.2	99.3
Empirical formula (*apfu*)													
Si	5.88	5.87	5.69	5.94	6.04	6.03	5.98	5.99	6.14	5.85	5.99	6.05	6.11
Al^{IV}	2.12	2.13	2.31	2.06	1.96	1.97	2.02	2.01	1.86	2.15	2.01	1.95	1.89
ΣT	8.00	8.00	8.00	8.00	8.00	8.00	8.00	8.00	8.00	8.00	8.00	8.00	8.00
Ti	0.28	0.28	0.28	0.45	0.32	0.28	0.29	0.30	0.31	0.31	0.28	0.29	0.29
Al	2.55	2.53	2.77	2.33	2.21	2.31	2.39	2.40	2.15	2.57	2.41	2.20	2.19
Al^{VI}	0.43	0.40	0.46	0.27	0.25	0.34	0.37	0.39	0.28	0.42	0.40	0.25	0.30
Fe^{tot}	1.09	1.11	1.38	1.39	1.98	1.35	1.45	1.80	1.92	1.66	1.16	1.93	1.79
Fe^{3+}	0.25	0.30	0.12	0.00	0.37	0.38	0.36	0.21	0.20	0.00	0.29	0.35	0.25
Mg	3.18	3.21	2.87	2.90	2.46	3.03	2.89	2.51	2.49	2.61	3.16	2.53	2.62
Ca	1.97	1.95	1.99	1.90	1.87	1.89	1.90	1.91	1.87	1.91	1.92	1.90	1.89
Mn	0.02	0.00	0.01	0.00	0.00	0.00	0.00	0.00	0.00	0.00	0.00	0.00	0.00
Fe^{2+}	0.84	0.81	1.26	1.39	1.61	0.97	1.09	1.59	1.73	1.67	0.87	1.58	1.54
Ba	0.00	0.00	0.00	0.00	0.00	0.00	0.00	0.00	0.00	0.00	0.00	0.00	0.00
Na	0.68	0.69	0.67	0.76	0.72	0.73	0.72	0.77	0.75	0.82	0.73	0.70	0.74
K	0.27	0.28	0.25	0.15	0.25	0.17	0.18	0.21	0.28	0.19	0.20	0.26	0.25
OH	2.00	2.00	2.00	2.00	2.00	2.00	2.00	2.00	2.00	2.00	2.00	2.00	2.00
O	22.9	22.9	22.9	22.9	22.8	22.8	22.8	22.9	22.9	22.9	22.9	22.8	22.9
$Mg/(Mg+Fe^{2+})$	0.79	0.80	0.70	0.68	0.60	0.76	0.73	0.61	0.59	0.61	0.78	0.62	0.63
Species	P	P	P	P	M	M	P	P	P	P	P	M	P

Empirical formula is calculated on the basis of T+C=13.

Petrographic type: TD — trachydacite; BTA — basaltic trachyandesite; BA — basalt; TB — trachybasalt; TA — trachyandesite; BAA — basaltic andesite

Species: M - magnesiohastingsite; P - pargasite

BDL: below detection limit

apfu: atoms per formula unit

Table S1 (continued): Representative compositions of amphibole.

Sample	**UB4**	**UB4**	**UB4**	**UB4**	**UB7**	**UB7**	**UB7**	**UB7**	**UB7**	**UB7**	**UB7**	**UB7**	**UB7**	**UB7**
Petrographic type	**TA**	**TA**	**TA**	**TA**	**BAA**	**BAA**	**BAA**	**BAA**	**BAA**	**BAA**	**BAA**	**BAA**	**BAA**	**BAA**
SiO_2	41.3	39.1	40.2	40.7	40.1	40.8	40.7	40.8	40.6	40.5	40.3	39.9	40.6	40.9
TiO_2	2.57	2.77	2.58	2.52	3.44	3.51	3.54	3.66	3.50	3.48	3.29	3.55	3.50	3.51
Al_2O_3	12.5	12.8	14.0	12.9	13.5	12.8	13.8	13.1	12.9	12.7	13.4	13.0	13.6	12.5
MgO	13.7	10.9	13.0	13.2	12.9	13.7	14.4	13.8	13.2	13.3	13.0	12.6	12.7	13.3
CaO	11.9	11.7	11.9	11.7	11.5	12.0	12.3	12.0	11.7	11.8	11.5	11.7	11.8	11.6
MnO	0.11	0.25	0.20	0.18	<BDL	0.12	<BDL	0.14	0.16	0.12	0.13	0.13	0.17	0.10
FeO	10.2	15.3	11.5	11.2	12.0	10.7	9.3	10.8	11.2	11.3	11.7	12.8	12.3	12.0
BaO	<BDL	<BDL	0.06	<BDL	<BDL	<BDL	<BDL	<BDL	<BDL	<BDL	<BDL	<BDL	<BDL	<BDL
Na_2O	2.54	2.59	2.52	2.58	2.00	2.00	2.02	2.09	2.04	2.06	1.99	2.05	1.97	2.03
K_2O	1.01	1.08	0.98	0.89	0.85	0.89	0.92	0.91	0.84	0.76	0.85	0.87	0.89	0.80
H_2O	2.01	1.97	2.02	2.00	2.03	2.03	2.05	2.04	2.02	2.01	2.03	2.01	2.04	2.03
Total	97.8	98.5	99.0	98.0	98.4	98.7	99.2	99.3	98.3	98.0	98.4	98.7	99.7	98.8
Empirical formula (*apfu*)														
Si	6.17	5.96	5.97	6.09	5.93	6.03	5.95	5.98	6.03	6.03	5.96	5.94	5.96	6.03
Al^{IV}	1.83	2.04	2.03	1.91	2.07	1.97	2.05	2.02	1.97	1.97	2.04	2.06	2.04	1.97
ΣT	8.00	8.00	8.00	8.00	8.00	8.00	8.00	8.00	8.00	8.00	8.00	8.00	8.00	8.00
Ti	0.29	0.32	0.29	0.28	0.38	0.39	0.39	0.40	0.39	0.39	0.37	0.40	0.39	0.39
Al	2.20	2.30	2.44	2.27	2.35	2.23	2.38	2.26	2.26	2.22	2.34	2.28	2.35	2.17
Al^{VI}	0.38	0.26	0.41	0.37	0.29	0.27	0.33	0.25	0.29	0.25	0.31	0.22	0.31	0.20
Fe^{tot}	1.27	1.95	1.42	1.40	1.49	1.32	1.13	1.32	1.39	1.40	1.45	1.59	1.51	1.48
Fe^{3+}	0.15	0.34	0.32	0.29	0.63	0.37	0.34	0.42	0.45	0.44	0.61	0.55	0.50	0.60
Mg	3.06	2.47	2.87	2.95	2.84	3.02	3.15	3.03	2.93	2.96	2.88	2.79	2.79	2.93
Ca	1.90	1.91	1.90	1.88	1.82	1.90	1.92	1.89	1.86	1.88	1.83	1.87	1.86	1.83
Mn	0.00	0.00	0.00	0.00	0.00	0.00	0.00	0.00	0.00	0.00	0.00	0.00	0.00	0.00
Fe^{2+}	1.13	1.61	1.10	1.10	0.86	0.96	0.79	0.90	0.94	0.96	0.84	1.04	1.02	0.88
Ba	0.00	0.00	0.00	0.00	0.00	0.00	0.00	0.00	0.00	0.00	0.00	0.00	0.00	0.00
Na	0.74	0.77	0.72	0.75	0.57	0.57	0.57	0.59	0.59	0.60	0.57	0.59	0.56	0.58
K	0.19	0.21	0.19	0.17	0.16	0.17	0.17	0.17	0.16	0.15	0.16	0.16	0.17	0.15
OH	2.00	2.00	2.00	2.00	2.00	2.00	2.00	2.00	2.00	2.00	2.00	2.00	2.00	2.00
O	22.9	22.8	22.8	22.9	22.7	22.8	22.8	22.8	22.8	22.8	22.7	22.7	22.8	22.7
$Mg/(Mg+Fe^{2+})$	0.73	0.61	0.72	0.73	0.77	0.76	0.80	0.77	0.76	0.75	0.77	0.73	0.73	0.77
Species	P	M	P	P	M	M	M	M	M	M	M	M	M	M

Empirical formula is calculated on the basis of T+C=13.

Petrographic type: TD — trachydacite; BTA — basaltic trachyandesite; BA — basalt; TB — trachybasalt; TA — trachyandesite; BAA — basaltic andesite

Species: M - magnesiohastingsite; P - pargasite

BDL: below detection limit

apfu: atoms per formula unit

Table S2: Representative compositions of clinopyroxene.

Sample	**UB1B**	**UB2**	**UB2**	**UB2**	**UB2**	**UB2**	**UB2**	**UB2**	**UB2**	**UB2**	**UB3**	**UB3**	**UB3**
Petrographic type	**BTA**	**BA**	**BA**	**BA-C**	**BA-R**	**BA-C**	**BA-R**	**BA**	**BA**	**BA**	**TB**	**TB-PR**	**TB-PR**
SiO_2	49.0	51.8	49.9	50.4	48.5	52.2	46.6	50.1	48.9	50.1	50.6	47.1	47.0
TiO_2	1.10	0.51	0.89	0.66	0.92	0.42	2.06	0.97	0.66	1.01	0.80	1.67	1.72
Al_2O_3	6.13	3.25	5.08	4.25	5.8	2.6	7.01	3.57	4.87	3.31	3.56	6.92	6.90
MgO	13.8	15.8	14.4	15.1	13.4	16.1	11.9	13.7	11.3	13.6	14.7	12.7	12.5
CaO	23.1	24.1	23.7	23.6	23.2	23.7	22.4	22.6	22.5	22.3	21.8	21.7	21.6
MnO	0.11	<BDL	<BDL	0.11	0.19	0.12	0.24	0.26	0.29	0.18	0.16	0.16	0.18
FeO	5.38	4.21	5.31	4.84	6.6	4.08	9.43	8.52	10.8	8.48	7.75	8.64	8.66
Na_2O	0.49	0.28	0.33	0.30	0.36	0.21	0.44	0.36	0.75	0.28	0.50	0.64	0.44
Total	99.2	99.9	99.6	99.3	99.1	99.5	100.1	100.0	100.1	99.3	99.8	99.5	99.1
Empirical formula (*apfu*)													
Si	1.83	1.90	1.85	1.87	1.82	1.92	1.76	1.87	1.85	1.89	1.88	1.78	1.78
Al^{IV}	0.17	0.10	0.15	0.13	0.18	0.08	0.24	0.13	0.15	0.11	0.12	0.22	0.22
ΣT	2.00	2.00	2.00	2.00	2.00	2.00	2.00	2.00	2.00	2.00	2.00	2.00	2.00
Ti	0.03	0.01	0.02	0.02	0.03	0.01	0.06	0.03	0.02	0.03	0.02	0.05	0.05
Al	0.27	0.14	0.22	0.19	0.26	0.11	0.31	0.16	0.22	0.15	0.16	0.31	0.31
Al^{VI}	0.10	0.04	0.07	0.06	0.08	0.04	0.07	0.03	0.07	0.03	0.04	0.08	0.09
Fe^{tot}	0.00	0.00	0.00	0.00	0.00	0.00	0.00	0.00	0.00	0.00	0.00	0.00	0.00
Fe^{3+}	0.07	0.07	0.08	0.08	0.10	0.05	0.12	0.10	0.14	0.07	0.10	0.13	0.10
Mg	0.77	0.86	0.80	0.84	0.75	0.89	0.67	0.77	0.64	0.77	0.81	0.71	0.70
Ca	0.92	0.95	0.94	0.94	0.94	0.94	0.91	0.91	0.91	0.90	0.87	0.88	0.88
Mn	0.00	0.00	0.00	0.00	0.01	0.00	0.01	0.01	0.01	0.01	0.01	0.01	0.01
Fe^{2+}	0.09	0.06	0.09	0.07	0.10	0.08	0.17	0.17	0.20	0.20	0.14	0.14	0.18
Na	0.04	0.02	0.02	0.02	0.03	0.02	0.03	0.03	0.06	0.02	0.04	0.05	0.03
O	6.00	6.00	6.00	6.00	6.00	6.00	6.00	6.00	6.00	6.00	6.00	6.00	6.00
Fe/(Fe+Mg)*	0.18	0.13	0.17	0.16	0.22	0.13	0.32	0.27	0.36	0.26	0.23	0.28	0.29
Species	D	D	D	D	D	D	D	D	D	D	A	A	A

Empirical formula is calculated on the basis of O=6.

* $Fe=Fe^{tot}+Mn$

Petrographic type: BTA — basaltic trachyandesite; BA — basalt; TB — trachybasalt; TA — trachyandesite, BAA — basaltic andesite; PR — prismatic sector, PY — pyramidal sector, C — core, R — rim

Species: D — diopside; A — augite

BDL: below detection limit

apfu: atoms per formula unit

Table S2 (continued): Representative compositions of clinopyroxene.

Sample	**UB3**	**UB3**	**UB3**	**UB3**	**UB3**	**UB3**	**UB3**	**UB3**	**UB3**	**UB3**	**UB3**	**UB4**	**UB4**
Petrographic type	**TB-PY**	**TB-PY**	**TB**	**TB**	**TB**	**TB**	**TB**	**TB**	**TB**	**TB-C**	**TB-R**	**TA-C**	**TA-R**
SiO_2	50.8	52.0	47.9	50.2	50.8	50.7	49.1	52.6	50.6	51.9	48.3	51.1	49.8
TiO_2	1.58	0.31	1.44	0.81	0.84	0.74	1.12	0.48	0.81	0.49	1.26	0.29	0.70
Al_2O_3	2.61	0.16	6.47	3.58	4.47	3.42	5.29	0.94	3.70	2.75	5.74	2.04	3.00
MgO	14.8	12.3	13.0	14.4	14.4	14.6	13.3	14.8	14.6	15.8	13.3	12.0	11.1
CaO	22.4	21.5	22.1	21.7	22.3	21.9	22.1	22.4	22.0	23.2	22.3	22.7	22.8
MnO	0.20	0.37	0.22	0.22	0.20	0.18	0.23	0.31	0.19	0.11	0.20	0.70	0.74
FeO	7.60	12.5	7.90	7.63	7.31	7.61	7.96	8.00	7.15	4.60	7.95	9.93	10.7
Na_2O	0.45	0.48	0.53	0.50	0.40	0.39	0.43	0.33	0.42	0.29	0.48	0.88	0.73
Total	100.4	99.7	99.6	99.1	100.8	99.6	99.5	99.9	99.5	99.1	99.5	99.7	99.6
Empirical formula (*apfu*)													
Si	1.89	1.98	1.80	1.89	1.87	1.89	1.84	1.96	1.89	1.92	1.82	1.94	1.90
Al^{IV}	0.11	0.01	0.20	0.11	0.13	0.11	0.16	0.04	0.11	0.08	0.18	0.06	0.10
ΣT	2.00	1.99	2.00	2.00	2.00	2.00	2.00	2.00	2.00	2.00	2.00	2.00	2.00
Ti	0.04	0.01	0.04	0.02	0.02	0.02	0.03	0.01	0.02	0.01	0.04	0.01	0.02
Al	0.11	0.01	0.29	0.16	0.19	0.15	0.23	0.04	0.16	0.12	0.25	0.09	0.13
Al^{VI}	0.00	0.00	0.09	0.04	0.07	0.04	0.07	0.00	0.05	0.04	0.07	0.03	0.04
Fe^{tot}	0.00	0.00	0.00	0.00	0.00	0.00	0.00	0.00	0.00	0.00	0.00	0.00	0.00
Fe^{3+}	0.08	0.07	0.11	0.09	0.07	0.07	0.08	0.05	0.07	0.04	0.12	0.12	0.12
Mg	0.82	0.70	0.73	0.81	0.79	0.81	0.74	0.82	0.81	0.87	0.75	0.68	0.63
Ca	0.89	0.88	0.89	0.87	0.88	0.87	0.89	0.90	0.88	0.92	0.90	0.92	0.93
Mn	0.01	0.01	0.01	0.01	0.01	0.01	0.01	0.01	0.01	0.00	0.01	0.02	0.02
Fe^{2+}	0.15	0.33	0.14	0.15	0.16	0.17	0.17	0.20	0.15	0.10	0.13	0.20	0.23
Na	0.03	0.04	0.04	0.04	0.03	0.03	0.03	0.02	0.03	0.02	0.04	0.06	0.05
O	6.00	6.00	6.00	6.00	6.00	6.00	6.00	6.00	6.00	6.00	6.00	6.00	6.00
Fe/(Fe+Mg)*	0.23	0.37	0.26	0.24	0.23	0.23	0.26	0.24	0.22	0.14	0.26	0.34	0.37
Species	D	A	D	A	D	A	D	D	D	D	D	D	D

Empirical formula is calculated on the basis of O=6.

* $Fe=Fe^{tot}+Mn$

Petrographic type: BTA — basaltic trachyandesite; BA — basalt; TB — trachybasalt; TA — trachyandesite, BAA — basaltic andesite; PR — prismatic sector, PY — pyramidal sector, C — core, R — rim

Species: D — diopside; A — augite

BDL: below detection limit

apfu: atoms per formula unit

Table S2 (continued): Representative compositions of clinopyroxene.

Sample	**UB4**	**UB4**	**UB4**	**UB7**	**UB7**	**UB7**	**UB7**
Petrographic type	**TA**	**TA**	**TA**	**BAA**	**BAA-C**	**BAA.R**	**BAA-R**
SiO_2	48.2	50.6	50.3	48.5	51.5	51.1	50.9
TiO_2	1.07	0.47	0.61	1.49	0.73	0.70	0.87
Al_2O_3	4.80	2.66	3.19	5.45	2.93	2.82	3.13
MgO	10.0	11.3	12.0	13.5	15.2	14.8	14.5
CaO	22.2	22.5	22.7	22.1	22.0	21.6	21.9
MnO	0.61	0.68	0.42	0.23	0.22	0.22	0.14
FeO	12.1	10.4	9.75	7.87	7.47	7.76	7.41
Na_2O	0.95	0.76	0.59	0.28	0.23	0.20	0.22
Total	100.0	99.4	99.5	99.4	100.3	99.2	99.1
Empirical formula (*apfu*)							
Si	1.84	1.93	1.90	1.82	1.90	1.91	1.91
Al^{IV}	0.16	0.07	0.10	0.18	0.10	0.09	0.09
ΣT	2.00	2.00	2.00	2.00	2.00	2.00	2.00
Ti	0.03	0.01	0.02	0.04	0.02	0.02	0.02
Al	0.22	0.12	0.14	0.24	0.13	0.12	0.14
Al^{VI}	0.06	0.05	0.05	0.06	0.03	0.04	0.04
Fe^{tot}	0.00	0.00	0.00	0.00	0.00	0.00	0.00
Fe^{3+}	0.15	0.09	0.08	0.08	0.06	0.04	0.03
Mg	0.57	0.64	0.68	0.76	0.84	0.83	0.81
Ca	0.91	0.92	0.92	0.89	0.87	0.86	0.88
Mn	0.02	0.02	0.01	0.01	0.01	0.01	0.00
Fe^{2+}	0.24	0.24	0.22	0.17	0.17	0.20	0.21
Na	0.07	0.06	0.04	0.02	0.02	0.01	0.02
O	6.00	6.00	6.00	6.00	6.00	6.00	6.00
Fe/(Fe+Mg)*	0.43	0.36	0.33	0.25	0.22	0.23	0.23
Species	D	D	D	D	A	A	A

Empirical formula is calculated on the basis of O=6.

* $Fe=Fe^{tot}+Mn$

Petrographic type: BTA — basaltic trachyandesite; BA — basalt; TB — trachybasalt; TA — trachyandesite, BAA — basaltic andesite; PR — prismatic sector, PY — pyramidal sector, C — core, R — rim

Species: D — diopside; A — augite

BDL: below detection limit

apfu: atoms per formula unit

Table S3: Representative compositions of dark mica.

Sample	**UB1A**	**UB1A**	**UB1A**	**UB1A**	**UB1A**	**UB1A**	**UB1A**	**UB1A**
Petrographic type	**TD**	**TD**	**TD**	**TD**	**TD**	**TD**	**TD**	**TD**
SiO_2	35.9	36.5	36.1	36.7	36.4	35.8	36.4	36.3
TiO_2	4.65	4.55	4.31	4.52	4.65	4.68	4.54	4.65
Al_2O_3	14.5	14.6	15.0	14.4	14.8	14.5	14.6	14.6
MgO	14.0	14.2	13.7	14.2	14.0	14.2	14.3	14.3
MnO	0.18	0.14	0.14	0.16	0.15	0.11	0.21	0.20
FeO	15.3	15.7	17.3	15.6	15.8	15.5	15.8	15.9
BaO	0.93	0.79	0.71	0.83	0.95	0.82	0.81	0.87
Na_2O	0.92	1.03	0.69	0.81	0.83	0.78	0.82	0.71
K_2O	8.73	8.65	8.3	8.65	8.56	8.53	8.62	8.69
H_2O	3.96	4.01	3.99	4.00	4.00	3.95	4.00	3.99
Total	99.1	100.2	100.3	99.9	100.2	98.9	100.1	100.0
Empirical formula (*apfu*)								
Si	2.72	2.74	2.70	2.75	2.73	2.71	2.73	2.72
Al^{IV}	1.28	1.26	1.30	1.25	1.27	1.29	1.27	1.28
ΣT	4.00	4.00	4.00	4.00	4.00	4.00	4.00	4.00
Ti	0.27	0.26	0.24	0.26	0.26	0.27	0.26	0.26
Al	1.29	1.29	1.32	1.27	1.31	1.30	1.29	1.29
Al^{VI}	0.02	0.02	0.03	0.03	0.03	0.01	0.02	0.01
Mg	1.58	1.58	1.52	1.59	1.56	1.60	1.60	1.60
Mn	0.01	0.01	0.01	0.01	0.01	0.01	0.01	0.01
Fe^{tot}	0.97	0.98	1.08	0.98	0.99	0.99	0.99	1.00
Ba	0.03	0.02	0.02	0.02	0.03	0.02	0.02	0.03
Na	0.14	0.15	0.10	0.12	0.12	0.11	0.12	0.10
K	0.84	0.83	0.79	0.83	0.82	0.83	0.82	0.83
OH	2.00	2.00	2.00	2.00	2.00	2.00	2.00	2.00
O	10.0	10.0	10.0	10.0	10.0	10.0	10.0	10.0
$Mg/(Mg + Fe^{tot})$	0.62	0.62	0.59	0.62	0.61	0.62	0.62	0.62
Species	B	B	B	B	B	B	B	B

Empirical formula is calculated on the basis of O=11.

Petrographic type: TD — trachydacite

Species: B — biotite

apfu: atoms per formula unit

Table S4: Representative compositions of feldspar.

Sample	**UB1A**	**UB1A**	**UB1A**	**UB1A**	**UB1A**	**UB1A**	**UB1A**	**UB1A**	**UB1A**	**UB1A**	**UB1A**	**UB1A**	**UB1B**
Petrographic type	**TD**	**TD**	**TD**	**TD**	**TD**	**TD**	**TD**	**TD**	**TD**	**TD**	**TD**	**TD**	**BTA**
SiO_2	54.8	56.3	58.4	56.2	57.7	52.7	54.0	55.3	54.2	53.6	56.4	57.9	56.7
Al_2O_3	27.8	27.0	25.6	27.1	26.5	29.6	28.7	28.0	28.5	29.5	26.9	26.3	26.8
MgO	<BDL	<BDL	<BDL	<BDL	<BDL	<BDL	<BDL	<BDL	<BDL	<BDL	<BDL	<BDL	<BDL
CaO	10.4	8.95	7.49	9.17	8.12	12.0	10.8	9.50	10.9	11.4	8.92	7.88	9.46
FeO	0.32	0.34	0.38	0.41	0.34	0.36	0.39	0.32	0.34	0.30	0.36	0.30	0.31
BaO	<BDL	0.08	<BDL	0.08	<BDL	<BDL	<BDL	<BDL	<BDL	<BDL	<BDL	<BDL	<BDL
Na_2O	5.78	6.33	7.31	6.26	6.90	4.67	5.37	6.07	5.37	5.09	6.51	6.95	6.13
K_2O	0.38	0.48	0.62	0.44	0.58	0.26	0.33	0.45	0.30	0.31	0.49	0.60	0.55
Total	99.4	99.4	99.8	99.6	100.1	99.5	99.6	99.7	99.7	100.2	99.6	100.0	99.9
Empirical formula (*apfu*)													
Si	2.49	2.56	2.66	2.55	2.62	2.40	2.46	2.52	2.47	2.44	2.57	2.63	2.58
Al	1.49	1.45	1.37	1.45	1.42	1.58	1.54	1.50	1.53	1.58	1.44	1.41	1.44
Mg	0.00	0.00	0.00	0.00	0.00	0.00	0.00	0.00	0.00	0.00	0.00	0.00	0.00
Ca	0.51	0.44	0.37	0.45	0.40	0.58	0.52	0.46	0.53	0.56	0.43	0.38	0.46
Fe	0.01	0.01	0.01	0.02	0.01	0.01	0.01	0.01	0.01	0.01	0.01	0.01	0.01
Ba	0.00	0.00	0.00	0.00	0.00	0.00	0.00	0.00	0.00	0.00	0.00	0.00	0.00
Na	0.51	0.56	0.64	0.55	0.61	0.41	0.47	0.54	0.47	0.45	0.57	0.61	0.54
K	0.02	0.03	0.04	0.03	0.03	0.02	0.02	0.03	0.02	0.02	0.03	0.03	0.03
O	8.00	8.00	8.00	8.00	8.00	8.00	8.00	8.00	8.00	8.00	8.00	8.00	8.00
Or (mol. %)	2.1	2.7	3.4	2.5	3.2	1.5	1.9	2.5	1.7	1.8	2.7	3.4	3.1
Ab	49.1	54.6	61.7	53.9	58.6	40.8	46.6	52.3	46.3	43.9	55.3	59.4	52.3
An	48.8	42.7	34.9	43.6	38.1	57.7	51.5	45.2	52.0	54.4	41.9	37.2	44.6

Sample	**UB1B**	**UB1B**	**UB1B**	**UB1B**	**UB1B**	**UB1B**	**UB1B**	**UB1B**	**UB1B**	**UB1B**	**UB1B**	**UB1B**	**UB1B**
Petrographic type	**BTA**	**BTA**	**BTA**	**BTA**	**BTA**	**BTA**	**BTA**	**BTA**	**BTA**	**BTA**	**BTA**	**BTA**	**BTA**
SiO_2	54.3	53.9	54.0	54.1	57.1	53.1	46.9	54.4	52.8	45.7	50.5	53.3	54.5
Al_2O_3	28.8	28.1	28.2	27.8	25.8	28.6	32.6	28.0	29.2	34.0	30.7	29.0	27.7
MgO	<BDL	<BDL	<BDL	<BDL	<BDL	0.06	<BDL	<BDL	<BDL	<BDL	<BDL	<BDL	<BDL
CaO	11.5	11.3	11.6	11.1	8.6	12.1	16.8	11.0	11.9	17.6	14.3	12.1	10.9
FeO	0.44	0.36	0.43	0.33	0.49	0.46	0.45	0.64	0.56	0.51	0.48	0.43	0.46
BaO	<BDL	<BDL	<BDL	<BDL	0.185	<BDL	<BDL	<BDL	<BDL	<BDL	<BDL	<BDL	<BDL
Na_2O	4.94	5.00	5.12	5.26	6.49	4.87	1.98	5.34	4.78	1.58	3.48	4.67	5.27
K_2O	0.39	0.38	0.42	0.39	0.65	0.28	0.10	0.58	0.37	0.06	0.20	0.34	0.42
Total	99.3	100.3	100.0	99.6	98.8	100.1	100.3	99.7	100.5	100.0	100.4	99.1	99.7
Empirical formula (*apfu*)													
Si	2.47	2.45	2.46	2.46	2.60	2.41	2.13	2.47	2.40	2.08	2.30	2.43	2.48
Al	1.55	1.51	1.51	1.49	1.38	1.53	1.75	1.50	1.56	1.82	1.65	1.55	1.49
Mg	0.00	0.00	0.00	0.00	0.00	0.00	0.00	0.00	0.00	0.00	0.00	0.00	0.00
Ca	0.56	0.55	0.57	0.54	0.42	0.59	0.82	0.54	0.58	0.86	0.70	0.59	0.53
Fe	0.02	0.01	0.02	0.01	0.02	0.02	0.02	0.02	0.02	0.02	0.02	0.02	0.02
Ba	0.00	0.00	0.00	0.00	0.00	0.00	0.00	0.00	0.00	0.00	0.00	0.00	0.00
Na	0.44	0.44	0.45	0.46	0.57	0.43	0.17	0.47	0.42	0.14	0.31	0.41	0.47
K	0.02	0.02	0.02	0.02	0.04	0.02	0.01	0.03	0.02	0.00	0.01	0.02	0.02
O	8.00	8.00	8.00	8.00	8.00	8.00	8.00	8.00	8.00	8.00	8.00	8.00	8.00
Or (mol. %)	2.2	2.2	2.3	2.2	3.7	1.6	0.6	3.2	2.1	0.3	1.1	2.0	2.4
Ab	42.7	43.5	43.3	45.2	55.6	41.5	17.5	45.3	41.1	13.9	30.3	40.3	45.6
An	55.1	54.3	54.4	52.6	40.7	57.0	82.0	51.5	56.8	85.7	68.6	57.8	52.0

Empirical formula is calculated on the basis of O=8.

Petrographic type: TD — trachydacite; BTA — basaltic trachyandesite; BA — basalt; TB — trachybasalt; TA — trachyandesite; BAA — basaltic andesite

BDL: below detection limit

apfu: atoms per formula unit

Table S4 (continued): Representative compositions of feldspar.

Sample	**UB1B**	**UB1B**	**UB1B**	**UB1B**	**UB1B**	**UB1B**	**UB1B**	**UB1B**	**UB1B**	**UB2**	**UB2**	**UB2**	**UB2**
Petrographic type	**BTA**	**BTA**	**BTA**	**BTA**	**BTA**	**BTA**	**BTA**	**BTA**	**BTA**	**BA**	**BA**	**BA**	**BA**
SiO_2	53.1	55.5	52.8	55.2	54.7	46.5	44.3	53.8	54.8	46.6	45.9	45.5	49.1
Al_2O_3	28.7	26.7	29.1	28.0	28.1	33.2	33.4	28.5	27.4	33.7	33.8	35.2	32.2
MgO	0.07	<BDL	0.07	0.05	0.05	0.05	<BDL	<BDL	<BDL	<BDL	<BDL	<BDL	<BDL
CaO	12.1	10.1	12.2	10.7	10.8	17.2	18.4	11.6	10.3	16.8	17.1	17.7	14.7
FeO	0.49	0.58	0.57	0.41	0.49	0.39	0.43	0.37	0.41	0.59	0.54	0.45	0.53
BaO	<BDL	0.087	<BDL	<BDL	0.084	<BDL	<BDL	0.078	0.121	<BDL	<BDL	<BDL	<BDL
Na_2O	4.53	5.63	4.36	5.45	5.34	1.70	0.90	5.01	5.77	2.05	1.84	1.49	3.23
K_2O	0.34	0.50	0.32	0.43	0.46	0.06	0.04	0.36	0.44	0.12	0.09	0.07	0.21
Total	98.9	99.4	99.5	99.0	100.0	99.6	99.5	99.7	99.8	99.3	99.3	99.2	99.5
Empirical formula (*apfu*)													
Si	2.42	2.53	2.40	2.51	2.49	2.12	2.01	2.45	2.49	2.12	2.09	2.07	2.23
Al	1.54	1.43	1.56	1.50	1.51	1.78	1.79	1.53	1.47	1.81	1.81	1.89	1.73
Mg	0.00	0.00	0.00	0.00	0.00	0.00	0.00	0.00	0.00	0.00	0.00	0.00	0.00
Ca	0.59	0.49	0.60	0.52	0.53	0.84	0.90	0.57	0.50	0.82	0.83	0.86	0.72
Fe	0.02	0.02	0.02	0.02	0.02	0.01	0.02	0.01	0.02	0.02	0.02	0.02	0.02
Ba	0.00	0.00	0.00	0.00	0.00	0.00	0.00	0.00	0.00	0.00	0.00	0.00	0.00
Na	0.40	0.50	0.38	0.48	0.47	0.15	0.08	0.44	0.51	0.18	0.16	0.13	0.28
K	0.02	0.03	0.02	0.02	0.03	0.00	0.00	0.02	0.03	0.01	0.01	0.00	0.01
O	8.00	8.00	8.00	8.00	8.00	8.00	8.00	8.00	8.00	8.00	8.00	8.00	8.00
Or (mol. %)	2.0	2.9	1.9	2.4	2.6	0.4	0.2	2.1	2.5	0.7	0.5	0.4	1.2
Ab	39.5	48.8	38.5	46.9	45.9	15.1	8.1	42.9	49.1	18.0	16.2	13.2	28.1
An	58.5	48.4	59.7	50.7	51.5	84.6	91.7	55.1	48.5	81.3	83.2	86.4	70.7

Sample	**UB2**	**UB2**	**UB2**	**UB2**	**UB2**	**UB3**	**UB3**	**UB3**	**UB3**	**UB3**	**UB3**	**UB3**	**UB3**
Petrographic type	**BA**	**BA**	**BA**	**BA**	**BA**	**TB**	**TB**	**TB**	**TB**	**TB**	**TB**	**TB**	**TB**
SiO_2	49.3	45.6	48.4	63.5	49.0	47.7	46.8	47.1	51.1	47.4	51.7	48.0	50.5
Al_2O_3	31.7	34.1	32.7	20.3	32.3	32.0	32.2	32.4	30.8	32.4	29.8	33.3	29.9
MgO	<BDL	<BDL	<BDL	<BDL	<BDL	0.07	0.06	0.07	0.09	0.06	0.09	0.05	0.10
CaO	14.5	17.0	15.4	1.52	15.3	16.7	16.9	16.5	14.1	17.1	14.2	16.8	13.8
FeO	0.58	0.48	0.63	0.34	0.65	0.65	0.55	0.62	0.69	0.65	0.70	0.72	0.72
BaO	<BDL	<BDL	<BDL	<BDL	<BDL	<BDL	<BDL	<BDL	<BDL	<BDL	<BDL	<BDL	0.081
Na_2O	3.36	1.55	2.76	5.44	3.02	2.46	2.19	2.23	3.60	2.13	3.64	2.38	3.81
K_2O	0.23	0.10	0.16	8.52	0.15	0.10	0.08	0.10	0.20	0.08	0.21	0.12	0.26
Total	100.2	100.0	99.2	99.8	99.3	99.8	98.8	99.1	100.6	99.9	100.4	101.4	99.1
Empirical formula (*apfu*)													
Si	2.24	2.07	2.20	2.89	2.23	2.17	2.13	2.14	2.32	2.16	2.35	2.18	2.30
Al	1.70	1.83	1.75	1.09	1.73	1.72	1.73	1.74	1.65	1.74	1.60	1.78	1.60
Mg	0.00	0.00	0.00	0.00	0.00	0.00	0.00	0.00	0.01	0.00	0.01	0.00	0.01
Ca	0.71	0.83	0.75	0.07	0.74	0.82	0.83	0.81	0.68	0.83	0.69	0.82	0.67
Fe	0.02	0.02	0.02	0.01	0.02	0.02	0.02	0.02	0.03	0.02	0.03	0.03	0.03
Ba	0.00	0.00	0.00	0.00	0.00	0.00	0.00	0.00	0.00	0.00	0.00	0.00	0.00
Na	0.30	0.14	0.24	0.48	0.27	0.22	0.19	0.20	0.32	0.19	0.32	0.21	0.34
K	0.01	0.01	0.01	0.49	0.01	0.01	0.00	0.01	0.01	0.00	0.01	0.01	0.01
O	8.00	8.00	8.00	8.00	8.00	8.00	8.00	8.00	8.00	8.00	8.00	8.00	8.00
Or (mol. %)	1.3	0.6	0.9	47.2	0.9	0.6	0.4	0.6	1.1	0.5	1.2	0.7	1.4
Ab	29.2	14.1	24.3	45.8	26.1	20.9	18.9	19.5	31.3	18.3	31.2	20.3	32.9
An	69.5	85.3	74.8	7.1	73.0	78.5	80.7	80.0	67.6	81.3	67.6	79.1	65.7

Empirical formula is calculated on the basis of O=8.

Petrographic type: TD — trachydacite; BTA — basaltic trachyandesite; BA — basalt; TB — trachybasalt; TA — trachyandesite; BAA — basaltic andesite

BDL: below detection limit

apfu: atoms per formula unit

Table S4 (continued): Representative compositions of feldspar.

Sample	**UB3**	**UB3**	**UB3**	**UB3**	**UB3**	**UB3**	**UB3**	**UB3**	**UB3**	**UB3**	**UB3**	**UB3**	**UB3**
Petrographic type	**TB**	**TB**	**TB**	**TB**	**TB**	**TB**	**TB**	**TB**	**TB**	**TB**	**TB**	**TB**	**TB**
SiO_2	47.2	47.2	47.4	52.0	51.0	48.0	47.4	47.0	46.9	49.6	47.0	46.9	51.4
Al_2O_3	32.4	32.9	32.7	28.8	29.6	32.7	32.2	32.7	32.3	30.7	32.2	32.9	30.1
MgO	0.07	<BDL	0.07	0.09	0.11	0.06	0.07	<BDL	0.06	0.07	<BDL	0.05	0.06
CaO	16.9	17.2	16.8	12.9	13.2	16.8	17.0	16.7	17.1	14.5	16.9	17.0	13.5
FeO	0.48	0.52	0.62	0.80	0.84	0.57	0.54	0.54	0.49	0.63	0.58	0.44	0.76
BaO	<BDL	<BDL	<BDL	<BDL	<BDL	<BDL	<BDL	<BDL	<BDL	<BDL	<BDL	<BDL	<BDL
Na_2O	2.20	1.92	2.30	4.42	4.09	2.14	2.00	2.27	1.80	3.49	2.09	2.02	4.14
K_2O	0.06	0.09	0.10	0.30	0.26	0.09	0.09	0.05	0.07	0.18	0.09	0.10	0.23
Total	99.3	99.7	100.1	99.5	99.1	100.3	99.3	99.2	98.8	99.4	98.8	99.4	100.1
Empirical formula (*apfu*)													
Si	2.15	2.14	2.16	2.37	2.32	2.18	2.16	2.14	2.14	2.26	2.14	2.13	2.34
Al	1.74	1.76	1.75	1.55	1.59	1.75	1.73	1.75	1.73	1.65	1.72	1.76	1.61
Mg	0.00	0.00	0.00	0.01	0.01	0.00	0.00	0.00	0.00	0.00	0.00	0.00	0.00
Ca	0.82	0.84	0.82	0.63	0.64	0.82	0.83	0.81	0.83	0.71	0.82	0.83	0.66
Fe	0.02	0.02	0.02	0.03	0.03	0.02	0.02	0.02	0.02	0.02	0.02	0.02	0.03
Ba	0.00	0.00	0.00	0.00	0.00	0.00	0.00	0.00	0.00	0.00	0.00	0.00	0.00
Na	0.19	0.17	0.20	0.39	0.36	0.19	0.18	0.20	0.16	0.31	0.18	0.18	0.37
K	0.00	0.01	0.01	0.02	0.01	0.01	0.01	0.00	0.00	0.01	0.00	0.01	0.01
O	8.00	8.00	8.00	8.00	8.00	8.00	8.00	8.00	8.00	8.00	8.00	8.00	8.00
Or (mol. %)	0.4	0.5	0.6	1.7	1.5	0.5	0.5	0.3	0.4	1.0	0.5	0.6	1.3
Ab	19.0	16.7	19.7	37.5	35.5	18.6	17.4	19.7	15.9	30.1	18.2	17.6	35.3
An	80.7	82.8	79.7	60.8	63.0	80.9	82.1	80.0	83.7	68.9	81.3	81.9	63.5

Sample	**UB3**	**UB3**	**UB4**	**UB4**	**UB4**	**UB4**	**UB4**	**UB4**	**UB4**	**UB4**	**UB4**	**UB4**	**UB4**
Petrographic type	**TB**	**TB**	**TA**	**TA**	**TA**	**TA**	**TA**	**TA**	**TA**	**TA**	**TA**	**TA**	**TA**
SiO_2	48.2	51.1	53.0	53.3	56.5	57.6	65.5	54.6	54.4	54.1	51.4	57.0	42.8
Al_2O_3	31.8	30.1	28.6	29.0	26.2	26.0	19.5	28.3	28.3	28.3	29.8	26.0	35.7
MgO	0.07	0.11	<BDL	<BDL	<BDL	<BDL	<BDL	<BDL	<BDL	<BDL	<BDL	<BDL	<BDL
CaO	15.8	13.8	11.9	11.8	9.11	8.76	0.82	10.5	10.9	11.2	13.2	7.97	18.6
FeO	0.53	0.71	0.41	0.47	0.54	0.53	0.28	0.37	0.41	0.47	0.55	0.66	0.48
BaO	<BDL	<BDL	<BDL	<BDL	0.082	0.194	0.821	<BDL	0.093	<BDL	<BDL	0.115	<BDL
Na_2O	2.75	3.79	4.80	4.88	6.56	6.74	5.88	5.45	5.59	4.89	3.92	6.92	0.95
K_2O	0.11	0.19	0.28	0.29	0.58	0.80	7.93	0.43	0.41	0.34	0.25	0.80	0.02
Total	99.3	99.9	99.0	99.8	99.6	100.6	100.8	99.7	100.1	99.3	99.1	99.5	98.6
Empirical formula (*apfu*)													
Si	2.19	2.32	2.41	2.43	2.57	2.62	2.98	2.48	2.48	2.46	2.34	2.59	1.95
Al	1.70	1.61	1.53	1.55	1.41	1.40	1.05	1.52	1.52	1.52	1.60	1.39	1.91
Mg	0.00	0.01	0.00	0.00	0.00	0.00	0.00	0.00	0.00	0.00	0.00	0.00	0.00
Ca	0.77	0.67	0.58	0.58	0.44	0.43	0.04	0.51	0.53	0.55	0.64	0.39	0.91
Fe	0.02	0.03	0.02	0.02	0.02	0.02	0.01	0.01	0.02	0.02	0.02	0.03	0.02
Ba	0.00	0.00	0.00	0.00	0.00	0.00	0.01	0.00	0.00	0.00	0.00	0.00	0.00
Na	0.24	0.33	0.42	0.43	0.58	0.59	0.52	0.48	0.49	0.43	0.35	0.61	0.08
K	0.01	0.01	0.02	0.02	0.03	0.05	0.46	0.02	0.02	0.02	0.01	0.05	0.00
O	8.00	8.00	8.00	8.00	8.00	8.00	8.00	8.00	8.00	8.00	8.00	8.00	8.00
Or (mol. %)	0.6	1.1	1.6	1.6	3.2	4.4	45.2	2.4	2.3	2.0	1.4	4.4	0.1
Ab	23.8	32.8	41.4	42.0	54.8	55.7	50.9	47.2	47.0	43.2	34.5	58.4	8.5
An	75.6	66.1	56.9	56.3	42.1	40.0	3.9	50.4	50.7	54.8	64.0	37.2	91.5

Empirical formula is calculated on the basis of O=8.

Petrographic type: TD — trachydacite; BTA — basaltic trachyandesite; BA — basalt; TB — trachybasalt; TA — trachyandesite; BAA — basaltic andesite

BDL: below detection limit

apfu: atoms per formula unit

Table S4 (continued): Representative compositions of feldspar.

Sample	**UB4**	**UB4**	**UB4**	**UB4**	**UB4**	**UB4**	**UB4**	**UB4**	**UB4**	**UB4**	**UB4**	**UB4**	**UB4**
Petrographic type	**TA**	**TA**	**TA**	**TA**	**TA**	**TA**	**TA**	**TA**	**TA**	**TA**	**TA**	**TA**	**TA**
SiO_2	55.6	53.1	53.3	54.8	53.2	53.5	53.8	69.4	53.0	63.5	51.8	53.8	52.9
Al_2O_3	27.6	28.9	28.6	27.8	29.0	28.4	28.7	15.9	28.4	21.8	29.2	29.0	28.6
MgO	<BDL	<BDL	<BDL	<BDL	<BDL	<BDL	<BDL	<BDL	<BDL	<BDL	<BDL	<BDL	<BDL
CaO	9.59	11.3	10.9	10.5	12.2	10.9	11.3	0.35	11.4	3.75	12.4	11.6	12.0
FeO	0.33	0.32	0.49	0.41	1.27	0.39	0.45	0.50	0.43	0.35	0.40	0.48	0.46
BaO	<BDL	<BDL	<BDL	<BDL	<BDL	<BDL	<BDL	<BDL	<BDL	0.084	<BDL	<BDL	<BDL
Na_2O	6.35	5.09	5.25	5.71	4.85	5.31	5.11	4.65	4.96	7.81	4.65	5.12	4.69
K_2O	0.43	0.34	0.34	0.38	0.37	0.34	0.32	7.86	0.33	2.83	0.26	0.30	0.29
Total	99.9	99.0	98.8	99.6	100.9	98.9	99.7	98.9	98.5	100.1	98.6	100.3	99.0
Empirical formula (*apfu*)													
Si	2.53	2.41	2.42	2.49	2.42	2.44	2.45	3.16	2.41	2.89	2.36	2.45	2.40
Al	1.48	1.55	1.53	1.49	1.55	1.52	1.54	0.85	1.52	1.17	1.56	1.56	1.53
Mg	0.00	0.00	0.00	0.00	0.00	0.00	0.00	0.00	0.00	0.00	0.00	0.00	0.00
Ca	0.47	0.55	0.53	0.51	0.59	0.53	0.55	0.02	0.55	0.18	0.60	0.57	0.59
Fe	0.01	0.01	0.02	0.02	0.05	0.01	0.02	0.02	0.02	0.01	0.02	0.02	0.02
Ba	0.00	0.00	0.00	0.00	0.00	0.00	0.00	0.00	0.00	0.00	0.00	0.00	0.00
Na	0.56	0.45	0.46	0.50	0.43	0.47	0.45	0.41	0.44	0.69	0.41	0.45	0.41
K	0.02	0.02	0.02	0.02	0.02	0.02	0.02	0.46	0.02	0.16	0.01	0.02	0.02
O	8.00	8.00	8.00	8.00	8.00	8.00	8.00	8.00	8.00	8.00	8.00	8.00	8.00
Or (mol. %)	2.4	1.9	2.0	2.1	2.1	1.9	1.8	51.6	1.9	15.8	1.4	1.7	1.7
Ab	53.2	44.1	45.6	48.5	41.0	46.0	44.1	46.5	43.3	66.5	39.9	43.6	40.6
An	44.4	54.0	52.4	49.4	56.9	52.1	54.1	1.9	54.8	17.7	58.6	54.7	57.7

Sample	**UB4**	**UB4**	**UB4**	**UB4**	**UB4**	**UB4**	**UB4**	**UB4**	**UB4**	**UB4**	**UB4**	**UB4**	**UB4**
Petrographic type	**TA**	**TA**	**TA**	**TA**	**TA**	**TA**	**TA**	**TA**	**TA**	**TA**	**TA**	**TA**	**TA**
SiO_2	55.5	53.1	54.1	53.8	55.8	52.2	52.5	54.9	52.9	52.9	53.6	59.0	56.6
Al_2O_3	26.7	29.1	28.1	28.0	26.5	28.8	29.4	28.0	28.9	28.4	28.1	24.9	26.1
MgO	<BDL	<BDL	<BDL	<BDL	<BDL	<BDL	<BDL	<BDL	<BDL	<BDL	<BDL	<BDL	<BDL
CaO	9.43	11.6	10.7	11.1	9.44	12.4	12.3	10.2	11.7	11.7	11.1	6.70	8.65
FeO	0.55	0.40	0.41	0.43	0.53	0.46	0.38	0.30	0.53	0.39	0.42	0.54	0.47
BaO	0.124	<BDL	<BDL	<BDL	0.105	<BDL	<BDL	<BDL	<BDL	<BDL	<BDL	0.395	0.175
Na_2O	5.95	4.96	5.21	5.10	6.00	4.43	4.42	5.69	4.84	4.87	5.28	7.16	6.42
K_2O	0.56	0.31	0.35	0.35	0.46	0.31	0.29	0.37	0.27	0.28	0.35	0.71	0.64
Total	98.8	99.5	98.8	98.8	98.9	98.6	99.3	99.5	99.1	98.5	98.9	99.5	99.1
Empirical formula (*apfu*)													
Si	2.52	2.41	2.46	2.45	2.54	2.37	2.39	2.50	2.41	2.41	2.44	2.69	2.57
Al	1.43	1.56	1.51	1.50	1.42	1.55	1.57	1.50	1.55	1.52	1.51	1.34	1.40
Mg	0.00	0.00	0.00	0.00	0.00	0.00	0.00	0.00	0.00	0.00	0.00	0.00	0.00
Ca	0.46	0.57	0.52	0.54	0.46	0.60	0.60	0.50	0.57	0.57	0.54	0.33	0.42
Fe	0.02	0.02	0.02	0.02	0.02	0.02	0.01	0.01	0.02	0.01	0.02	0.02	0.02
Ba	0.00	0.00	0.00	0.00	0.00	0.00	0.00	0.00	0.00	0.00	0.00	0.01	0.00
Na	0.52	0.44	0.46	0.45	0.53	0.39	0.39	0.50	0.43	0.43	0.47	0.63	0.57
K	0.03	0.02	0.02	0.02	0.03	0.02	0.02	0.02	0.02	0.02	0.02	0.04	0.04
O	8.00	8.00	8.00	8.00	8.00	8.00	8.00	8.00	8.00	8.00	8.00	8.00	8.00
Or (mol. %)	3.2	1.8	2.0	2.0	2.7	1.8	1.6	2.1	1.5	1.6	2.0	4.1	3.6
Ab	51.6	42.8	45.9	44.4	52.1	38.6	38.7	49.1	42.2	42.3	45.3	63.2	55.2
An	45.2	55.4	52.0	53.6	45.3	59.6	59.7	48.8	56.2	56.1	52.7	32.7	41.1

Empirical formula is calculated on the basis of O=8.

Petrographic type: TD — trachydacite; BTA — basaltic trachyandesite; BA — basalt; TB — trachybasalt; TA — trachyandesite; BAA — basaltic andesite

BDL: below detection limit

apfu: atoms per formula unit

Table S4 (continued): Representative compositions of feldspar.

Sample	**UB4**	**UB4**	**UB7**	**UB7**	**UB7**	**UB7**	**UB7**	**UB7**	**UB7**	**UB7**	**UB7**	**UB7**
Petrographic type	**TA**	**TA**	**BAA**	**BAA**	**BAA**	**BAA**	**BAA**	**BAA**	**BAA**	**BAA**	**BAA**	**BAA**
SiO_2	46.7	53.3	44.8	45.8	50.1	50.6	44.9	44.7	50.0	46.1	50.3	44.8
Al_2O_3	32.9	27.9	34.0	33.2	30.6	30.4	34.4	34.6	30.5	33.6	30.1	33.4
MgO	<BDL	<BDL	<BDL	0.05	0.09	0.10	<BDL	<BDL	0.12	<BDL	0.13	0.05
CaO	17.2	11.4	18.5	17.4	14.3	13.9	18.1	18.0	14.2	17.7	14.5	18.3
FeO	0.52	0.48	0.52	0.52	0.53	0.50	0.43	0.42	0.59	0.56	0.50	0.86
BaO	<BDL	<BDL	<BDL	<BDL	<BDL	<BDL	<BDL	<BDL	<BDL	<BDL	<BDL	<BDL
Na_2O	1.65	5.10	0.83	1.42	2.87	3.10	0.97	0.98	3.01	1.25	2.81	1.03
K_2O	0.05	0.30	0.05	0.06	0.18	0.18	0.00	0.00	0.20	0.07	0.15	0.06
Total	98.9	98.5	98.8	98.5	98.8	98.9	98.7	98.7	98.5	99.2	98.5	98.5
Empirical formula (*apfu*)												
Si	2.12	2.43	2.04	2.08	2.28	2.30	2.04	2.03	2.27	2.09	2.29	2.04
Al	1.76	1.49	1.82	1.78	1.64	1.63	1.84	1.85	1.63	1.80	1.61	1.79
Mg	0.00	0.00	0.00	0.00	0.01	0.01	0.00	0.00	0.01	0.00	0.01	0.00
Ca	0.84	0.56	0.90	0.85	0.70	0.68	0.88	0.88	0.69	0.86	0.71	0.89
Fe	0.02	0.02	0.02	0.02	0.02	0.02	0.02	0.02	0.02	0.02	0.02	0.03
Ba	0.00	0.00	0.00	0.00	0.00	0.00	0.00	0.00	0.00	0.00	0.00	0.00
Na	0.15	0.45	0.07	0.12	0.25	0.27	0.09	0.09	0.27	0.11	0.25	0.09
K	0.00	0.02	0.00	0.00	0.01	0.01	0.00	0.00	0.01	0.00	0.01	0.00
O	8.00	8.00	8.00	8.00	8.00	8.00	8.00	8.00	8.00	8.00	8.00	8.00
Or (mol. %)	0.3	1.7	0.3	0.4	1.1	1.1	0.0	0.0	1.2	0.4	0.9	0.3
Ab	14.8	44.0	7.5	12.8	26.3	28.4	8.8	8.9	27.4	11.3	25.7	9.2
An	84.9	54.3	92.2	86.9	72.6	70.5	91.2	91.1	71.4	88.3	73.4	90.4

Empirical formula is calculated on the basis of O=8.

Petrographic type: TD — trachydacite; BTA — basaltic trachyandesite; BA — basalt; TB — trachybasalt; TA — trachyandesite; BAA — basaltic andesite

BDL: below detection limit

apfu: atoms per formula unit

Supplement B

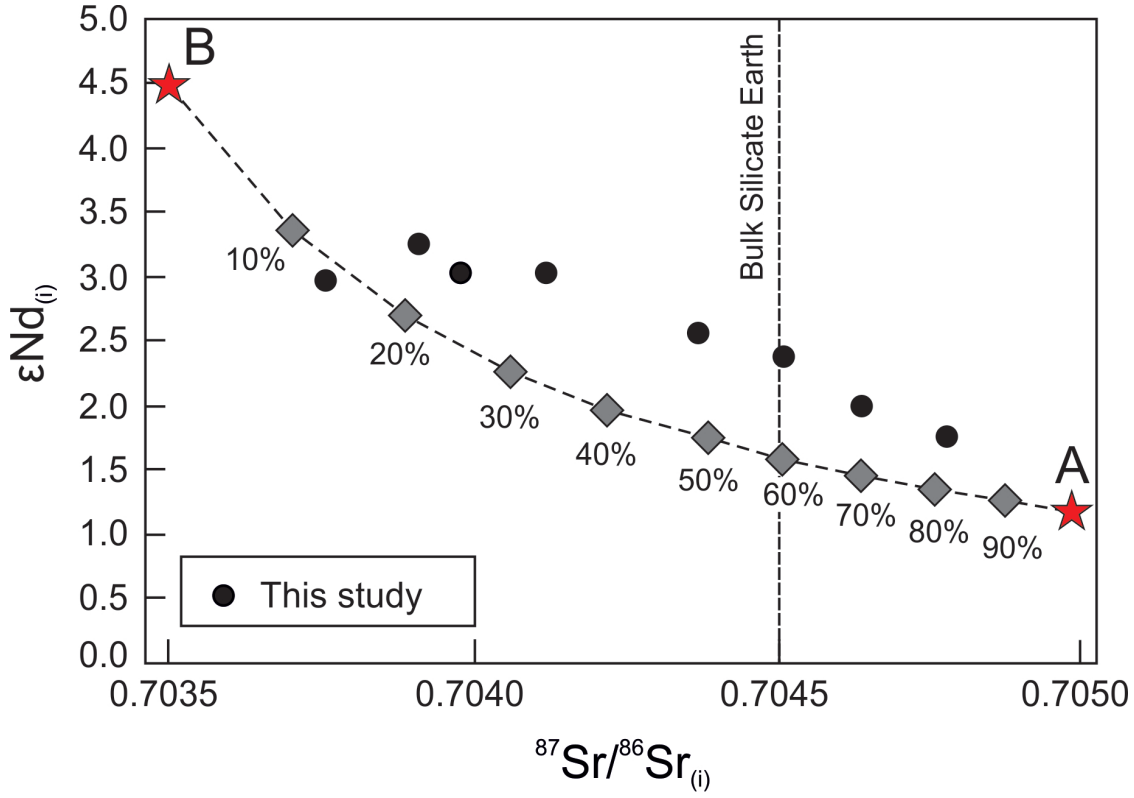

Initial $^{87}Sr/^{86}Sr$ *vs.* $^{143}Nd/^{144}Nd$ isotope ratios for rocks from the Uherský Brod area in comparison with result of two-component mixing between the amphibole-bearing metasome (A) and subcontinental lithospheric mantle (B). Two-component mixing line was calculated using the Sr–Nd isotope composition and concentration taken from Powell et al. (2014) and Medaris et al. (2009).

References

Medaris Jr. G., Ackerman L., Jelínek E., Toy V., Siebel W. & Tikoff B. 2009: The Sklené garnet peridotite: petrology, geochemistry, and structure of a mantle-derived boudin in Moldanubian granulite. *Journal of Geosciences* 54, 301–323.

Powell W., Zhang M., O'Reilly S.Y. & Tiepolo M. 2004: Mantle amphibole trace-element and isotopic signatures trace multiple metasomatic episodes in lithospheric mantle, western Victoria, Australia. *Lithos* 75, 141–171.